TOG domain-tubulin interactions and the function of the *Arabidopsis* Microtubule Organization 1 protein

by

Yi Zhang

B.Sc. (Honors Program in Life Science), China Agricultural University, 2006

A THESIS SUBMITTED IN PARTIAL FULFILLMENT OF
THE REQUIREMENTS FOR THE DEGREE OF

MASTER OF SCIENCE

in

The Faculty of Graduate Studies

(Botany)

THE UNIVERSITY OF BRITISH COLUMBIA

(Vancouver)

April 2010

ABSTRACT

Microtubules are indispensible cellular components involved in multiple core processes such as cell division and intra cellular trafficking. Elaborate regulatory mechanisms are required to direct the precise functioning of these highly dynamic structures. Microtubule-Associated Proteins (MAPs) often perform regulatory functions in controlling microtubule dynamics. Distortion of the function of *Arabidopsis* Microtubule Organization protein1 (MOR1) leads to various developmental defects. However, the mechanism through which MOR1 regulates microtubule function is poorly understood. We have hypothesized that each TOG domain of MOR1 physically binds with tubulin dimers to directly regulate their addition and removal from the microtubule polymer.

To address this hypothesis, we aimed to identify interaction sites between the MOR1 protein and tubulins through a genetic interaction strategy. Three left-handed twisting *mor1* mutants were each crossed with sixteen right-handed twisting *tubulin* mutants, and pronounced genetic interactions were detected by observing non-additive and allele-specific phenotypes. Notably, tubulin point mutations in the interface between the β-tubulin at the plus end of the microtubules and the α-tubulin of the incoming dimer generated the most synergistic phenotypes when combined with the *mor1* alleles. Live cell imaging of microtubules confirmed that allele-specific variations in growth phenotypes were correlated with altered microtubule dynamics.

The MOR1-tubulin interaction model was further tested through the characterization of a new *mor1* allele in the TOG3 domain of MOR1, *mor1-11*, which was determined to have a semi-dominant propyzamide-dependent right-handed twisting phenotype and microtubule organization and dynamics were found to be altered by propyzamide treatment. However, the distinct right-handed twisting phenotype, and to some extent the altered microtubule organization is lost at higher temperature, suggesting that the intrinsic increase in microtubule dynamics at 31 ℃ overrides *mor1-11*'s effect. The $tua6^{C213Y}$ single mutant, which was reported to have similar right-handed twisting upon

propyzamide treatment, continues to twist in a right-handed manner at 31 ℃ and *mor1-11tua6^{C213Y}* double mutants are indistinguishable from *tua6^{C213Y}* single mutants on propyzamide at either 21 ℃ or 31 ℃. Together, these observations suggest that tubulin is more likely than MOR1 to be a direct target of propyzamide and that the motif identified by the *mor1-11* mutation could play a key role in the interactions on MOR1 with α-tubulin.

TABLE OF CONTENTS

LIST OF TABLES

LIST OF FIGURES

LIST OF ABBREVIATIONS

BSA   bovine serum albumin

DMSO   dimethyl sulfoxide

EB1   end-binding protein 1

EDTA   ethylene diamine tetra-acetic acid

EGTA   ethylene glycol tetra-acetic acid

FESEM   field emission scanning electron microscopy

GFP   green fluorescent protein

MAP   microtubule-associated protein

min   minute

MT   microtubule

PBS   phosphate buffered saline

PCR   polymerase chain reaction

PIPES   piperazine-N,N'-bis (2-ethane-sulphonic acid)

SD   standard deviation

Tris [HCl]   2-amino-2(hydroxymethyl)-1,3-propanediol, hydrochloride

TUA   alpha tubulin

TUB   beta tubulin

WT   wild type

ACKNOWLEDGEMENTS

CHAPTER 1: General Introduction

1.1 Microtubule structure and microtubule dynamics

Microtubules are one very important component of the cytoskeleton. They serve as a structural network within cells and function in many cellular processes such as mitosis, cytokinesis and vesicular transport. Microtubules also have indispensable roles in cell shape maintenance.

Microtubules are long, hollow cylinders with a diameter of about 25nm. Each microtubule consists of 13 protofilaments and each protofilament is composed of repetitively ordered α- and β-tubulin, globular proteins that exist cytoplasmically as heterodimers. The GTP (Guanosine-5'-triphosphate) associated with α-tubulin is tightly bound with the tubulin polypeptides and it remains unhydrolysed in association with α-tubulin. In contrast, the GTP coupled with β-tubulin is less tightly bound and can be easily hydrolyzed to GDP. So the microtubule terminus where the β-tubulin is located is highly active to both hydrolyze GTP and to attach free tubulin heterodimers. The microtubule end with exposed GTP-bound β-tubulin has rapid tubulin dimer exchange and is referred to as the "plus end", whereas the other end where incoming GTP-tubulin is immediately converted to GDP-tubulin and subunit exchange is slow is referred to as the "minus end" (Hashimoto, 2003). When the rate of adding dimers is quicker than the rate of losing dimers, microtubules undergo "growth", while "disassembly" occurs when subunit removal exceeds subunit addition. Plus and minus ends have different critical concentrations. The critical concentration, which is defined as the concentration of free tubulin at which net assembly is zero, is higher at the minus end, it is possible for minus end shrinkage to occur simultaneously with growth at the plus end, resulting "treadmilling" behaviour (Hashimoto, 2003; Wasteneys and Collings, 2006; Sedbrook and Kaloriti, 2008; Wasteneys and Ambrose, 2009).

1.2 Microtubule-associated proteins and structures

There is a variety of Microtubule-Associated Proteins (MAPs) that associate with microtubules to regulate their spatial organization and/or dynamics. MAPs can be categorized according to their particular function in stabilizing, destabilizing or cross-linking microtubules, as well as to whether they bind to microtubule ends or bind along the microtubule lattice (Hashimoto, 2003). Microtubule plus-end tracking proteins (+TIPSs) target the plus ends of microtubules. They include CLIP-170 in mammalian cells (Akhmanova et al., 2001) and the END-BINDING PROTEIN1 (EB1) family, which has 3 homologues in *Arabidopsis* (Hashimoto, 2003). Members of the XMAP215 family are also active at the microtubule plus end where they promote tubulin polymerization and depolymerization, and are essential for microtubule dynamics, especially during cell division (Tournebize et al., 2000; Shirasu-Hiza et al., 2003; Hamada et al., 2004; Kawamura et al., 2006). The MAP65 class of proteins is well characterized in plants. These proteins serve to cross-link microtubules (Smertenko et al., 2000).

The XMAP215 family has a wide range of homologues, including XMAP215 from *Xenopus laevis* (Gard and Kirschner, 1987a, b), TOGp from human cells (Gergely et al., 2003), Suppressor of tubulin2 (Stu2) from the budding yeast *Sacharomyces cerevisiae* (Wang and Huffaker, 1997), ZYG-9 from *Caenorhabditis elegans* (Matthews et al., 1998), Microtubule-bundling polypeptide 200 (TMBP200) in tobacco (Yasuhara et al., 2002), Microtubule Organization protein 1(MOR1)/Gemini Pollen1 (GEM1) in *Arabidopsis* ((Park and Twell, 2001; Whittington et al., 2001; Twell et al., 2002).

It has been determined that members of the XMAP215 family have similar core structures. The most conserved feature of these proteins is the N-terminal region, which is characterized by having two or more TOG (Tumor Over-expressed Gene) domains, each approximately 240 amino acids in length (Ohkura et al., 2001). Each TOG domain is formed by six HEAT repeats (HRs), which are tandemly repeated, 37-47 amino acid-long modules that form α-helices linked by a turn region (Perry and Kleckner, 2003). These motifs are generally believed to function in protein to protein interaction (Neuwald and Hirano, 2000).

1.3 MAP-tubulin interaction analysis in the XMAP215 family

Several studies have shown that MAPs of the XMAP215 family, either in plants or animals, can have a variety of effects on microtubule dynamics, to either promote or inhibit growth and/or shrinkage, catastrophe frequency and/or rescue frequency (Tournebize et al., 2000; Brittle and Ohkura, 2005; Srayko et al., 2005; Al-Bassam et al., 2006; Kawamura and Wasteneys, 2008). To better understand the mechanism by which these MAPs affect microtubule dynamics, protein structural analysis as well as *in vitro* interaction assays have been carried out.

Both TOGp and XMAP215 have 5 N-terminal TOG domains, which share highly comparable amino acid sequences. Their homology is reflected by the fact that both proteins will form MAP-tubulin dimer complexes when they interact with microtubule protofilaments during polymerization and depolymerization processes (Spittle et al., 2000; Hamada et al., 2004). A model proposed in Spittle et al. (2000) suggests these MAPs bind along protofilaments and stabilize elongating microtubules. Another *in vitro* interaction assay with XMAP215 showed that this MAP can form a XMAP215:tubulin complex with the C-terminus extended from the complex. And size-exclusion chromatography indicates that the five TOG domains in XMAP215 form a complex with one tubulin dimer for each XMAP215 molecule. TEM images of such complexes suggested that one tubulin dimer is enclosed within each XMAP215 (Brouhard et al., 2008).

Stu2, the XMAP215 family member found in budding yeast, has 2 TOG domains at the N-terminus and a coiled coil at the C-terminus. It is suggested that Stu2 controls microtubule dynamics by using the first TOG domain (TOG1) to bind with one free tubulin dimer and the second TOG domain (TOG2) to associate with the ends of microtubule protofilaments. Two Stu2 proteins linked together by the coiled coils and a pair of tandemly arranged TOG1 and TOG2 domains will recruit free tubulin dimers, promote their binding to the microtubule end, and then dissociate from the protofilaments (Al-Bassam et al., 2006).

1.4 Organ twisting with microtubule dynamics

Various factors, including MAPs, regulate microtubule dynamics. Altering microtubule dynamics causes a variety of phenotypes, depending on the species. In the model plant *Arabidopsis*, altered microtubule dynamics is associated with organ twisting, which can be easily observed in petioles, petals, hypocotyls and roots.

Organ twisting as a consequence of altered microtubule dynamics can be either right- or left-handed, and the handedness is genotype-specific. When *Arabidopsis* roots are growing on hard agar surfaces that are positioned on a slight angle to the vertical axis, root twisting results in the skewing of the roots in one or other direction. The direction of skewing is diagnostic of the handedness of twisting. Left-handed twisting roots result in a sustained rightward root bending so it referred to hereafter as right skewing, even though when viewed from the upper side of the plate is seen to skew to the left side of plates, while right-handed twisting roots skew to the right side of plates (when viewed from the upper side) and result in left skewing.

One of the earliest reports of right-handed twisting roots was in a study by Furutani et al. (2000). In a screen for mutants that reverse the tendency of L*er* mutants to skew slightly to the left side of plates, they identified two mutant loci *spr1* and *spr2* that generated right-handed twisting. They correlated the right skewing (when viewed from the upper side of plates) with right-handed twisting and also found that cortical microtubules in root epidermal cells were arranged in a left-handed helix, suggesting that SPR1 and SPR2 might function in a microtubule-dependent process. Subsequent studies determined that SPR1 (Nakajima et al., 2004; Sedbrook et al., 2004) and SPR2 (Shoji et al., 2004) were indeed microtubule-associated proteins. Various mutations in tubulin-encoding genes have been identified that cause right-handed twisting in roots. These point mutations can occur in either α–tubulin or β–tubulin, and the twisting is associated with changes in the orientation of cortical microtubules as well as altered microtubule dynamics (Ishida et al., 2007b). Overexpression of α–tubulin with an N-terminal GFP tag or the Microtubule Binding Domain (MBD) of the vertebrate MAP4 also cause right-handed twisting phenotypes (Dixit and Cyr, 2004; Abe and Hashimoto, 2005).

Various genetic and pharmacological conditions cause left-handed twisting. The *lefty1* and *lefty2* mutants, which have equivalent point mutations in α–tubulin 4 and 6 respectively, are reported to have microtubule arrays arranged in right-handed helices and this is correlated with left-handed twisting and left skewing of roots (Thitamadee et al., 2002; Abe et al., 2004). More recently, several more left-handed twisting mutants have been described that have point mutations in either α or β–tubulin (Ishida et al., 2007b). Low concentrations of the microtubule-targeted drugs propyzamide and taxol also generate left-handed twisting (Hugdahl et al., 1993; Furutani et al., 2000; Nakamura et al., 2004). Several mutations in microtubule-associated proteins have been described that cause left-handed twisting. MAP18 was suggested to function in microtubule destabilization and stabilization, and overexpressing *MAP18* generated left-handed twisting roots (Wang et al., 2007). Left-handed twisted roots were also observed in a triple mutant of end-binding proteins EB1 (EB1a, EB1b and EB1c) in *Arabidopsis* (Bisgrove et al., 2008). In particular, three point mutations in MOR1, *mor1-1*, *mor1-2* and *rid5*, cause temperature-dependent microtubule disruption and left-handed twisting of most organs including roots (Whittington et al., 2001; Konishi and Sugiyama, 2003).

In summary, although different twisting directions can be induced by different chemical treatments or genetic mutations, the common point is that twisting appears to be consistently correlated with defects in microtubule dynamics. Mutations that cause twisting generally map to genes encoding α or β–tubulins or to MAPs or subunits of nucleating complexes. Some microtubule-targeted drugs that alter dynamics and/or the spatial organization of cortical microtubules also lead to twisting, and this too appears to have a handedness that is drug-specific. Thus, genetic as well as chemical-genetic approaches can be used to examine the microtubule basis for directional handedness of plant growth, just as they can be used to understand the essential role microtubules play in growth anisotropy (Sugimoto et al., 2000).

1.5 Objectives

Studies on the XMAP215 homologue in *Arabidopsis*, MOR1, indicate that this MAP plays an important role in regulating microtubule dynamics (Kawamura and Wasteneys 2008). Mechanisms of MAP-tubulin interactions have been deduced to some extent in MOR1's homologues XMAP215 and Stu2. Negative staining electron microscopy predicted that the MAP215/Dis1/TOGp/MOR1 proteins are approximately 60nm in length (Cassimeris et al., 2001) and it is known that each tubulin dimer is 8nm long. The C terminal has been shown to act as a microtubule-binding domain (Twell et al., 2002). Based on these structural data and microtubule dynamics measurements in *mor1-1* at restrictive temperature, a model was proposed that suggests **each TOG domain interacts with one tubulin heterodimer to increase the efficiency of tubulin addition and removal from microtubules** (Kawamura and Wasteneys 2008; Figure 1- 1).

One way to test this model will be to identify motifs in each TOG domain that interact with α- and β-tubulin. In this thesis, two major strategies to better understand MOR1-tubulin interactions were undertaken. In the first project, as described in chapter 2, a genetic approach was used to probe TOG-tubulin interaction analysis in the N-terminal-most TOG1A domain. Three left-handed twisting mutants caused by single amino acid substitutions in MOR1's TOG1A domain were each crossed with sixteen semi-dominant right-handed twisting mutants caused by amino acid substitutions in a range of tubulin proteins to assess the consequences on growth and microtubule dynamics and organization in the ensuing double mutants. The second major project, described in chapter 3, used a chemical-genetic strategy to characterize MOR1's function in controlling microtubule dynamics by analysis of a novel point mutation, *mor1-11*, identified in the fifth TOG domain.
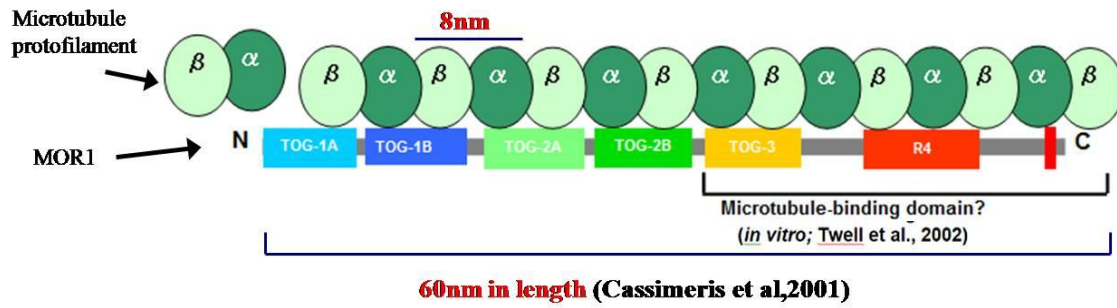
Figure 1- 1 Model for MOR1 interaction with free tubulin and protofilaments.

CHAPTER 2: MOR1 TOG-tubulin Interaction in TOG1

2.1 Introduction

2.1.1 The structure of MOR1 protein and related *mor1* alleles

Arabidopsis MICROTUBULE ORGANIZATION 1 (MOR1) protein is the first member of the MAP215/Dis1 family of microtubule-associated proteins to be identified in the plant kingdom (Whittington et al., 2001). The most highly conserved feature of the XMAP215 family is the presence of N-terminal TOG domains, so-called for the human homologue, Tumour-Overexpressed Gene protein. MOR1 has five of these TOG domains, each of which has a core of 6 HEAT repeats (HRs). These motifs are believed to function in protein to protein interaction (Neuwald and Hirano, 2000). Like MOR1, its homologue XMAP215 of *Xenopus laevis* has 5 TOG domains, while the Zyg-9 protein of C.*elegans* has 3 and Stu2 of *S. cerevisiae* has 2 TOG domains respectively (Ohkura et al., 2001).

In the N-terminal TOG domain of MOR1, three point mutations have been identified and described: *mor1-1*^{L174F}, *mor1-2*^{E195K} and *rid5*^{C96Y}. Both the temperature-sensitive *mor1-1*^{L174F} and *mor1-2*^{E195K} mutations are located in the fifth HR of the first TOG domain. At restrictive temperatures (29 to 31 ℃), microtubule organization is disrupted and the plants undergo left-handed organ twisting (Whittington et al., 2001). The *root initiation defective5 (rid5)* mutant was identified as another temperature-sensitive allele of *mor1* (Konishi and Sugiyama, 2003). The *rid5* mutation also substitutes an amino residue in the first TOG domain of MOR1 but unlike the *mor1-1* and *mor1-2* mutations, which are located in the fifth HR, the *rid5* substitutes an amino acid in the third HR.

The Wasteneys lab has also used a reverse genetics approach called TILLING to obtain a series of additional mutant alleles in MOR1, which comprise a variety of point mutations in TOG domains interior to the N-terminus and in the C-terminal region. Studies on these mutant lines will be discussed in Chapter 3.

2.1.2 MOR1 can alter microtubule dynamics

Previous research has demonstrated that microtubule disorganization in both *mor1-1* and *mor1-2* are temperature-dependent, with shorter and disordered microtubules forming at temperatures above 28 ℃ (Whittington et al., 2001). In addition to the temperature–sensitive phenotype, studies of *mor1-1* and *mor1-2* mutants have shown that they are hypersensitive to microtubule-targeted drugs (Collings et al., 2006). Mitotic spindles and cytokinetic phragmoplasts are shorter in *mor1-1* than they are in the wild type (Kawamura et al., 2006). Most recently it was also shown that at restrictive temperature, microtubule dynamics, including growth and shrinkage rates, are reduced in *mor1-1*. This demonstrates that the MOR1 protein has an important function in promoting microtubule dynamics (Kawamura and Wasteneys, 2008).

2.1.3 Previous research on MOR1 interaction with β-tubulin

The mechanism by which MOR1 affects microtubule dynamics and how the MOR1 protein interacts with microtubules or free tubulin dimers still needs further studies.

Structural analysis by X-ray diffraction of the third TOG domain of MOR1's homologue from *C.elegans,* Zyg9, indicated that TOG domains have a flat, paddle-like shape and that the turns between the α-helices of the HEAT repeats are likely to constitute the tubulin binding sites (Al-Bassam et al., 2007). This observation suggests that the first TOG domain in MOR1, where *mor1-1, mor1-2 and rid5* mutations are situated, is likely to have tubulin binding sites at equivalent positions.

Genetic studies conducted in yeast led Al-Bassam et al (2006) to speculate that there is an interaction between TOG domains and tubulin. In a screen for suppressors of a temperature-sensitive β-tubulin mutation, the yeast TOGp homologue Stu2 was identified (Wang and Huffaker, 1997). The *stu2-1* and *stu2-2* mutations are located in the second TOG domain's fifth HR while *mor1-1* and *mor1-2* are in the first TOG domain's fifth HR. This suggests the fifth HR in the first TOG domain of MOR1 might also interact with β-tubulin. It is worth noting that the *stu2-1* mutation in combination with an independent

tubulin mutation, *tub2-404,* is synthetically-lethal, which demonstrates that allele-specific phenotypes can vary from suppression through to lethality.

The inhibition of microtubule growth and shrinkage rates in *mor1-1* at restrictive temperature (Kawamura and Wasteneys, 2008) is possibly caused by a partially impaired interaction between MOR1 and the exposed active β-tubulin. As the *stu2* and *mor1-1* and *mor1-2* mutations occur in the same HR but in different TOG domains, we need to confirm that the fifth HR in each TOG domain regulates microtubule dynamics through a specific interaction with β-tubulin (Figure 2- 1).
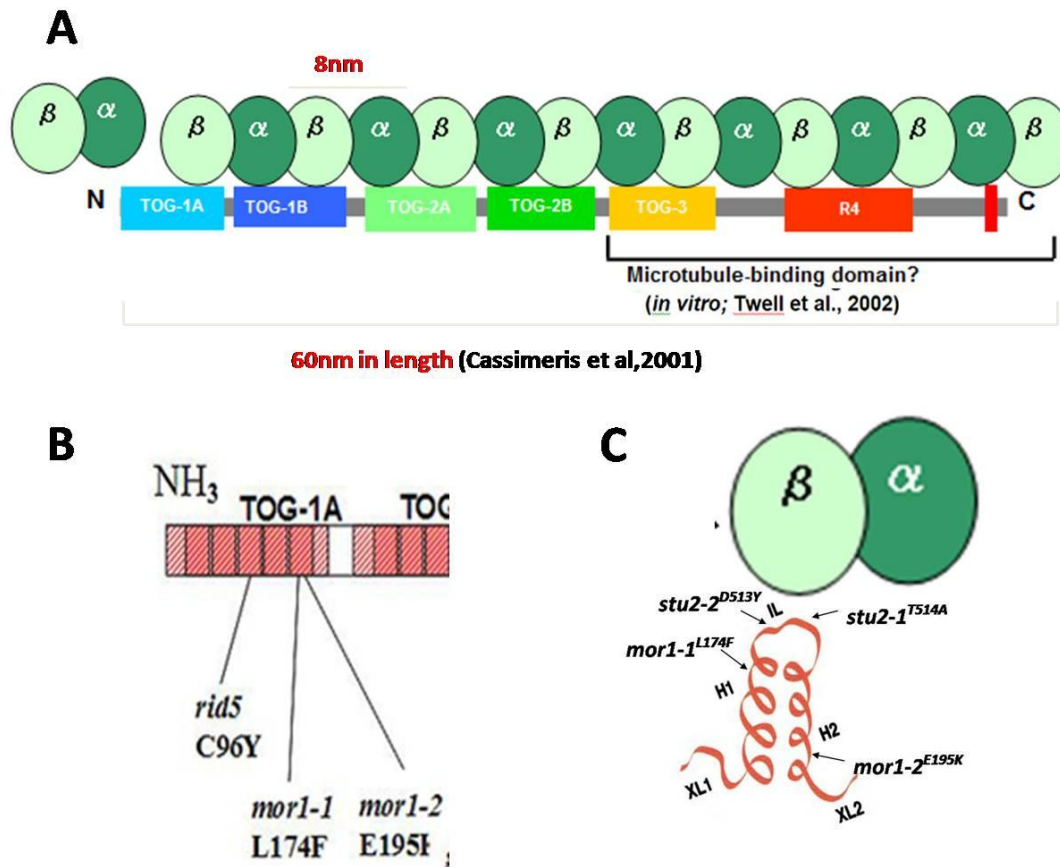
Figure 2- 1 A. A hypothetical model of MOR1-tubulin interaction from Kawamura and Wasteneys (2008). B. The N-terminal TOG-1A domain showing putative heat repeats (red boxes). *mor1-1* **and** *mor1-2* **mutations are located in the fifth HR of the first TOG domain and** *rid5* **is located at the third HR of the same TOG domain. C. Putative interaction of the fifth HR with β–tubulin, showing the locations of residue substitutions caused by the** *mor1-1* **and** *mor1-2* **mutations from MOR1's TOG-1A domain, and the** *stu2-1* **and** *stu2-2* **mutations from the TOG-1B domain of the Stu2 homologue of MOR1 from** *S. cereviseae***. (HR structure is modified from Perry and Klechner (2003), Figure1 A)**

2.1.4 Mutations in tubulin dimers alter microtubule dynamics

From a mutant screening project carried out in the Hashimoto lab (Nara Institute of Science and Technology, Japan), various tubulin mutants with point mutations in either α-tubulin or β-tubulin were identified that showed either left-handed or right-handed organ twisting phenotypes (Ishida et al., 2007b). These tubulin mutants have twisting in roots, hypocotyls and usually cotyledon petioles during the early seedling stage. Under normal growth conditions, the organization of cortical microtubules in root epidermal cells was reported to be helical, with the predominant orientation of microtubules tilted with respect to the transverse axis. Microtubule dynamics were also suggested to be affected by these point mutations.

In this study, I used a genetic strategy to identify MOR1-tubulin protein-protein interaction sites. To achieve this, I crossed all three of the left-handed twisting *mor1* alleles with sixteen tubulin mutants that cause right-handed twisting. The latter were obtained from the tubulin mutant collection described in Ishida et al (2007), as highlighted in Figure 2- 2 (Ishida et al., 2007b). These tubulin mutants comprise a variety of amino acid substitutions in various domains of both α- and β-tubulins, including the lateral contact regions, the GTPase-activating region of α-tubulin, within the GTPase-activating region of β-tubulin, as well as the interdimer regions (Figure 2- 2). By comparing the phenotypes of double mutants to look for allele-specific interactions, it is hoped that this genetic interaction assay will provide insights into the MOR1 motifs that interact with specific tubulin binding sites, and specifically test the prediction that the motif on the MOR1 protein at which the *mor1-1* and *mor1-2* mutations occur interacts with β-tubulin.
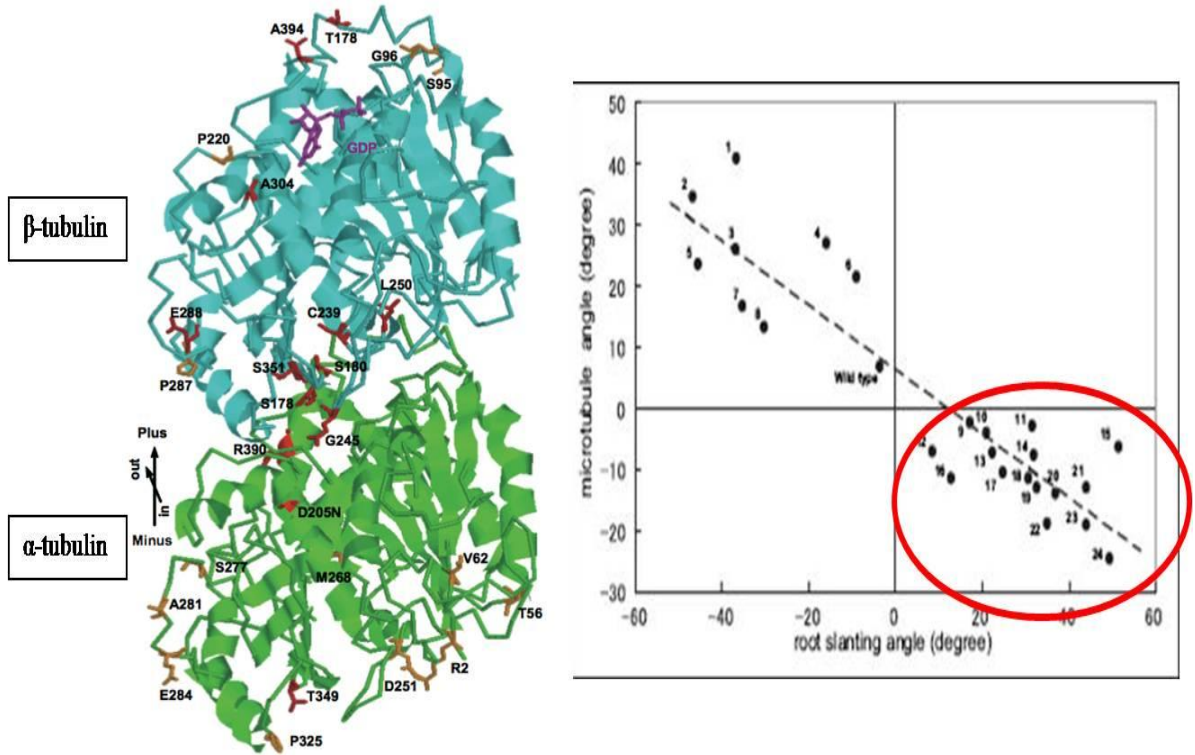
Figure 2- 2 Tubulin mutations used in the current study are generally mapped to the inter-dimer and intra-dimer regions. Among these mutants, some showed left-handed twisting roots, with minus root slanting angles and positive microtubule angles (microtubule orientation to cell long axis), while others show right-handed twisting with positive root slanting angles and minus microtubule angles (Modified from (Ishida et al., 2007b) Figure 2 and Figure 3, with permission).

2.2 Material and methods

2.2.1 Plant material and growth conditions

In this part of study, three alleles of *mor1* mutants (*mor1-1*^{L174F}, *mor1-2*^{E195K} and *rid5*^{C96Y}) and sixteen tubulin mutants were crossed individually. Seeds of *rid5* were provided by the Sugiyama Lab (The University of Tokyo, Japan) and *tubulin* seeds were provided by the Hashimoto lab (Nara Institute of Science and Technology, Japan).

Seeds were sterilised by treatment with 3% (v/v) hydrogen peroxide and 50% (v/v) ethanol in distilled water for 2 min, then rinsed in distilled water three times. Sterilised seeds were then planted on nutrient-solidified Hoaglands' medium (90 μM Fe-EDTA, 5mM $Ca(NO_3)_2$, 1mM KH_2PO_4, 2mM KNO_3, 2mM $MgSO_4$, 46 μM H_3BO_3, 9.2 μM $MnCl_2$, 0.77 μM $ZnSO_4$, 0.32 μM $CuSO_4$, 0.11 μM MoO_3, 530 μM Inositol (Sigma, Canada), 50 μM Thiamine Hydrochloride (Lancaster Synthesis), 3% (w/v) Sucrose (Fisher Chemical), 1.2% (w/v) Bacto Agar (BD Chemical). Approximately 20 seeds were planted on round plates, while 50 seeds were planted on square plates (Fisher Brand). Then plates were sealed with microtape (Micropore, 3M, USA) and vertically placed in wooden racks. After 2 days treatment at 4 °C, plates were moved to 21 °C under continuous light (80-100 μmol/m^2/s).

2.2.2 Temperature shift assays

The *mor1* mutants used in this study have temperature-sensitive phenotypes. The seedlings show left-handed twisting and swollen roots after incubation at 31 °C for 1 or 2 days. Therefore in order to confirm *mor1* homozygosity in all double mutants, it was important to standardize the mutant detection process. Thus, seedlings were grown at 21 °C for 7 days then at 31 °C for 2 days, and images were taken for further quantitative analysis.

2.2.3 Evaluation of segregation ratio

Approximately 500 F2 seedlings from each *mor1-tubulin* cross were planted to segregate double mutants. Seedlings, planted on regular Hoagland's medium, were examined after the standard temperature shift assay. Because of the semi-dominant nature of the tubulin mutants, seedlings were scored as candidate genotypes according any distinguishable phenotypes, especially their growth behaviour at 31 ℃. Then, segregation ratios were calculated and the goodness of fit tested by Chi-square analysis. The wild type and single mutant control lines were segregated from the same F2 lines. Putative double mutants and control lines were transplanted to soil for further genotyping and seed harvesting.

2.2.4 Genomic DNA extraction, genotyping and sequencing analysis

All of the putative double mutants and control lines were genotyped by sequencing to confirm their genotypes.

Genomic DNA was extracted from 7 to 10 day old leaf tissue using the DNA extraction method (Weigel and Glazebrook, 2002).

To amplify the region of DNA containing the point mutation, primer sets for sequencing across each tubulin point mutation were designed. Forward and reverse primers were determined by putting the mutation point at the center of 500bp length fragment. All primer sets for this work are listed in Table 2-1.

After combining the genomic DNA and specific primers, PCR reactions were carried out as follows: 94 ℃ for 2 min, 94 ℃ for 30 sec, 55 ℃ for 30 sec, 68 ℃ for 1:30 min, and then go back to 94 ℃ 30 sec for 35 cycles, then 68 ℃ for 5 min, 4 ℃ forever.

PCR products were purified using a QIA kit to remove extra salts or primers, and the purified PCR products were then added to the sequencing PCR reaction (96 ℃ for 1 min, 96 ℃ for 10 sec, 50 ℃ for 5 sec, 60 ℃ for 4 min, and then back to 96 ℃ 10 sec for 25 cycles, then 4 ℃ forever). Samples were sent to the NAPS Unit at UBC for sequencing and the sequencing results were analyzed by BioEdit software to determine the genotypes.

Table 2- 1 Primer sets used for tubulin mutants genotyping.

Targeted mutation	Primer 1	Primer 2
$tua2^{E284K}$	5'-ACACCAACCTCAACCGTCTC-3'	5'-CACAGCTCTCTGGACTTTAGCA-3'
$tua4^{R2K}$	5'-AGAAAATACGCAGCTCACGA-3'	5'-CAGAAATCCGGAGAACAAGG-3'
$tua4^{T56I}$	5'-ACCTGTTTAGATCTGAGTTTGACA-3'	5'-GGAGGAGAGATCCAAGACCA-3'
$tua4^{V62I}$	5'-TTGACATAGATTTCTTGTTGGTTGA-3'	5'-TTGGACTTTTTCCCGTAGTCA-3'
$tua4^{M268I}$	5'-TGTAGCCAGCCTCAACCAGTCT-3'	5'-TGATGGTGCCAACAGCTGCGT-3'
$tua4^{S277F}$	5'-GACGCTCCCTAAGCATTGAG-3'	5'-AGCAAGATCACCTCCTGGAA-3'
$tua5^{D251N}$	5'-CCCTTCTCCTCAGGTACTCTTTC-3'	5'-CTGAACAGTCCTCTTTGTCTTGA-3'
$tua6^{S277F}$	5'-ACACCAACCTCAACCGTCTCGT-3'	5'-ACTCGTAAGAGTTTCGAGCCCCCA-3'
$tua6^{A281T}$	5'-ACACCAACCTCAACCGTCTCGT-3'	5'-ACTCGTAAGAGTTTCGAGCCCCCA-3'
$tua6^{P325S}$	5'-ACGCTCCCTTAACATTGAGA-3'	5'-TCTCCTTCTTCCATACCCTCA-3'
$tub1^{S96F}$	5'-CGTGGAACGAGAATGATTACAA-3'	5'-TGTTCTTTGCATCCCACATC-3'
$tub2^{P287L}$	5'-TGCTTTGATTCTTTTCTCATCGT-3'	5'-CACTCACTCGCCTGAACATC-3'
$tub3^{P287L}$	5'-CATTGATGACTATCGATTTGTGAA-3'	5'-CACTCACTCGCCTGAACATC-3'
$tub4^{G96D}$	5'-TCATATCCAAGGCGGTCAAT-3'	5'-GAGTTCCCATTCCAGATCCA-3'
$tub4^{P220S}$	5'-CGTGGAACGAGAATGATTACAA-3'	5'-TGTTCTTTGCATCCCACATC-3'
$tub4^{P287L}$	5'-TGCAGCTTGTGTATTCATGTAGTGTGA-3'	5'-AGCTTACGAATCCGAGGGAGCCA-3'

2.2.5 GFP reporter detection in double mutants

To detect changes in microtubule dynamics in *mor1-tubulin* double mutants, several different GFP reporters were initially compared. *Pro35S*::GFP-TUB (Nakamura et al., 2004), a GFP-β-tubulin reporter, was chosen because it does not produce a root twisting phenotype. In contrast, the *Pro35S*::GFP-TUA6 reporter line (Ueda et al, 1999), which expresses GFP tagged to the N-terminal region of α-tubulin 6, generates constitutive right-handed root twisting. Two microtubule end-binding 1 protein GFP reporter lines, *Pro35S*::EB1-GFP and *ProEB1*::EB1-GFP were used for specifically measuring growth rates on microtubule plus ends (Chan et al., 2005). Wild-type plants homozygous for each of the reporter lines were crossed with all of the confirmed double mutants to segregate putative double mutants expressing the GFP reporter as well as control lines. 5 to 7 day-old seedlings were screened by stereo-fluorescence. All the mutant genotypes were confirmed by sequencing analysis.

2.2.6 Live cell imaging of GFP plants and image processing

I chose three different GFP reporters to track microtubule dynamics. However, in this thesis I will mainly describe the data detected using the *Pro35S*::GFP-TUB reporter line, which enabled both microtubule growth and shrinkage rates to be measured.

All the seedling samples prepared for live cell imaging were grown for 7 days at 21 °C, or 5 days at 21 °C then 2 days at 31 °C. To control the temperature of samples when they were removed from the growth chambers, samples were prepared on a heat block (Labnet) set to the specified temperature. All tools and solutions were pre-cooled or pre-warmed. Cotyledons of seedlings were cut and placed at the center part of every slide, upon which a drop of distilled water at the required temperature was added. To secure the 22×22 mm coverslips, silicon vacuum grease (Dow Corning) was applied along all four edges, and the coverslips applied gently to the slides to prevent air bubble formation.

Samples were observed on a Leica DMI6000 inverted microscope, equipped with a Quorum-customized Wave FX system incorporating a modified Yokogawa CSU-10

spanning disk scan head (Yokogawa Electric Corporation, Tokyo, Japan). A 63×NA 1.3 glycerol lens (Leica) was used to detect fluorescence signals generated by the 488nm laser. Images were acquired using a Hamamatsu 9100-13 EM-CCD (ImagEM) camera (Hamamatsu, Japan). GFP signals were detected using a 502/35 emission band filter (Chroma Technology, Rockingham VT; (Figure 2- 3 A).

To maintain the temperature of samples during the imaging process, a temperature controlled stage was placed on the microscope sample stage area, connected to Bionomic controller BC-110 and Heat Exchanger HEC-400 (20/20 Technology Inc.) (Figure 2- 3 B). The objective lens was also warmed by applying an Objective Heater (Bioptechs Inc.; Figure 2- 3 C). The temperature of the glycerol on cover slips was monitored constantly with a temperature detector (thermocouple, Fisher Brand) to determine the actual temperature of the sample.

All images were captured using a 802 ms exposure time. An approximate 0.5 μm thick optical depth was recorded at each time point by scanning 3 frames every 5 seconds over a 3 minute period.

The ImageJ plugin Image5D was used to align three-frame maximized images. The ImageJ Manual Tracking plugin was used to track the growth and shrinkage of single microtubule. If the images showed XY drifting, the ImageJ Stabilizer plugin was applied.
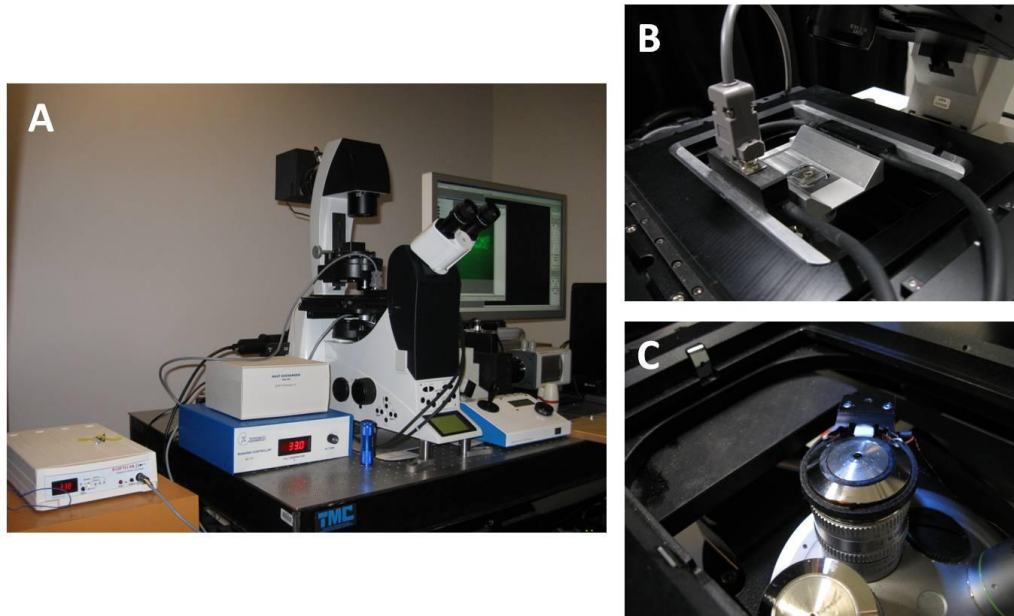
Figure 2- 3 A. The Leica inverted microscope with a Quorum Wave FX spinning disc confocal scanning system. B. A temperature-controlled stage was used to maintain the permissive or restrictive temperatures during imaging processing. C. Objective lens heater.

2.3 Results

2.3.1 *mor1* TOG domain 1a mutants have temperature sensitive phenotypes

As reported previously (Whittington et al., 2001), the *mor1-1* and *mor1-2* alleles had temperature-sensitive phenotypes. Both mutants grew normally at 21 °C but at restrictive temperature, such as after treatment for 6 days at 31 °C, the seedlings skewed to the left side of the plate (observed from the front side of the plate), roots became radially swollen (Figure 2- 4 A. B. E. and F.), and cotyledons twisted in an anti-clockwise manner (Figure 2- 4 A. and B.).

According to a previous study (Konishi and Sugiyama, 2003), *rid5* has a similar temperature-sensitive phenotype as *mor1-1* and *mor1-2*, with normal root growth at 21 °C and left-handed twisting and swollen roots at 31 °C. However, I determined that the *rid5* mutant, when grown on Hoaglands' medium at 21 °C, showed left-handed twisting. The phenotype, however, became stronger at the restrictive temperature, with roots undergoing noticeable radial swelling after seedlings were transferred to 31 °C for 1 or 2 days (Figure 2- 4 C. and G.).

2.3.2 *tubulin* mutants have no temperature sensitive phenotypes

Due to the *mor1* mutants' temperature-dependent phenotypes, it was necessary to test whether the right-handed twisting *tubulin* mutants have altered phenotypes at the *mor1* mutants' restrictive temperature. All 16 alleles were planted on the Hoaglands' medium at 21 °C for 7 days, and then moved to 31 °C for 2 days (Figure 2- 4 D. and H.). To ensure their validity, the assays were repeated at least three times. According to the observations, none of the 16 tubulin mutants has any temperature-specific response. After shifting to 31 °C, the tubulin seedlings continued to skew to the right side of the Petri plates (as viewed from the upper side), and none underwent radial swelling.
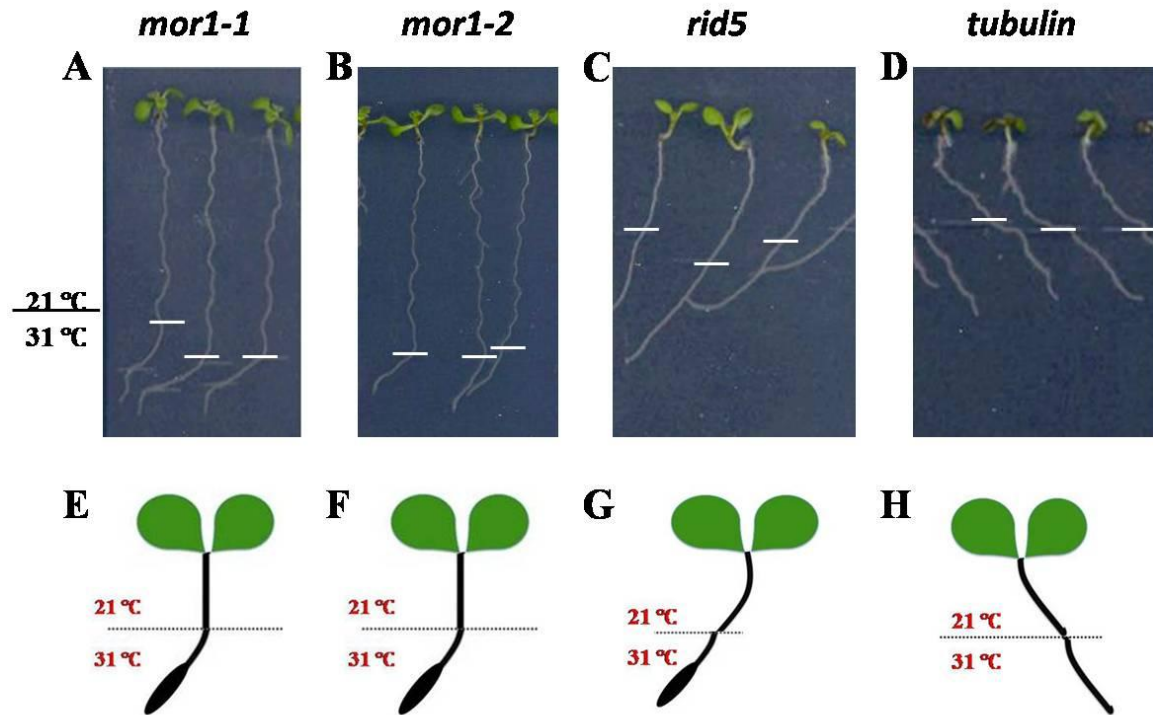
Figure 2- 4 Phenotypes of *mor1* mutants and tubulin mutants at 21 ℃ and 31 ℃, showed in actual images (A to D) and schematic drawings (E to H). The white line indicated where temperature shift occurred. *mor1-1* and *mor1-2* have straight root growth at 21 ℃ and left-handed twisting and swollen roots at 31 ℃ (A. B. E and F.). *rid5* showed consistent left-handed twisting root at both 21 ℃ and 31 ℃, but in addition formed swollen roots at 31 ℃ (C. G). None of the 16 *tubulin* mutants had temperature-dependent phenotypes, undergoing consistent right-handed twisting at either temperature (*tua5*[D251N] was presented in D, H).

2.3.3 *mor1-tubulin* double mutant screening and phenotypes

All three left-handed twisting *mor1* alleles were crossed with the sixteen right-handed twisting *tubulin* mutants (provided by the Hashimoto lab, as highlighted in Figure 2- 2) (Ishida et al., 2007b). Since all the mutants have significant root twisting or swelling phenotypes, we designed a combination of phenotypic and molecular approaches to identify double homozygous mutants from the F2 generation. Since it had been confirmed that none of the tubulin mutants had a temperature-sensitive phenotype, it was possible to identify F2 seedlings that were homozygous for the *mor1* mutations by checking for radial swelling of roots at 31 ℃. Sanger sequencing following PCR amplification was subsequently conducted to determine the zygosity of the *TUB* loci, as well as to confirm the genotypes at the *MOR1* locus.

For all 48 crosses, F2 segregation analysis was carried out to identify double mutants. For each cross, 500 F2 seedlings were categorized into different candidate genotypes according to the root growth behaviours, first at 21 ℃ and then at 31 ℃. After Chi-square analysis and genotype confirmation (as described above), phenotypes were assessed for the F3 progeny from all 48 confirmed double mutants as well as azygous and single mutant controls.

The phenotypes of all double mutants were examined to identify any non-additive or allele-specific phenotypes in order to identify any combinations indicating site-specific functional interactions between MOR1 and the various tubulins. Apart from one exception (the *tua5*^{D251N} mutant described below), *mor1-1* and *mor1-2* usually behaved similarly when combined with a particular tubulin mutation (see Appendix 1), which is consistent with that *mor1-1* and *mor1-2* locate in the same HR motif and the fact that these two mutants have indistinguishable temperature-sensitive phenotypes. Therefore, unless specifically noted, in all comparisons between the *rid5-tubulin* and *mor1-1-tubulin* double mutants, it can be assumed that the *mor1-2-tubulin* double mutant has the same phenotype as *mor1-1-tubulin*.

Most of the mutant combinations were additive, suggesting that there was no significant functional interaction between the sites affected by the point mutations in the MOR1 and tubulin proteins. An example for an additive double mutant phenotype is the $tub3^{P287L}$-$mor1$ double mutants (Table 2- 2). At 21 ℃, both the $tub3^{P287L}mor1-1$ and $tub3^{P287L}rid5$ double mutants displayed right-handed twisting hypocotyls and roots, with the root twisting leading to skewing of roots to the right side of the plates. At 31 ℃, the roots changed direction and instead skewed to the left side of the plate as a result of left-handed cell file twisting. The roots, as with the $mor1$ single mutants, also underwent radial swelling at 31 ℃.

Five double mutants were identified that displayed non-additive phenotypes that were specific to either $mor1-1$ or $rid5$ alleles (Table 2- 2).
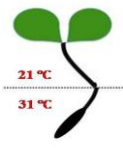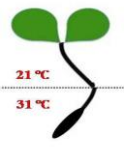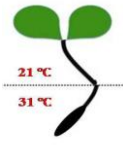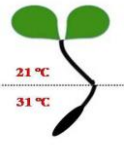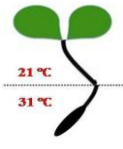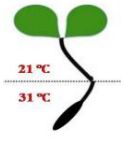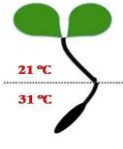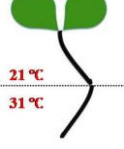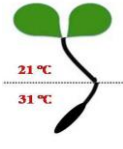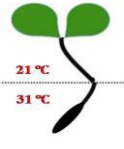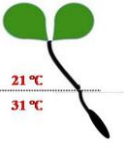
The $tub4^{G96D}$ mutation is located in the interdimer region of β-tubulin. At 21 ℃, the hypocotyls of the $tub4^{G96D}$ $mor1-1$ double mutant did not show the right-handed twisting that is detected in $tub4^{G96D}$ single mutant. The roots, however, behaved in the same manner as double mutant with additive phenotypes, undergoing right-handed twisting at 21 ℃, and left-handed twisting and radial swelling at 31 ℃. In contrast, the $tub4^{G96D}$ $rid5$ double mutant had the right-handed twisting hypocotyls and roots at 21 ℃ but relatively weak left-handed twisting and radial swelling at 31 ℃.

The $tua4^{T56I}$ mutation is located at the lateral contact region of microtubule protofilaments. Both the $tua4^{T56I}mor1-1$ and $tua4^{T56I}rid5$ had very weak right-handed cell file twisting in hypocotyls, and right skewing of roots at 21 ℃, followed by left root skewing and swelling at 31 ℃. At 31 ℃, however, $tua4^{T56I}mor1-1$ showed the right-handed helical cell files, while there was no sign of cell file twisting in $tua4^{T56I}rid5$, which had cell files that were aligned in the direction of root growth.

Another mutation in α–tubulin, located at the interdimer region, $tua6^{P325S}$, also showed allele-specific phenotypes in combination with different $mor1$ alleles. The root swelling phenotype was lost in $tua6^{P325S}rid5$ but existed in $tua6^{P325S}mor1-1$.

An interesting tubulin mutant, $tua5^{D251N}$, substitutes a conserved amino acid in the domain of α-tubulin that is known to activate the GTPase activity of β-tubulin upon docking at the microtubule plus end. As a single mutant, $tua5^{D251N}$ generated right-handed twisting. The $tua5^{D251N}mor1-1$ double mutant was seedling-lethal. After seedlings, which had germinated on plates, were transferred to soil, the seedlings died. In contrast $tua5^{D251N}mor1-2$ and $tua5^{D251N}rid5$ double mutants were able to proceed into reproductive phase and to produce seeds.

Table 2- 2 Phenotypes of some *tubulin-mor1-1* and *tubulin-rid5* double mutants.

mutations	*tubulin-mor1-1*	*tubulin-rid5*
$tub3^{P287L}$ Lateral contact region		
$tub4^{G96D}$ Interdimer αβ-tubulin region	No hypocotyl twisting	
$tua6^{T56I}$ Lateral contact region		No cell file twisting at 31 ℃
$tua6^{P325S}$ Interdimer αβ-tubulin region		No root swollen at 31 ℃
$tua5^{D251N}$ GTPase-activing region	Seedling-lethal	
$tub4^{P220S}$ Interdimer αβ-tubulin region	Straight root growth at 31 ℃	Right-handed twisting at 31 ℃

2.3.4 Double mutants of *tub4^P220S^-mor1* show allele-specific genetic interaction

The *tub4^P220^-mor1* mutants were chosen for in-depth analyses because of the sophisticated allele-specific synthetic phenotypes. This β-tubulin mutation replaces a hydrophobic proline residue located in the interdimer region with a hydrophilic serine, resulting in the constitutive and strong right-handed twisting. Double homozygous *tub4^P220S^mor1-1* seedlings resembled the *tub4^P220S^* mutant at 21 ℃ but after two days at 31 ℃, the swollen region of roots grew straight rather than skewing to the left side of plates (Figure 2- 5 A. and C.). In the *tub4^P220S^rid5* double mutant, root twisting failed to reverse handedness at 31 ℃, and swollen roots continued right-handed twisting and skewing to the right side of the Petri dish (Figure 2- 5 B. and D.). In both of the double mutants, root radial swelling occurred. This suggests that the *tub4^P220S^* mutant's ability to suppress the *mor1* or *rid5* phenotype was limited to the left-twisting aspect.
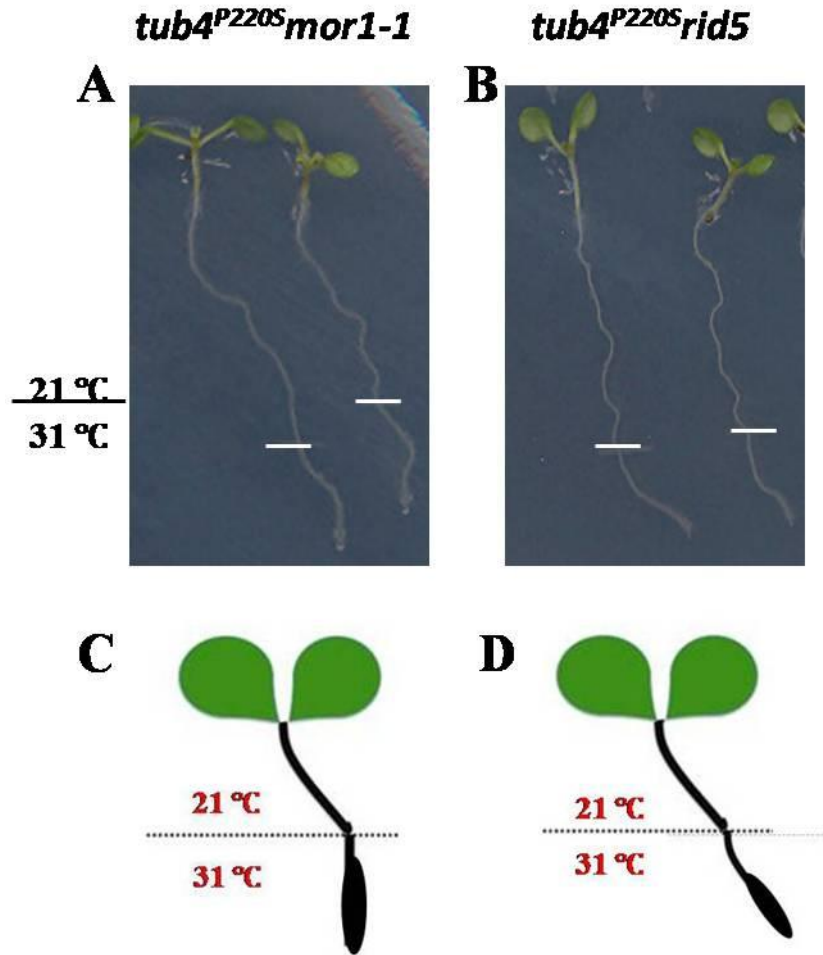
Figure 2- 5 Schematically illustrated phenotypes of double mutants of *tub4^{P220S}mor1-1*and *tub4^{P220S}rid5* after growing them at 21 ℃ for 7 days and at then at 31 ℃ for 2 days, showed in actual images (A. and B.) and schematic drawings (C. and D.). The white line indicated where temperature shift occurred. The difference between these two double mutants was occurred at 31 ℃, at which *tub4^{P220S}mor1-1*had swelling and straight growth roots (A. and C.) whereas *tub4^{P220S}rid5* showed right-handed twisting and radial swelling (B. and D.).

2.3.5 Microtubule dynamics in *tub4^{P220S}mor1-1* and *tub4^{P220S}rid5* double mutants

Because the combination of *tub4^{P220S}* with *mor1-1* resulted in a different phenotype from the *tub4^{P220S}rid5* double mutant at 31 °C, it is possible that these differences will be reflected in the microtubule dynamics and organization in these two double mutants.

In order to track microtubule behaviours, the microtubule reporter construct, *Pro35S*::GFP-TUB, was introgressed by cross-pollination into selected double mutants and the homozygous double mutants with GFP reporter and related controls were segregated and genotyped from the F2 generation. Microtubules were observed in cotyledon pavement cells rather than roots for several reasons. First, cotyledons are also affected by the *tubulin* and *mor1* mutations, as indicated by petiole twisting. Second, measuring microtubule dynamics is relatively easy in pavement cells owing to the generally mixed orientation pattern, which enables the free ends of microtubules to be observed unequivocally. Third, the GFP-TUB reporter, which when expressed generates no twisting phenotypes, does not label microtubules in root cells. In contrast, the GFP-MBD microtubule reporter, which can be used to image microtubules in root cells, generates a right-handed twisting phenotype so is inappropriate for investigating microtubule dynamics in mutants that are undergoing organ twisting. To ensure that the data collected were reproducible, for every mutant at each temperature, approximately 15 movies were acquired from 1 or 2 cells each from 10 cotyledons, with a minimum length of 3 minutes.

Representative images of the seedling phenotypes and microtubule organization in cotyledon epidermal cells are shown in Figure 2-6. In the single *mor1-1* mutant at restrictive temperature, shorter microtubules were observed (Figure 2- 6 D), compared with that at 21 °C (Figure 2- 6 C) and wild type at both temperatures (Figure 2- 6 A. and B). Microtubules in the *rid5* allele appeared to be overall shorter and less coordinated into arrays (Figure 2- 6 F). In the *tub4^{P220S}* mutant, microtubule length did not appear to be affected at 21 °C (Figure 2- 6 G), but at 31 °C, the microtubules were organized into parallel arrays in contrast to the mixed orientation typical at the outer face of pavement cells (Figure 2- 6 H). In the *tub4^{P220S}mor1-1* double mutant, microtubule organization

was similar to that of the wild type at 21 ℃ (Figure 2- 6 I) but microtubules became short at 31 ℃ (Figure 2- 6 J). Similar microtubule organization to the $tub4^{P220S}mor1\text{-}1$ double mutant was observed in the $tub4^{P220S}rid5$ double mutant at both temperatures (Figure 2- 6 K. and L).
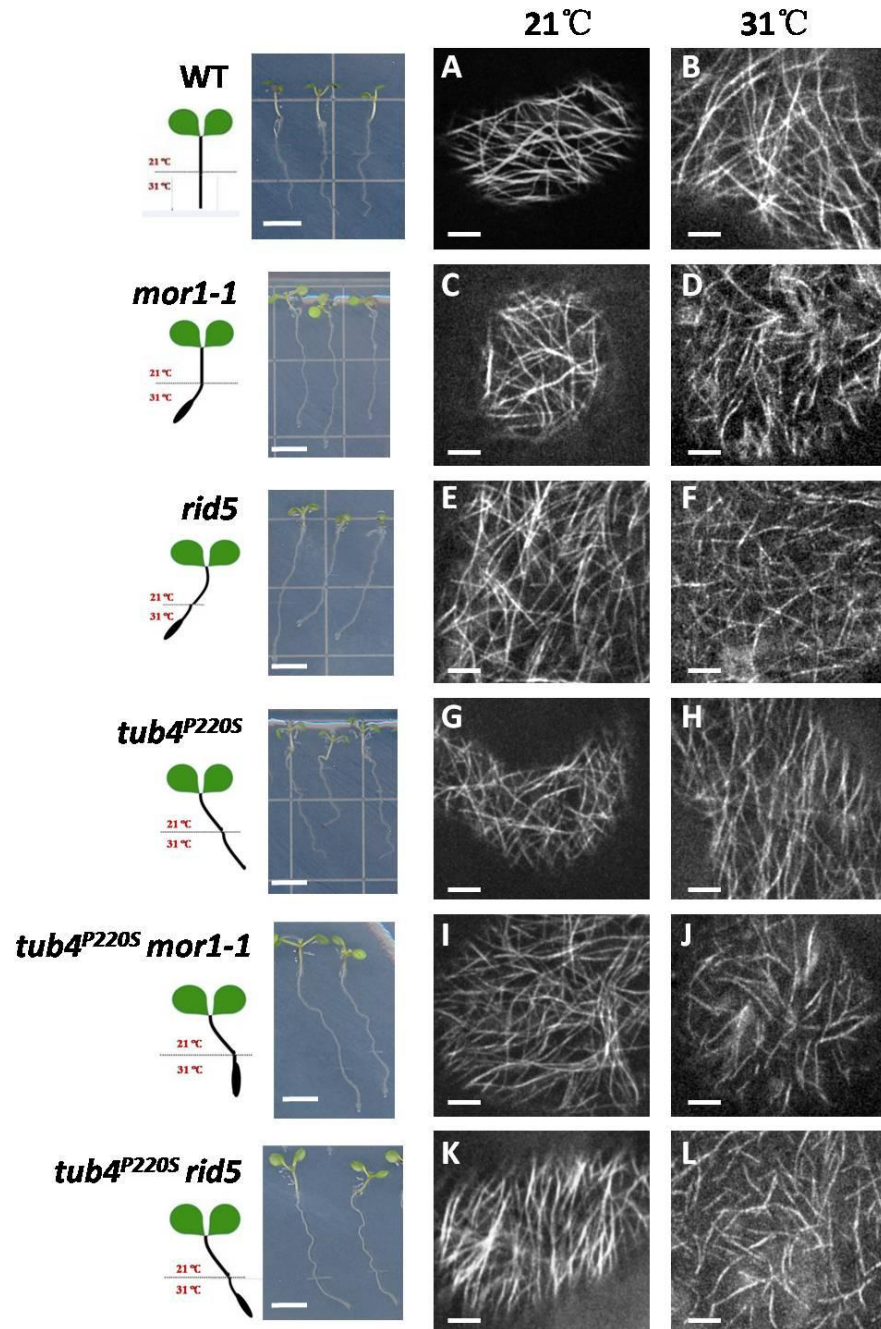
Figure 2- 6 Microtubule organization of *tub4*^*P220S*^*mor1-1* **and** *tub4*^*P220S*^*rid5* **double mutants and related controls. For each genotype, the mutant root growth phenotypes at 21 ℃ and 31 ℃ are illustrated schematically in the left panel, and representative images of actual seedlings grown at for 7 days at 21 ℃ followed by 2 days at 31 ℃ are shown in the second panel from the left (Scale bar=0.5mm). Cortical microtubule organization patterns in cotyledon pavement cells are shown for each genotype at 21 ℃ (A, C, E, G, I, K) and 31 ℃ (B, D, F, H, J, L). Scale bar = 5 μm.**

Although comparisons of microtubule organization patterns in the two double mutants did not reveal any clear differences that would explain the allele-specific growth phenotypes, qualitative analysis of microtubule dynamics indicated that there were some striking differences. According to these assays, microtubule dynamics increased in wild-type cells by shifting the temperature from 21 ℃ to 31 ℃, while in *mor1-1* mutants, dynamics was greatly reduced (Figure 2- 7 A. B. C. and D), in agreement with published data (Kawamura and Wasteneys, 2008). In *rid5* at 21 ℃, microtubules grew more slowly than microtubules in wild-type cells at the same temperature (Figure 2- 7 C). At 31 ℃, microtubule growth was dramatically reduced; there was no detectable change in microtubule lengths over a 50 second period (Figure 2- 7 D), and very little change over a 3 minutes period (data not shown). In the *tub4*^{P220S} mutant, growth and shrinkage of microtubules at 21 ℃ were also slower than in wild-type cells (Figure 2- 7 G) and it was difficult to detect any dynamics at 31 ℃ over a 3 minute period (Figure 2- 7 H).

WT
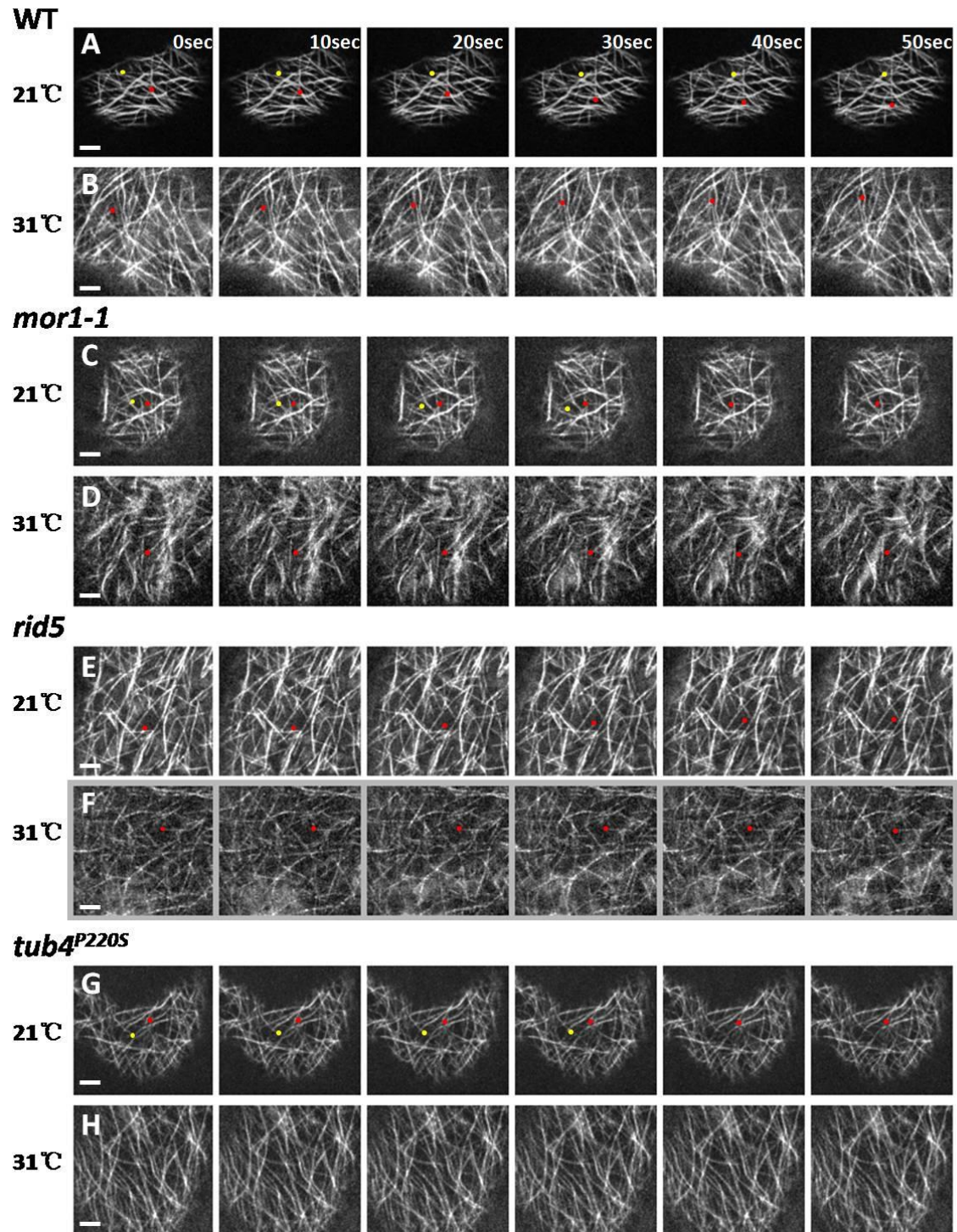
Figure 2- 7 Comparison of microtubule dynamics in wild type and single mutants at two different temperatures. Red dots show growing microtubules, and yellow ones show shrinking microtubules. Frames are shown for images taken at 10 sec intervals. Scale bar=5 μm.

In the *tub4^{P220S}mor1-1* double mutant, microtubule dynamics were similar to those observed in *tub4^{P220S}* single mutant at 21 ℃ (Figure 2- 8 A). At 31 ℃, microtubules resembled the *mor1-1* phenotype in being very short but like the *tub4^{P220S}* phenotype, these short microtubules became hyperstabilized (Figure 2- 8 B) and changes in lengths could only be observed over time lapses greater than 3 minutes (data not shown). In the *tub4^{P220S}rid5* double mutant, most microtubules were stabilized at 21 ℃, with very little change in microtubule lengths detected over a 1 minute period (Figure 2- 8 C). At 31 ℃, the short microtubules displayed no dynamic events over the 3 minute time course (Figure 2- 8 D).

tub4^{P220S} mor1-1
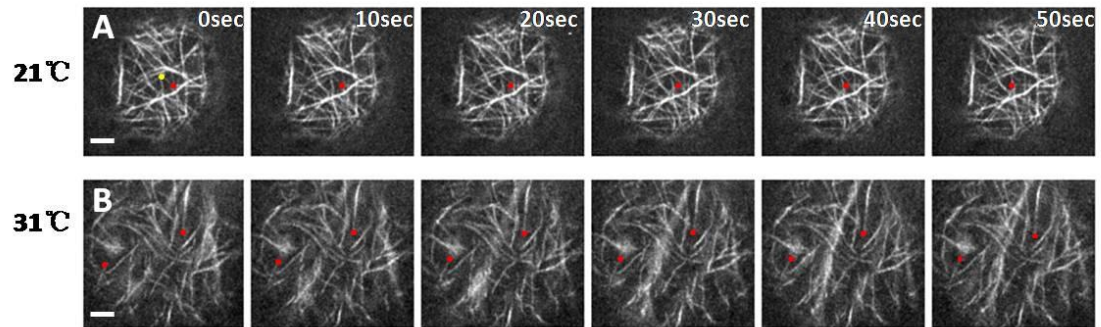
tub4^{P220S} rid5
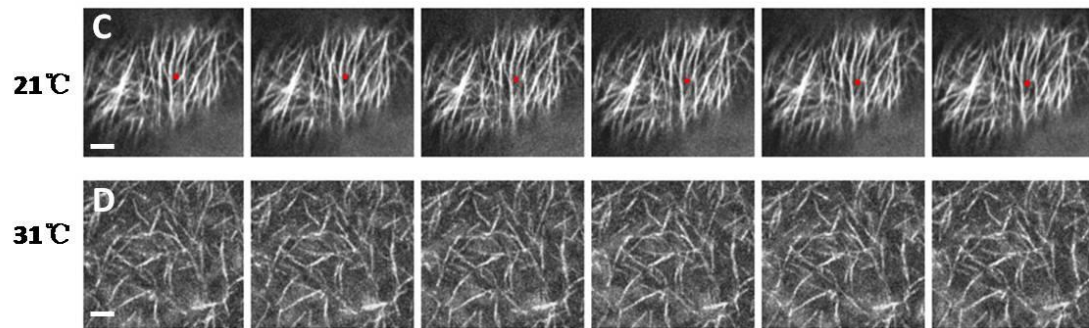
Figure 2- 8 Comparison of microtubule dynamics in *tub4^{P220S}mor1-1* and *tub4^{P220S}rid5* double mutants at 21 ℃ and 31 ℃. Red dots indicate the growing plus ends of microtubules, and yellow ones show shrinking microtubules. Scale bar=5 μm.

2.4 Discussion

In this study, a genetic interaction assay was carried out with three *mor1* mutants and sixteen *tubulin* mutants to map the possible MOR1-tubulin interaction domains in TOG1. The phenotypes generated from various *tubulin- mor1* combinations indicated the regions in tubulin dimer where 5 *tubulin* mutations located, showing non-additive or allele specific phenotype in *tubulin-mor1-1* and *tubulin-rid5*.

2.4.1 Allele-specific double mutant phenotypes indicate possible interaction domains in TOG1

The organ twisting phenotypes of all the 48 double mutants at two different temperatures were documented and non-additive or allele-specific phenotypes were observed in some *mor1-tubulin double* mutant combinations. Strikingly, the five *tubulin* mutations, all of them showed non-additive phenotypes when combined with *mor1-1* or *rid5*, were found in the region of interface between the β-tubulin at the plus end of the microtubule and the α-tubulin of the incoming dimer (Figure 2- 9). It is possible that these particular *tubulin* mutations alter microtubule dynamics on their own but in combination with the abnormal MOR1 protein, cause stronger effect leading to peculiar root growth phenotypes.

Among these five mutations, *tua5*^{D251N} is located in the GTPase activating domain and has been reported to have left-handed oblique microtubule arrays and suppressed microtubule dynamics (Ishida et al., 2007b). When this mutation combined with *mor1*, *tua5*^{D251N}*mor1-1* was seedling-lethal whereas *tua5*^{D251N}*mor1-2* and *tua5*^{D251N}*rid5* double mutants were healthy throughout development. That suggests that the interaction of MOR1 and TUA5 is more severely affected when the *tua5*^{D251N} mutation is combined with the *mor1-1* mutant, than it is with *mor1-2* or *rid5* positions on MOR1. The seedling lethality in the *tua5*^{D251N}*mor1-1* double mutant is probably caused by strongly suppressed GTPase activity, which could generate the microtubules unable to disassemble. To test this idea, further microtubule observation in early seedling stage of *tua5*^{D251N}*mor1-1* will be informative.
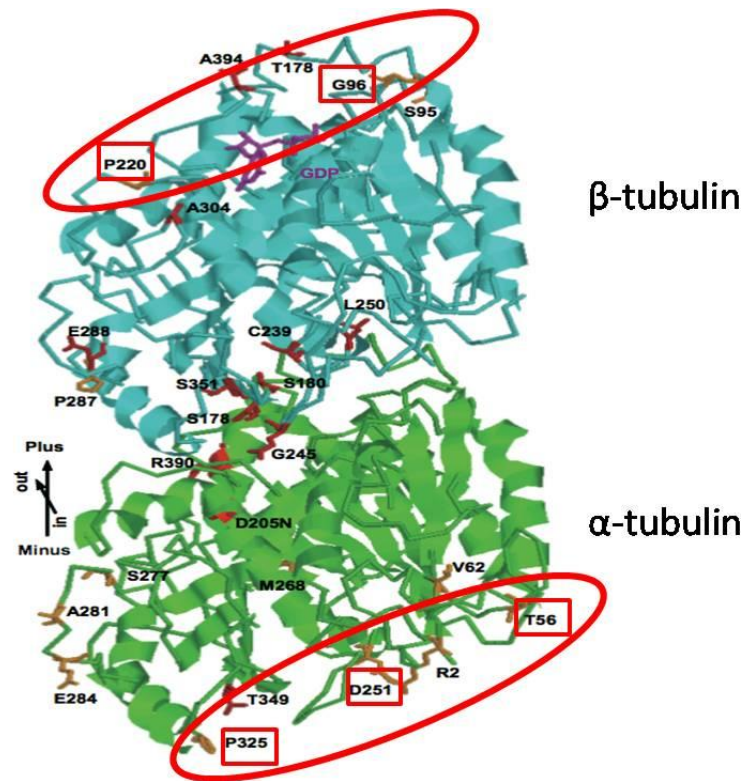
Figure 2- 9 Regions in the tubulin dimer where double mutants of *tubulin-mor1* had significant phenotypes. The five *tubulin* mutations, labelled with red boxes, generated non-additive or allele-specific phenotypes when combined with *mor1-1* or *rid5* and were found in the region of interface between the β-tubulin at the plus end of the microtubule and the α-tubulin of the incoming dimer, as red circles shown.

2.4.2 Microtubule dynamics were suppressed in *tub4*^{P220S}*mor1-1* and *tub4*^{P220S}*rid5* double mutants

tub4^{P220S}, located at the exposed β-tubulin of microtubule plus ends, showed distinguishable different root twisting directions in *tub4*^{P220S}*mor1-1* and *tub4*^{P220S}*rid5* double mutants at 31 ℃. These allele-specific phenotypes are probably related with that in TOG1, *mor1-1* is located in the fifth HR while *rid5* is in the third HR, leading the physical interaction differences with β-tubulin and altering microtubule dynamics in different levels. To detect whether the microtubule behaviours are different in these two double mutants, live cell imaging from GFP-fused cells were analyzed.

It was presented before that during a 3 minute time series, growing microtubules were detectable in *tub4*^{P220S}*mor1-1* but hard to track in *tub4*^{P220S}*rid5* at 21 ℃. At 31 ℃, the growth of microtubules was very slow in *tub4*^{P220S}*mor1-1* whereas in *tub4*^{P220S}*rid5*the movement was rare. The stronger microtubule dynamic defects observed at 31 ℃ partly resemble the hyperstabilized microtubules in *tub4*^{P220S} at 31 ℃. However, due to the large sample size and time limitation, no quantitative dynamic data was presented in this study, resulting in no indubitable interaction model can be established at this stage.

2.5 Future directions

This genetic interaction assay results provides possible insights into the function of MOR1 motifs that interact with specific tubulin binding sites. Although there is no evidence listed for the identification of protein-protein interaction sites, the genetic strategy preformed in this study could be useful for specifically testing the prediction that the site on the MOR1 protein at which the *mor1-1* and *mor1-2* mutations occur interacts with β-tubulin.

To get more informative results from $tub4^{P220S}mor1-1$ and $tub4^{P220S}rid5$ double mutants, microtubule dynamics tracking by *Pro35S*::EB1-GFP or *ProEB1*::EB1-GFP will be useful to get more quantitative data, especially at 31 ℃, at which the microtubule dynamics were hard to track by *Pro35S*::GFP-TUB6.

At the same time, biochemical studies of the interaction between the MOR1 protein with induced point mutations and free tubulin dimers will be one effective way to develop and refine interaction models, as described in Chapter 4.

CHAPTER 3: MOR1 Interactions with Tubulin via the fifth TOG Domain

3.1 Introduction

In Chapter 2, the interaction between tubulin dimers and the first TOG domain (TOG1A) of the MOR1 protein was investigated using a genetic strategy. Three alleles of *MOR1* with point mutations in TOG1A causing left-handed twisting were each crossed to sixteen *tubulin* mutants that generate right-handed twisting. In this Chapter I characterized the phenotype of a novel point mutation in the TOG domain closest to the C-terminus, TOG3.

3.1.1 TILLING project

TILLING (Targeted Induced Local Lesions IN Genomes) is a reverse genetics method in which point mutations in specifically targeted genes or regions of genes can be identified (McCallum et al., 2000). Seeds are exposed to the chemical mutagen EMS in order to cause random point mutations throughout the genome. DNA from M2 plants is then pooled for PCR-based identification of the mutations, using specific primers to amplify the sequence of interest. The PCR products are heated and cooled to let wild type and mutant DNA strands form heterodimers, which can then be cleaved by CEL 1 endonuclease so that lines with point mutations in sequence of interest can be identified by the separation of the two resulting fragments of DNA when run on a gel. Several series of TILLING lines have been generated for the *Arabidopsis* TILLING Project (ATP), as a mean to identify point mutations in known genes of interest. This high-throughput and low cost method can provide more insights into protein function than can be determined by other reverse genetics approaches such as T-DNA insertion mutagenesis (Till et al., 2003).

3.1.2 Previous results of MOR1 TILLING alleles

Using this powerful method, a series of new *mor1* mutations has been identified in the Wasteneys Lab, to add to the previously described *mor1-1, mor1-2 and rid5* alleles, which were identified in forward genetics screens of EMS-mutagenized seedlings. The collection now includes 3 point mutations in TOG2B and 5 in TOG3 (Figure 3- 1). Preliminary analysis showed that at least one of the mutants identified by TILLING caused right-handed root twisting (*mor1-11*, Figure 3- 2) under the normal growth conditions, in contrast to the left-handed twisting observed in *mor1-1*, *mor1-2* and *rid5* alleles. In addition, *mor1-11* M3 generation plants, when grown on soil, are dwarf, have curved leaves and tiny flower buds.
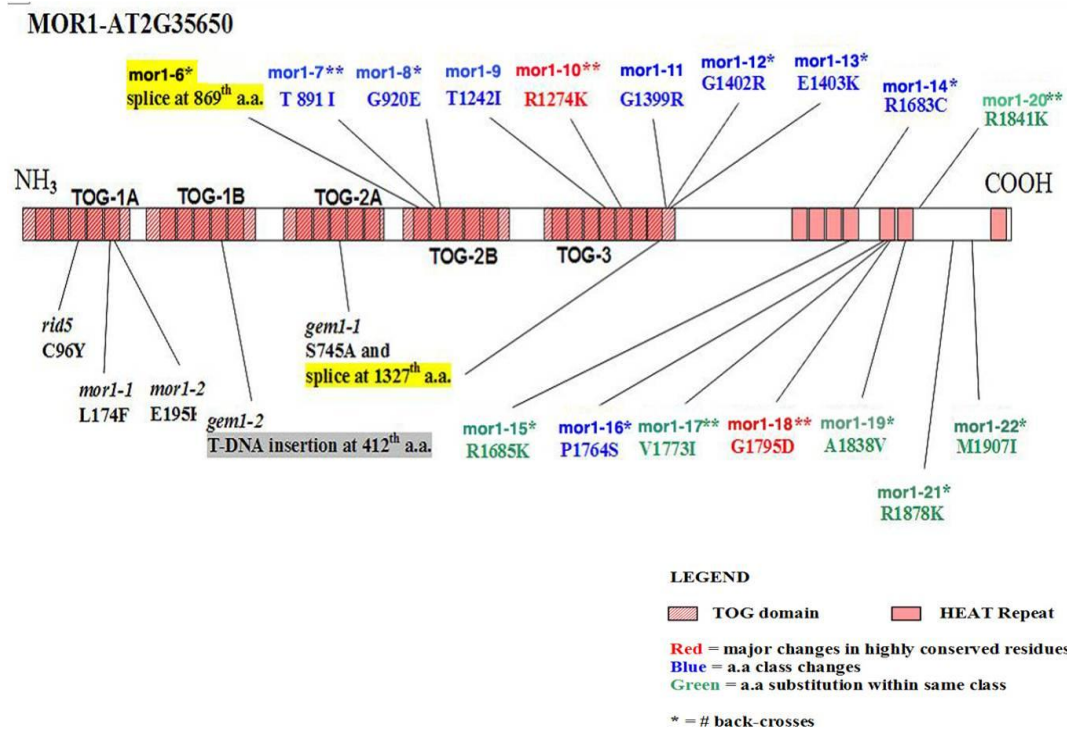
Figure 3- 1 Mutations in the MOR1 protein. Besides *mor1-1*, *mor1-2* and *rid5* located in the first TOG domain, and the homozygous-lethal *gem1-1* and *gem1-2* alleles that most likely generated truncated proteins, the TILLING method identified additional *mor1* alleles in other TOG domains.
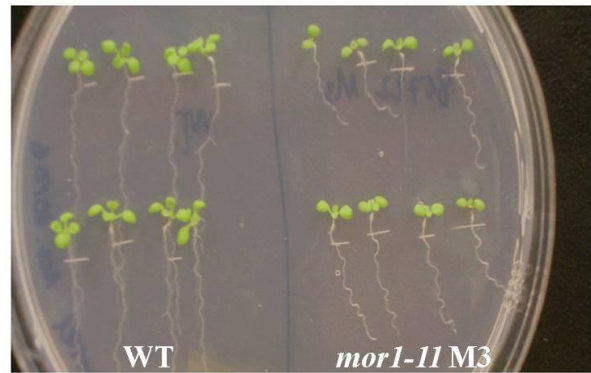
Figure 3- 2 *mor1-11* **M3 generation seedlings show right-handed twisting roots at 21 ℃. (From David Chen)**

3.1.3 Microtubule-targeted drugs

There are various microtubule drugs that can alter microtubule dynamics, either stabilizing or destabilizing microtubules, such as propyzamide, oryzalin and taxol. It had indicated that low effective concentrations of propyzamide caused wild type seedlings form left-handed helical root growth (Furutani et al., 2000), and the microtubules were destabilized and less dynamic (Nakamura et al., 2004). The alpha tubulin mutants *lefty1* and *lefty2*, which showed left-handed twisting caused by point mutations, had increased sensitivity to microtubule-targeted drugs, showing depolymerized and disrupted microtubules (Thitamadee et al., 2002). The hypersensitive responses to microtubule-specific drugs were also observed in two alleles from microtubule-associate proteins, *spr1* and *mor1-1* (Furutani et al., 2000; Collings et al., 2006).

Among these three microtubule drugs, both propyzamide and taxol at low concentrations can cause left-handed twisting of roots and petioles in wild-type seedlings (Furutani et al., 2000; Nakamura et al., 2004). However, these two drugs have opposite effects on microtubule dynamics. Propyzamide is a microtubule-destabilizing drug whereas taxol can promote microtubule polymerization and stabilization. It is already published that taxol can bind to β-tubulin in intact microtubules (Nogales et al., 1995). In contrast, the mechanism by which propyzamide binds to microtubules and/or free tubulin to affect microtubule dynamics is still unknown.

Another microtubule-targeting drug, oryzalin, at low concentrations reduces microtubule assembly rates, resulting in shorter roots (Nakamura et al., 2004).

The subject of this chapter is to explore the nature of a novel point mutation in the *MOR1* gene, which causes a propyzamide-dependent phenotype. The analysis will include genetic interactions with a tubulin mutation generating a similar propyzamide-specific phenotype.

3.2 Materials and methods

3.2.1 Plant materials and growth conditions

In this study, one allele from identified in the MOR1 TILLING project, designated *mor1-11* was backcrossed six times and then used for further analysis. The wild-type control line was segregated from the same F2 line to ensure the control and mutants have the same genetic background.

Another plant material, *tua6*^{C213Y} (Ishida and Hashimoto, 2007), was provided by the Hashimoto lab at the Nara Institute of Science and Technology, Japan.

Details can be found in Chapter 2 about regular planting and growth conditions. Generally, seedlings were planted and placed at 4 ℃ for 2 days, then moved to 21 ℃. For the higher temperature treatments, seedlings were grown at 21 ℃ for 5 to 7 days, and then moved to 31 ℃ for 2 days.

3.2.2 Backcrossing and genotyping

EMS-mutagenized *mor1-11* was backcrossed into Col-0 background to remove other mutations. Plants used for crossing were around 1 month old. (All the backcross information can be found in Cross Records for the Wasteneys Lab).

To genotype the plants carrying *mor1-11* mutations, a SNP primer set was designed to specific identify the existence of mutations. Several primer design methods were used and a series of genotyping primers were designed for several of the MOR1 TILLING alleles. For the detailed design methods and PCR procedure, see Appendix 2.

3.2.3 Drug screening

All the drug stock solutions were prepared in the solvent dimethysulfoxide (DMSO). The stock concentration was 10mM for all the three drugs. The stock solutions were added according to the final concentrations to the autoclaved Hoagland's medium (with 1.2% (w/v) Bacto Agar) just before pouring plates. DMSO was added to the liquid medium so that the final DMSO concentration was the same for all drug concentrations and control treatments.

Seeds were sterilized and planted on plates over a wide range of drugs concentrations. For each treatment, approximately 400 *mor1-11* seeds, 100 wild-type seeds and 50 *tua6*^{C213Y} seeds were used.

All the plates were observed and images recorded after 7 days treatment. Root twisting angles and root lengths were measured from the images using ImageJ software.

3.2.4 Whole root immunofluorescence

To do the immunolabelling on whole roots, 7-day old seedlings were fixed in small Petri dishes with 4% formaldehyde (v/v), 0.1% glutaraldehyde made up in 1x PMEG (25mM PIPES, 0.5mM MgSO$_4$, 2.5mM EGTA and 2% glycerol, pH6.9) for 1 hour. Then PBS containing 0.05% Triton X-100 was used to rinse three times, for 5 min. After this, whole seedlings were transferred to digestion solution (0.1% pectolyase, 0.05% cellulase, 0.5% Triton X-100, dissolved in PME buffer) for 30 min, and then were rinsed again twice with PME for 10 min. The samples were then treated for 1 hour in 3%BSA/PBS to block non-specific binding. To remove the lipids from the samples for better antibody diffusion, seedlings were detergent extracted in PME containing 0.5% Triton for 30 min, then rinsed 3 times for 5 min each time in PBS (with no Triton X-100).

For immunolabelling, DM1A (FITC-conjugated anti-tubulin) was used at a 1:1000 dilution in 3%BSA/PBS for 1hour. If needed, this step can be done at 30 ℃ incubation. Finally, the seedlings were rinsed in PBS (no Triton X-100) 3 times for 10 min. During

the rinsing, slides used for mounting were coated twice with poly-L-Lysine (Sigma 1524, at 1 or 0.5 mg/ml in distilled water). To mounting samples, 20 μl Citifluor (#AF1, Electron Microscope Science) was applied to the centre of each slide, then roots were cut off 2cm above the tip and placed in the mounting medium. Cover slips were then applied, sealed with nail polish, and the samples stored at 4 °C.

3.2.5 Confocal laser scanning microscopy

To study cortical microtubule organization in *Arabidopsis* root, images were taken in the late elongation zone, where cell file twisting was observed (Sugimoto et al., 2000). All the immunolabelled roots were observed using an upright AxioImager M1 microscopy (Carl Zeiss, Germany), housing a Zeiss Pascal Excite two channel scan head. A 63×oil-immersion lens (Zeiss) was used to collect images using fluorescence generated by the 488nm laser, and 488nm to 505nm emission filter.

ImageJ software was used for microtubule array measurements. Images were rotated to place the root vertically, with the tip at the bottom. The orientation of microtubules was measured relative to the cell long axis, from 10 randomly picked microtubules per cell, 4 to 5 cells per root, 3 to 4 roots per treatment.

3.2.6 GFP reporter detection in mutants

To quantify microtubule dynamics in *mor1-11*, a GFP reporter protein is used to track the microtubules. A GFP-β-tubulin reporter line, *Pro35S*::GFP-TUB (Nakamura et al., 2004), was chosen because this line has no root twisting phenotype. Wild-type plants homozygous for the GFP-TUB transgene were crossed with homozygous *mor1-11* plants. To detect GFP in seedlings of the F1 or F2 generation, seedlings were screened by stereo-fluorescence. The genotypes of the putative double homozygous lines were subsequently confirmed by PCR-based genotyping.

3.2.7 Live cell imaging of GFP-TUB6 plants

Although *Pro35S*::GFP-TUB has high expression levels in *Arabidopsis*, the weakness of this reporter line is that the fluorescent signals in roost are very weak. Since *mor1-11* also has a synchronous twisting phenotype in the petioles of leaves and hypocotyls on propyzamide, images were captured in 7 days old cotyledons.

All details of sample preparation, spinning disc confocal microscopy observation and data analysis can be found in Chapter 2.

To measure microtubule velocity, for every sample line, 3 to 5 microtubules per cell were tracked from 3 to 5 cells, 10 cotyledons. The velocity data was analyzed using Microsoft Excel. Growth rate was presented as positive value while shrinkage rate was negative value.

3.3 Results

3.3.1 *mor1-11*, one of the TILLING alleles, has different phenotype before and after backcrosses

Since all TILLING alleles were generated by EMS mutagenesis, which causes numerous C/G to A/T point mutations, it was necessary to remove undesired non-specific background mutations by back-crossing the mutants with the Col-0 background several times. Good molecular markers that confirm the presence of specific point mutations in phenotype-free heterozygotes can dramatically reduce backcrossing times by eliminating the needs to carry out F2 segregations after each backcross. Such markers also enhance double mutant segregation analysis by distinguishing between heterozygous and homozygotes of one of the parent mutations. A SNP (Single Nucleotide Polymorphism) marker was designed in order to identify the presence of the *mor1-11* mutation at each round of backcrossing. Six sequential backcrosses were conducted in *mor1-11* within two years using the quick and effective SNP primer sets for genotyping.

In the M3 generation, *mor1-11* mutants had a pronounced right-handed root twisting phenotype on the regular Hoagland's medium. This right-handed twisting results in a sustained leftward bending of the root as it grows downward on a steeply inclined hard agar surface so is referred to hereafter as left skewing, even though the root appears to be growing towards the right side of the plate when viewed from the upper side of the vertically held Petri dish. However, after several backcrosses, the twisting phenotype was lost (Figure 3- 3). After the fifth backcrossing homozygous *mor1-11* plants displayed no detectable right-handed twisting (left root skewing) under regular growth conditions. The plants on the soil had the similar sizes and growth rates as the wild type.
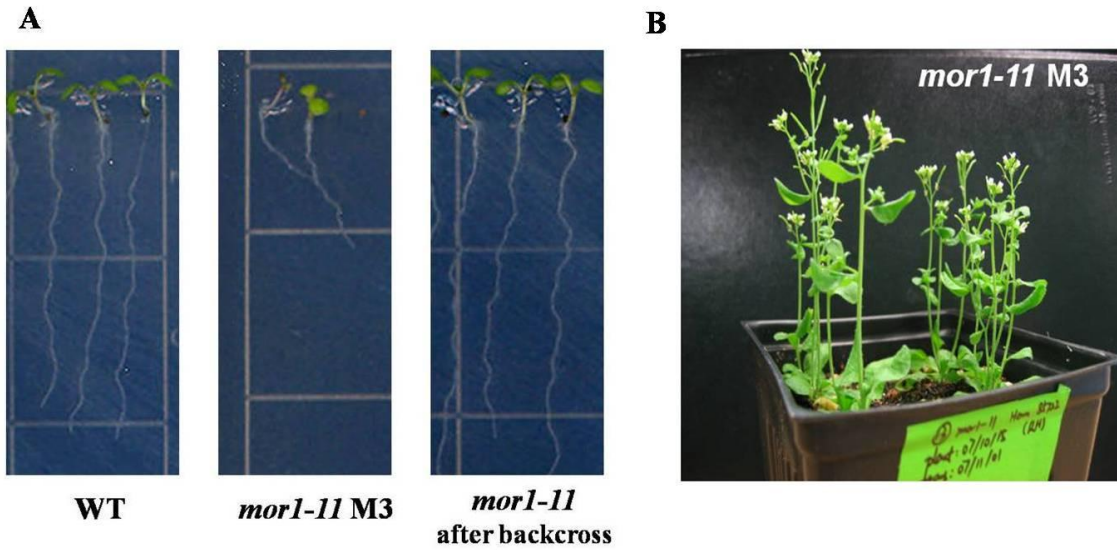
Figure 3- 3 **(A) In the M3 generation, *mor1-11* showed right-handed twisting, evident by left root skewing (the root grows to the right side of the plate when viewed from the upper side as a result of a sustained leftward bend). In homozygous *mor1-11* seedlings segregating after six backcrosses to the Col wild type, there is no organ twisting when grown on regular Hoagland's medium. (B) When grown on soil, *mor1-11* M3 seedlings were dwarf.**

3.3.2 *mor1-11* has a cryptic propyzamide-dependent, semi-dominant phenotype

Loss of the right-handed twisting phenotype after backcrossing confirmed that the *mor1-11* mutation on its own does not lead to right-handed twisting. It is therefore plausible that the *mor1-11* M3 phenotype was either caused entirely by an independent mutation or by one or more independent mutations working in combination with *mor1-11*. Examination of F2 segregating lines after the second and subsequent backcrosses demonstrated that the frequency of right-handed twisting was reduced gradually over several subsequent generations, indicating that the phenotype was dependent on the presence of the *mor1-11* mutation (data not shown). We therefore hypothesized that the *mor1-11* mutation may cause a cryptic phenotype that is only manifested under certain conditions, and tested this hypothesis by treatment with low concentrations of microtubule-targeted drugs. There are many examples in the literature of mutants with altered sensitivity or responses to microtubule-targeted drugs when applied at low concentrations. The conditional *mor1-1* and *mor1-2* mutants, for example, are hypersensitive to various microtubule-targeted drugs (Collings et al., 2006). It has also been reported that a C to Y substitution at amino acid 213 of α-tubulin (*tua6^{C213Y}*), causes right-handed root twisting when treated with low concentration of propyzamide, a microtubule-destabilizing drug that causes left-handed twisting responses in wild-type plants (Ishida and Hashimoto, 2007). In the absence of this drug, this mutant was indistinguishable from wild type.

To determine whether isogenic lines of *mor1-11* have any conditional phenotype under treatment with drugs that disrupt microtubule functions, with the effects of three different microtubule-targeted drugs – propyzamide, oryzalin and taxol were tested on *mor1-11* mutants.

Preliminary Assays

Initially, two drugs – propyzamide and oryzalin were tested. 3μM propyzamide was found to cause wild-type seedlings to undergo significant left-handed twisting, as previously reported (Nakamura et al., 2004), and 150nM oryzalin reduced wild-type root elongation rates. These oryzalin and propyzamide concentrations were therefore used to determine whether *mor1-11* has any altered sensitivity or response. The F2 generation from the fifth backcross was used for the drug assay, which was conducted on azygous, heterozygous and homozygous *mor1-11* seedlings at day 7 post germination.

Among 225 F2 seedlings, the 3μM propyzamide treatment had no effect on approximately one quarter of them (62 seedlings), caused another quarter of the seedlings to undergo strong left skewing (61 seedlings), and the remaining half of the seedlings' roots to undergo a weaker left skewing (102 seedlings). These data approximately fit a 1:2:1 segregation ratio expected for a semi-dominant phenotype (Figure 3- 4) and also fit Chi-square analysis. Close inspection of the roots indicated that the left skewing corresponded with right-handed twisting, which is opposite to the usual left-handed twisting induced by propyzamide in wild-type roots. PCR-based genotyping confirmed that the stronger phenotypes occurred exclusively in *mor1-11* homozygotes and that the heterozygous segregants had the intermediate response. The skewing angles of wild type, homozygous *mor1-11*, F1 seedlings and F2 seedlings generated from 5th backcross were measured. The F2 seedlings had a wide range of skewing angles, which corresponded with the angles from other three genotypes. This skewing angle analysis also proved *mor1-11*'s semi-dominant response on 3μM propyzamide (Figure 3- 5). Taken together, these data indicate that *mor1-11* has a cryptic semi-dominant phenotype that causes root twisting of opposite handedness under low concentrations of propyzamide.

In contrast, *mor1-11* homozygotes and heterozygotes responded to 150nM oryzalin treatment in the same manner as the wild type, with reduced root lengths.

From this preliminary drug test, we were able to conclude that *mor1-11* has a cryptic semi-dominant altered response to propyzamide phenotype. However, treatment with just

two drugs at a narrow concentration range is insufficient to assess *mor1-11*'s phenotype. To determine *mor1-11*'s microtubule behaviour, a larger scale drug screening assay was needed utilizing different microtubule-specific drugs at a range of concentrations. A more extensive growth assay was therefore conducted using propyzamide, oryzalin and taxol over a wide range of concentrations.
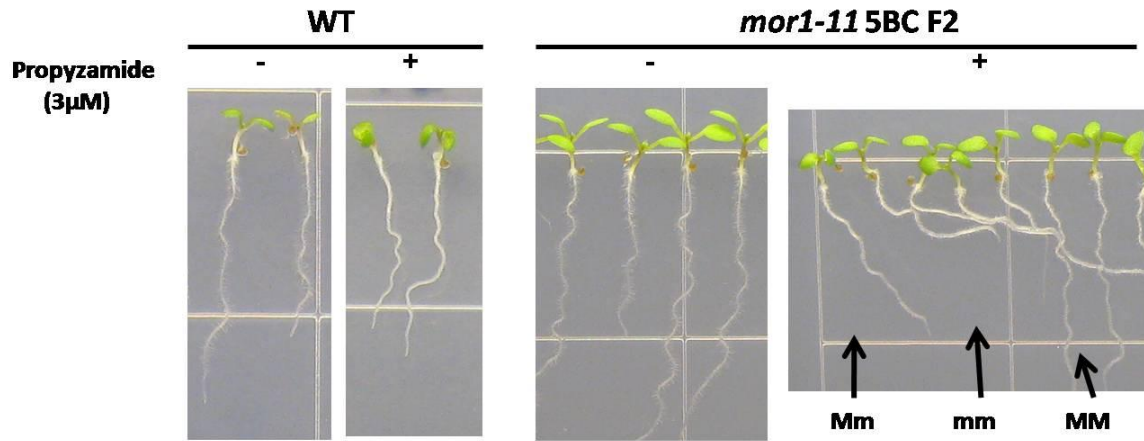
Figure 3- 4 In a *mor1-11* F2 generation after 5 backcrosses (5BC), treatment with 3 μM propyzamide causes approximately one quarter of the seedlings to undergo strong left root skewing relative to the growth direction (arrowed as mm), while another quarter showed straight root growth (arrowed as MM) and the rest had an intermediate left skewing phenotype (arrowed as Mm). This segregation approximated a 1:2:1 segregation ratio, confirmed by Chi-square analysis.
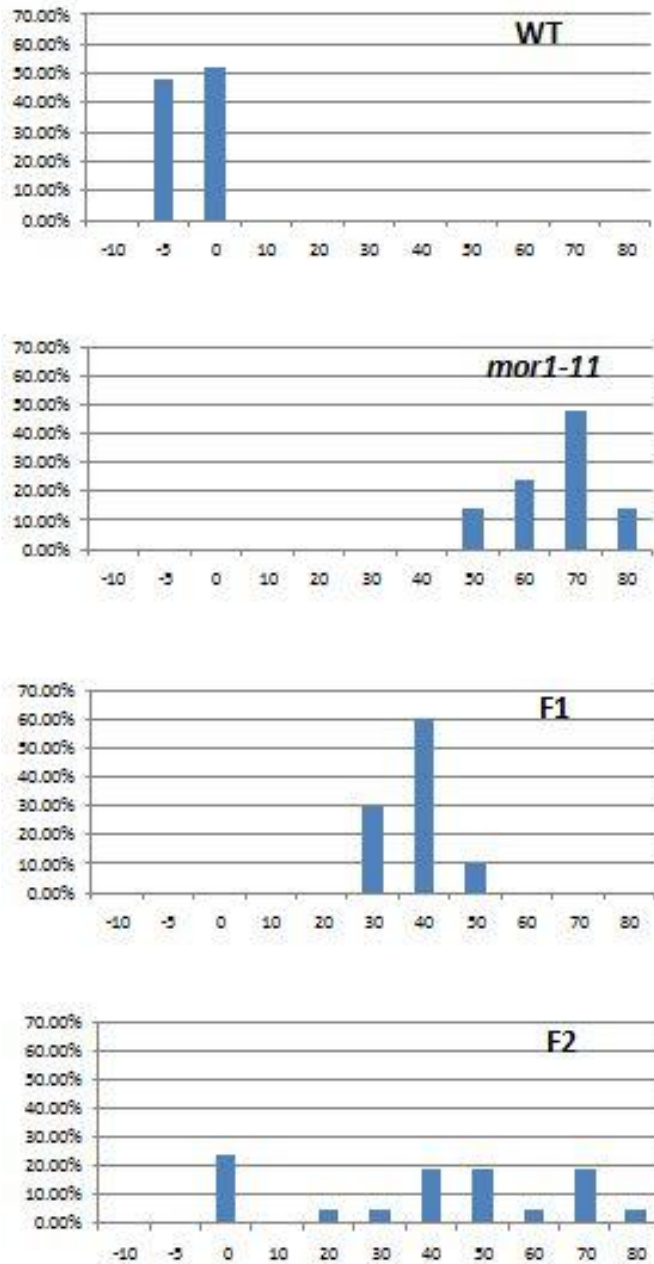
Figure 3- 5 *mor1-11* **has a semi-dominant left skewing phenotype when exposed to 3 μM propyzamide. The skewing angles were measured as they appear when viewed from the top side of Petri dishes from wild type, homozygous** *mor1-11***, F1 seedlings and F2 seedlings, all generated from 5th backcross. Approximately 50 seedlings were measured from F1 generation, while 100 seedlings for wild type, 100 for homozygous** *mor1-11* **and 100 for F2 generation.**

Propyzamide

We performed a larger scale treatment assay at four different concentrations (1μM, 2μM, 2.5μM and 3μM). Homozygous *mor1-11* seeds from a 5 times backcrossed line were used, while wild type and the *tua6^{C213Y}* mutant, which has previously been reported to also have a propyzamide-dependent right-handed root twisting phenotype (Ishida and Hashimoto, 2007), were used as controls. All the seeds from different genotypes were sterilized and planted on Hoagland's medium containing various DMSO or propyzamide concentrations. At 7 days, digital images of roots as well as cotyledon petioles were captured on a stereomicroscope for further analysis.

DMSO controls had no effect on the direction of root growth but propyzamide treatments showed genotype-specific response (Figure 3- 6). At 1μM propyzamide, there was no petiole twisting in any of the genotypes. Both mutants and the wild type grew toward the left side of the plates (right skewing), all at similar angles (Figure 3- 6 A; Figure 3- 7 A. and B). At 2μM propyzamide, wild type roots continued their right skewing and still showed no petiole twisting. However, both *tua6^{C213Y}* and *mor1-11* grew to the right side of plates (left skewing) and exhibited right-handed twisting in petioles (Figure 3- 6 B; Figure 3- 7 A. and B). At the higher propyzamide concentrations, mutants skewed at an even greater angle than after treatment with 2μM, while the wild-type roots continued right skewing (Figure 3- 6 C. and D; Figure 3- 7 A. and B). It is worth noting that the overall difference in twisting angle between *mor1-11* and wild type is greater (65 ° difference) at 3μM than at 2.5μM, at which there is only a 50 ° difference (Figure 3- 7 C).

However, propyzamide had no significant effects on root lengths in all wild type, *tua6^{C213Y}* and *mor1-11* (Figure 3- 8). Quantified roots length in wild type, *tua6^{C213Y}* and *mor1-11* showed similar reducing trends when propyzamide concentration increased, but there were no significant differences between wild type and mutants at every drug concentration.
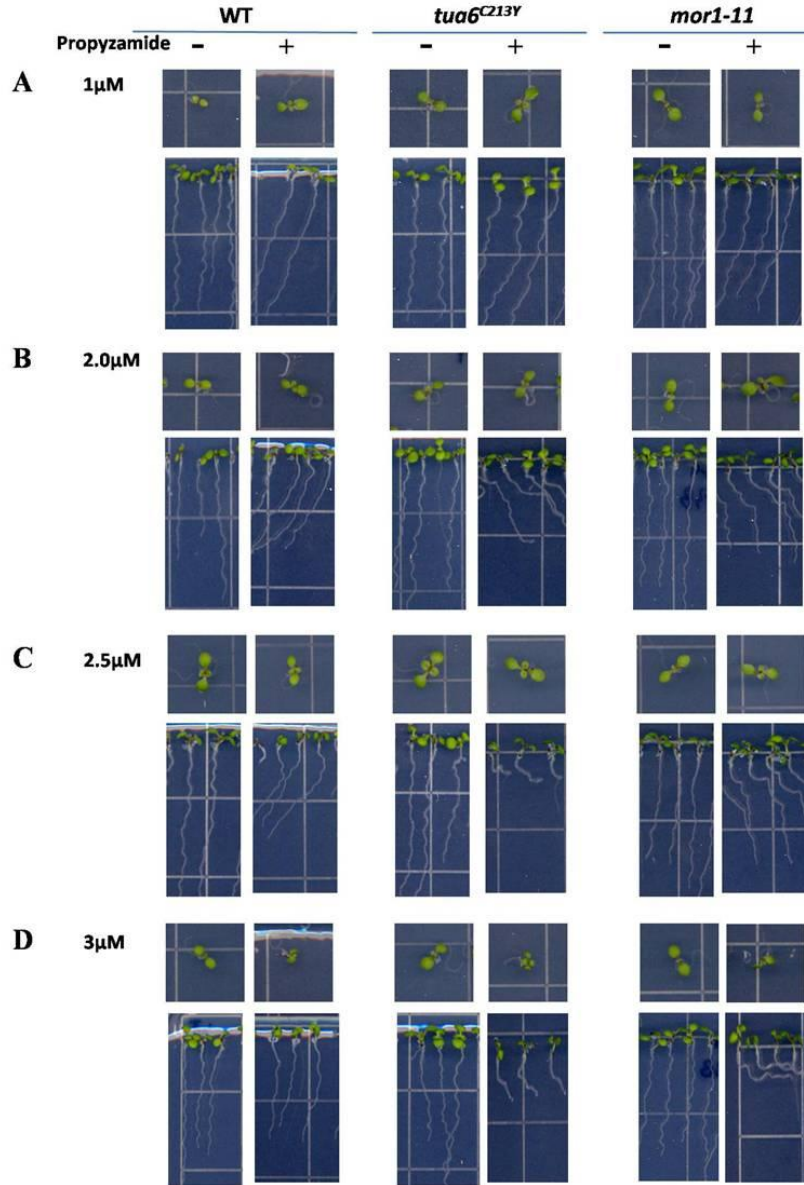
Figure 3- 6 Propyzamide dose responses on *mor1-11* and *tua6*^{C213Y}. A. At 1 μM propyzamide, the roots of wild type, *tua6*^{C213Y} and *mor1-11* all formed left-handed twisting and right skewing. B. Wild type kept the right skewing but both and *mor1-11* shifted to left skewing and showed right-handed twisting roots. C. At 2.5 μM propyzamide, *tua6*^{C213Y} had the stronger skewing angle than *mor1-11*, and wild type showed distinguish left-handed twisting. D. Compared with 2.5 μM, with 3 μM propyzamide treatment, the right skewing angle in wild-type roots was reduced, and left skewing in *mor1-11* was stronger than in *tua6*^{C213Y}. In all treatment, when no propyzamide applied, there was no root twisting effect on wild type, *tua6*^{C213Y} and *mor1-11*.
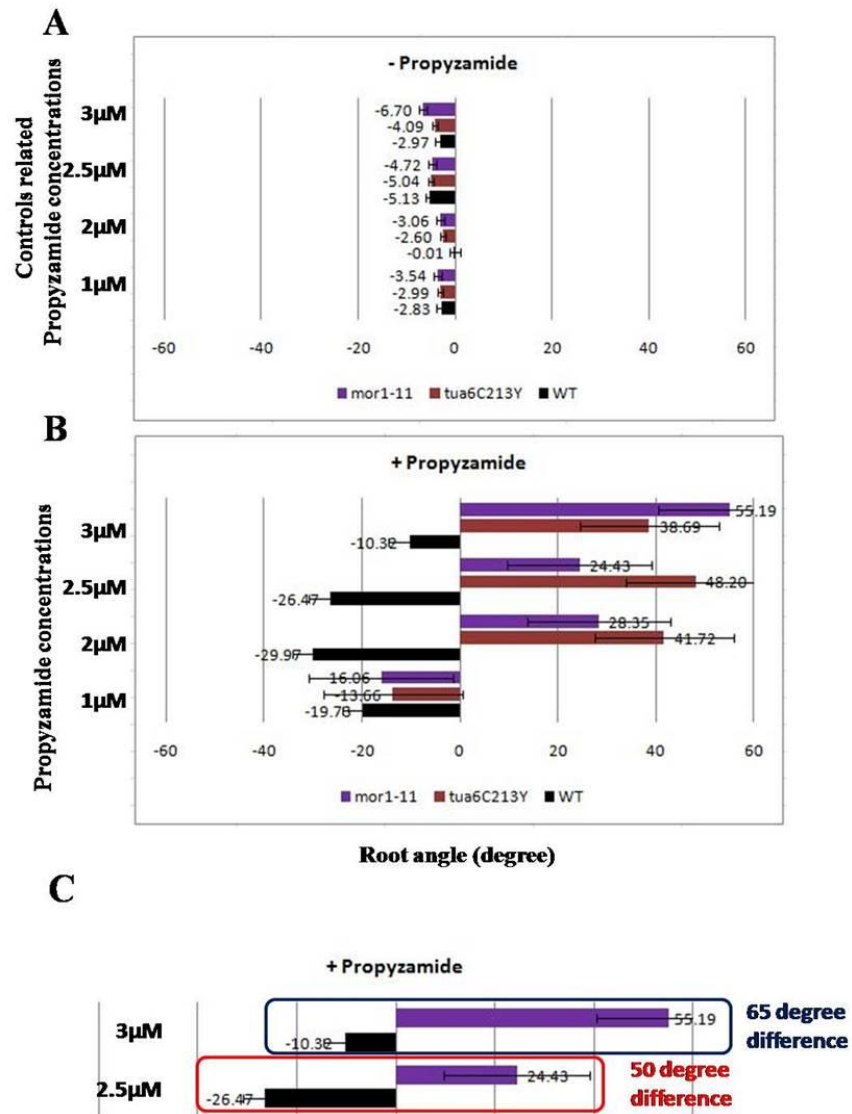
Figure 3- 7 Root skewing angles in wild type, $tua6^{C213Y}$ **and** $mor1-11$**with propyzamide treatments.**
Right skewing (left-handed twisting) was presented as negative values whereas left skewing (right-
handed twisting) as positive values. A. No propyzamide treatment controls. B. Root skewing angles
in wild type, $tua6^{C213Y}$ **and** $mor1-11$ **when different concentrations of propyzamide applied. These**
measured results quantificationally presented the phenotypes shown in Figure 3- 6. Wild type,
$tua6^{C213Y}$ **and** $mor1-11$ **showed same skewing direction at 1 µM propyzamide, while the strongest angle**
in $tua6^{C213Y}$ **was occurred at 2.5 µM propyzamide and in** $mor1-11$ **was at 3 µM. C. Data zoomed from**
B, specific showing the differences between wild type and $mor1-11$ **at 2.5 µM and 3 µM treatments.**
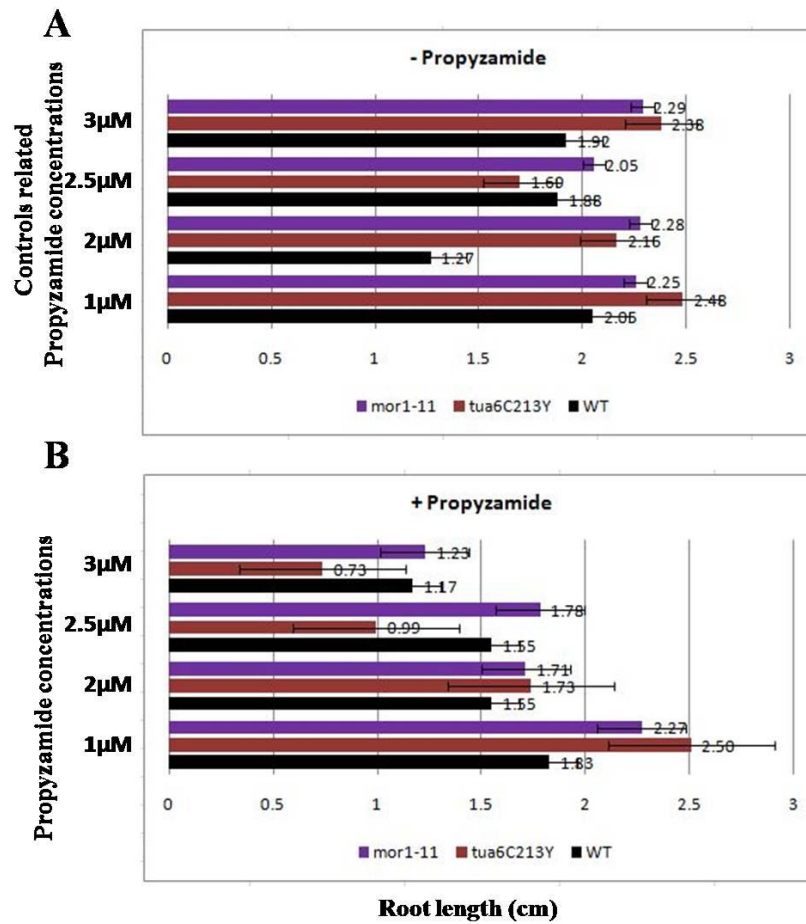
Figure 3- 8 Root lengths in wild type, *tua6*^{C213Y} **and** *mor1-11* **with propyzamide treatments. The root lengths in wild type,** *tua6*^{C213Y} **and** *mor1-11* **showed similar reducing trends when propyzamide concentration increased, but there were no significant differences between wild type and mutants.**

Taxol

Taxol also affects root growth direction and causes root swelling. Here I assessed the effects of three different taxol concentrations, 0.5μM, 1.0μM and 1.5μM (Figure 3- 9). At 0.5μM, taxol caused weak petiole twisting and maximum right root skewing in both *mor1-11* and the wild type (Figure 3- 9 A; Figure 3- 10). The angle of root skewing was slightly reduced at higher concentrations but there was no difference in responses of *mor1-11* and the wild type (Figure 3- 9 B. and C; Figure 3- 10). Among the concentrations of taxol presented in this study, no specific root length difference was observed in *mor1-11*compared with wild type (Figure 3- 11).
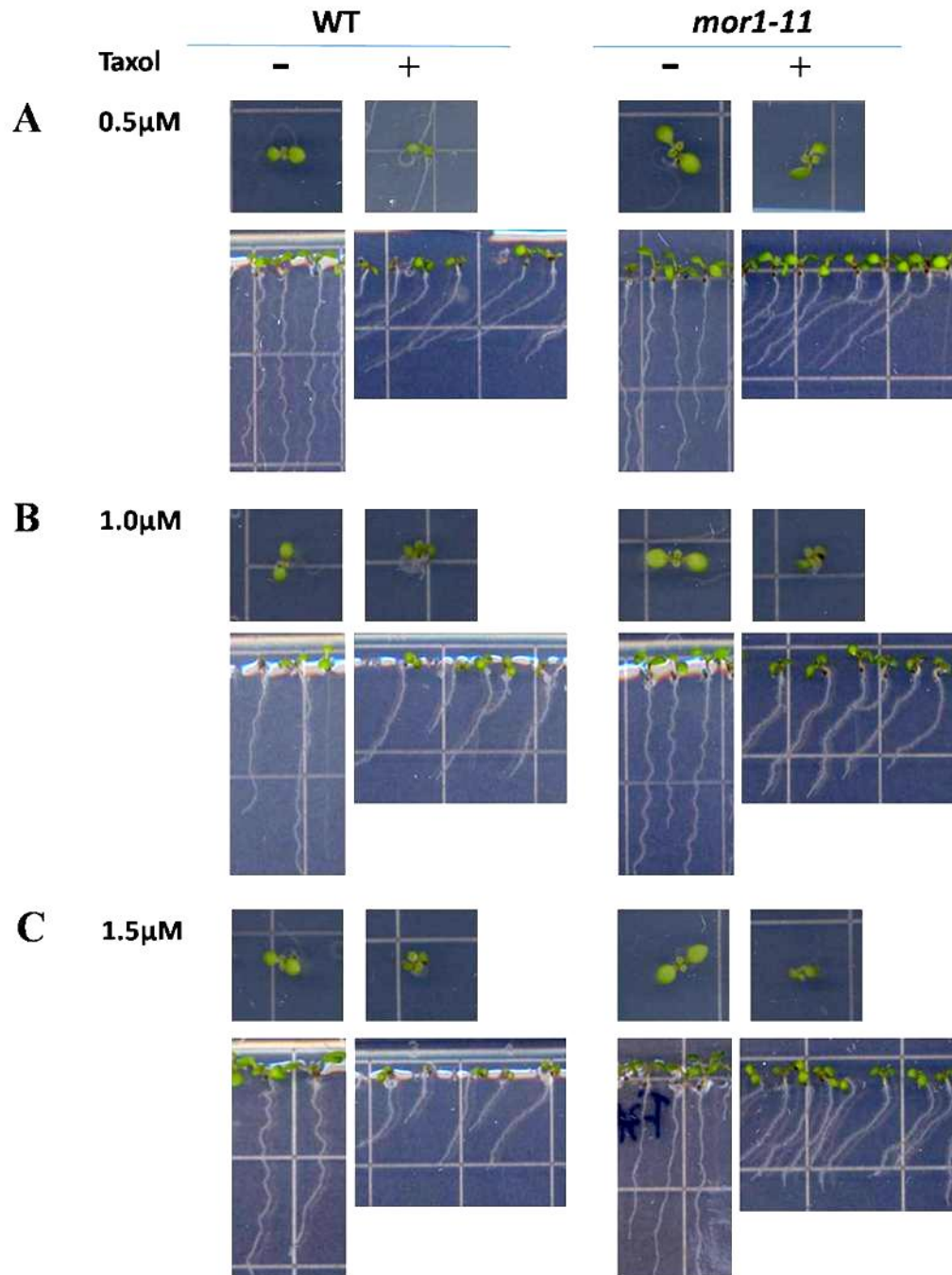
Figure 3- 9 Taxol screening with *mor1-11* at different concentrations. Both the root skewing angle and direction were similar between wild type and *mor1-11* in 0.5 μM (A), 1.0 μM (B), 1.5 μM (C) taxol treatments.

A

- Taxol

Controls related
Taxol concentrations

1.5μM -3.51 / -3.24
1.0μM -3.62 / -2.96
0.5μM -3.41 / -3.43

■ mor1-11 ■ WT

B

+ Taxol

Taxol concentrations

1.5μM -38.9 / -41.21
1.0μM -37.2 / -37.98
0.5μM -50.7 / -45.57

■ mor1-11 ■ WT

Root angle (degree)
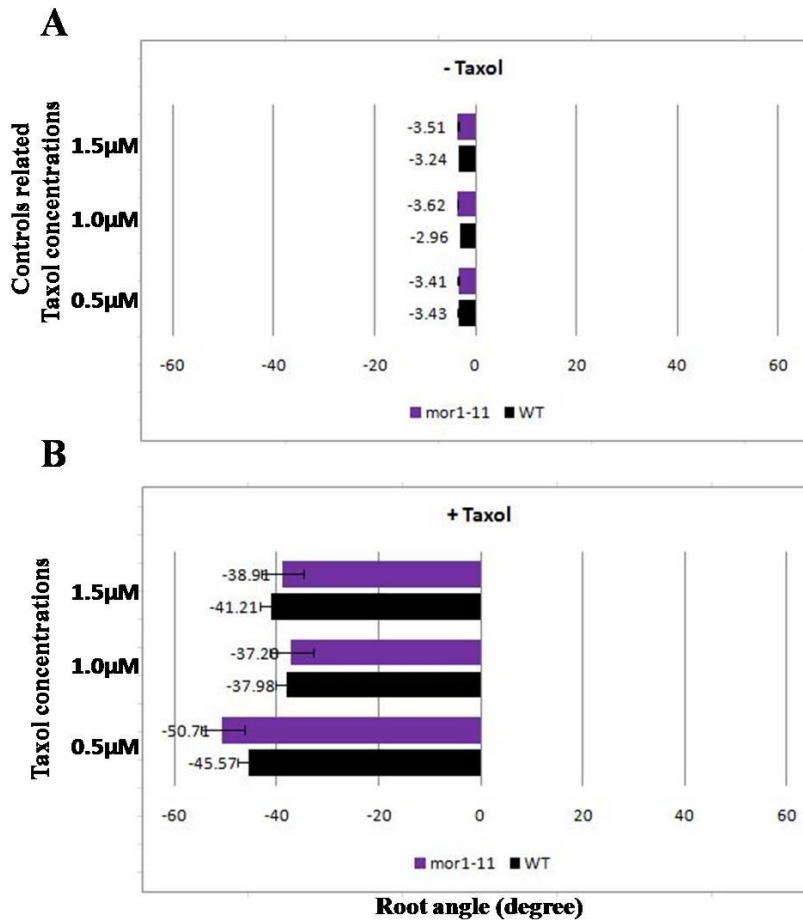
Figure 3- 10 Root skewing angles in wild type and *mor1-11* with taxol treatments. Compared with controls (A), wild type and *mor1-11* skewed to the same direction and with similar skewing angles in all three taxol concentrations (B). The maximum skewing angle of *mor1-11* was observed in 0.5 μM taxol treatment (B).
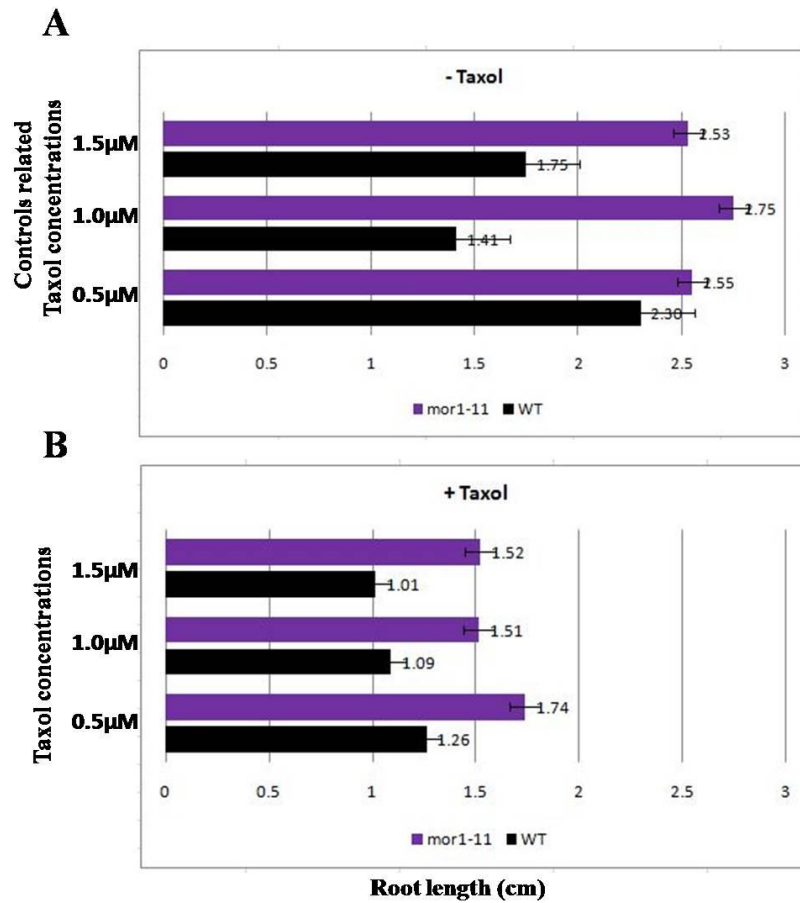
Figure 3- 11 Root lengths in wild type and *mor1-11* with taxol treatments. No obvious differences were found between wild type and *mor1-11* with taxol treatment at concentrations of 0.5 μM, 1.0 μM, 1.5 μM.

Oryzalin

Oryzalin was used at 100nM, 120nM, 150nM and 200nM (Figure 3- 12), and root skewing angle (Figure 3- 13) as well as root length (Figure 3- 14) were measured at each concentration. None of these four oryzalin concentrations caused root skewing or twisting effects in wild type and *mor1-11* (Figure 3- 13). But similar root length reduction effects were noted for *mor1-11* and the wild type at all concentrations. 100nM and 120nM oryzalin caused no significant root length change (Figure 3- 12 A. and B; Figure 3- 14), but 150nM caused a dramatic reduction in root length (Figure 3- 12 C; Figure 3- 14) and 200nM oryzalin caused roots to be short and swollen (Figure 3- 12 D; Figure 3- 14).
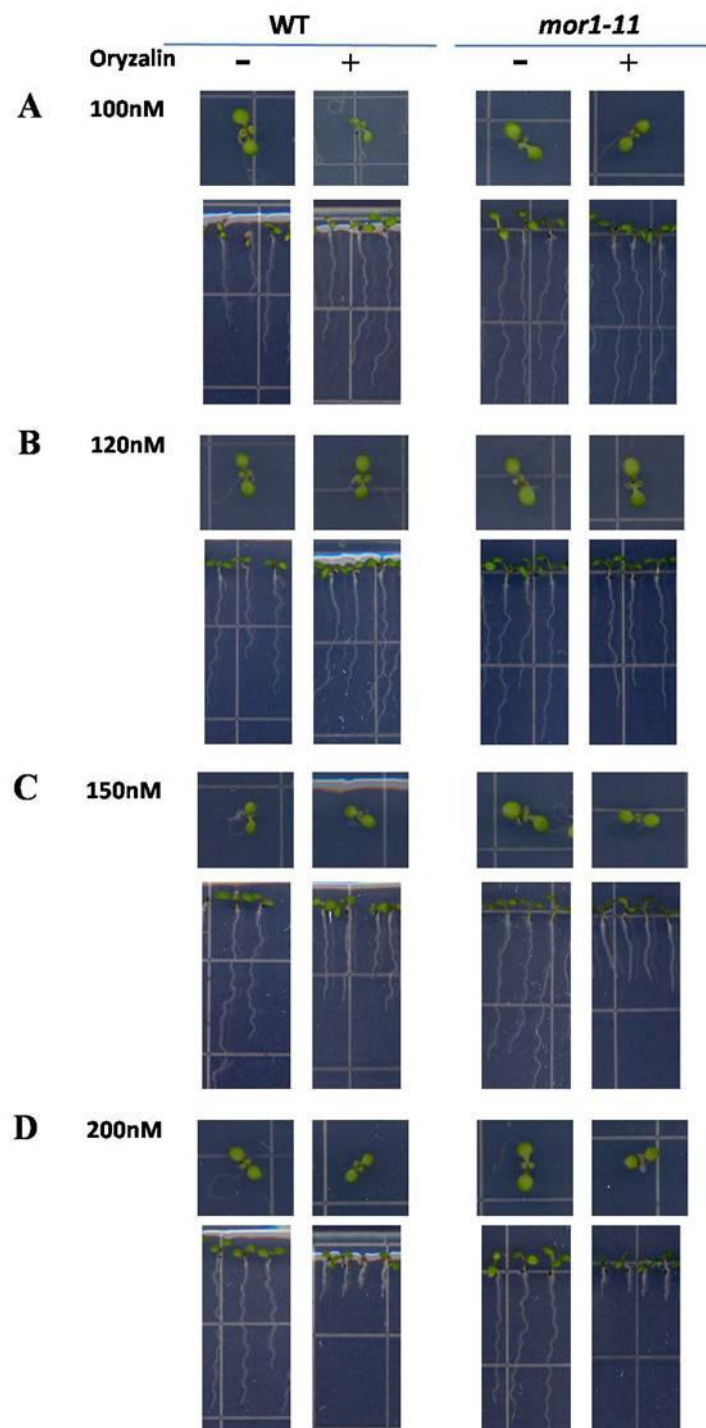
Figure 3- 12 Oryzalin dose responses on *mor1-11*. Similar effects of oryzalin defect were observed in wild type and *mor1-11* at all concentrations.
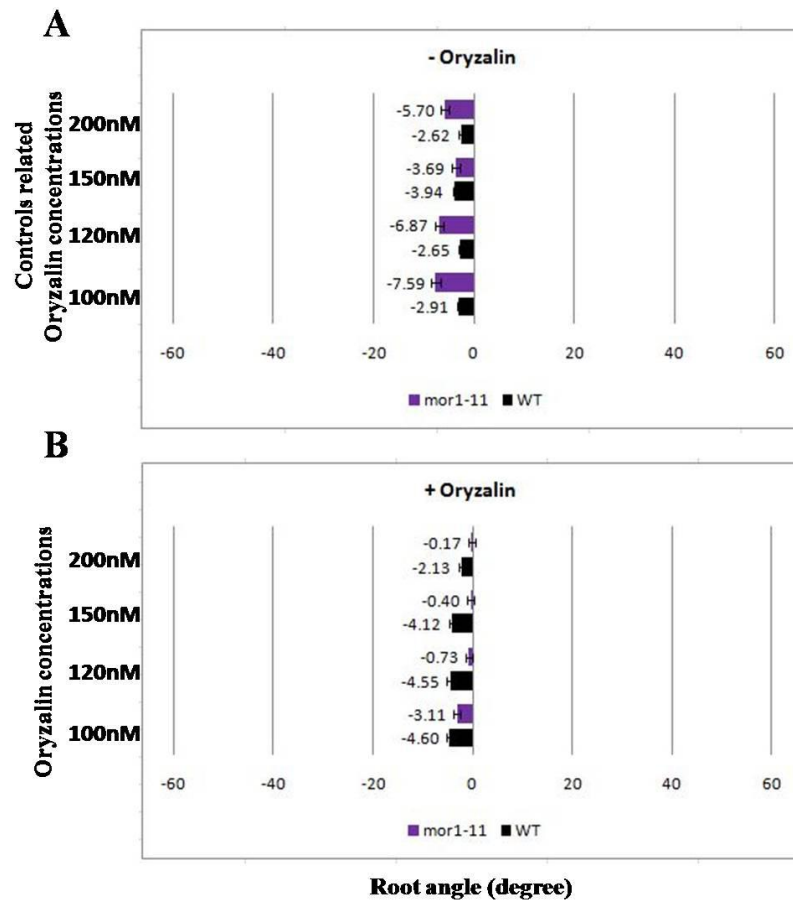
Figure 3- 13 Measured root skewing angles in wild type and *mor1-11* with oryzalin treatments. No root skewing or twisting phenotypes were generated by four different concentrations of oryzalin in wild type and *mor1-11*.
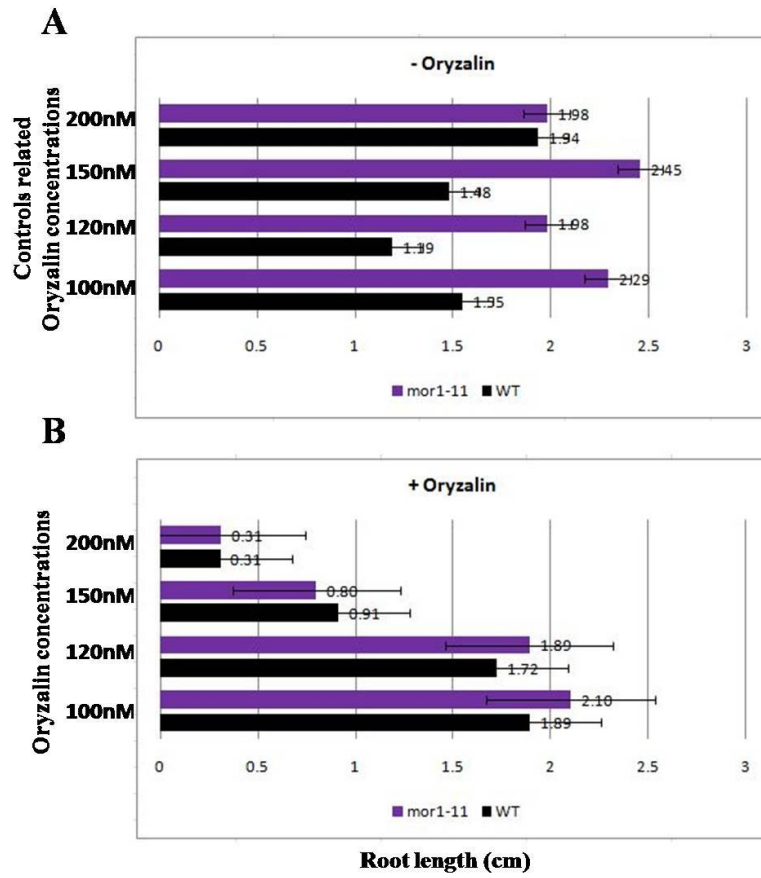
Figure 3- 14 Root lengths in wild type and *mor1-11* with oryzalin treatments. Wild type and *mor1-11* showed similar changes of root length at all four oryzalin concentrations.

Based on these drug screening results and primary drug test results, *mor1-11* has a semi-dominant propyzamide-dependent right-handed root twisting phenotype.

3.3.3 Roots of *mor1-11* shift from right-handed twisting to left-handed twisting when seedlings are moved from 21 ℃ to 31 ℃ on propyzamide

It was recently reported that microtubule dynamics undergoes dramatic increases when the temperature is shifted from 21 ℃ to 31 ℃ (Kawamura and Wasteneys, 2008). This is the same temperature regime that stimulates the expression of the *mor1-1* and *mor1-2* left-handed twisting and radial swelling phenotype (Whittington et al., 2001) as a consequence of greatly diminished microtubule dynamics (Kawamura and Wasteneys, 2008). Although preliminary screening of all of the *mor1* TILLING lines indicated that none had a temperature-sensitive phenotype (David Chen, unpublished results), the discovery of a propyzamide-specific phenotype in *mor1-11* prompted a reinvestigation of temperature effects in the presence of this inhibitor. The phenotype of homozygous *mor1-11* seedlings was confirmed to be the same as wild type on regular Hoagland's medium, whether at 21 ℃ or 31 ℃ (Figure 3- 15 A. C. E. and G). However, in the presence of 3 μM propyzamide the right-handed twisting of *mor1-11* roots at 21 ℃ (Figure 3- 15 D) rapidly changed to left-handed twisting upon shifting the temperature to 31 ℃ (Figure 3- 15 H). Wild-type roots, which undergo left-handed twisting on propyzamide at 21 ℃ (Figure 3- 15 B), continued left-handed twisting at 31 ℃ (Figure 3-15 F). This suggests that at 31 ℃, the *mor1-11* phenotype is rescued.
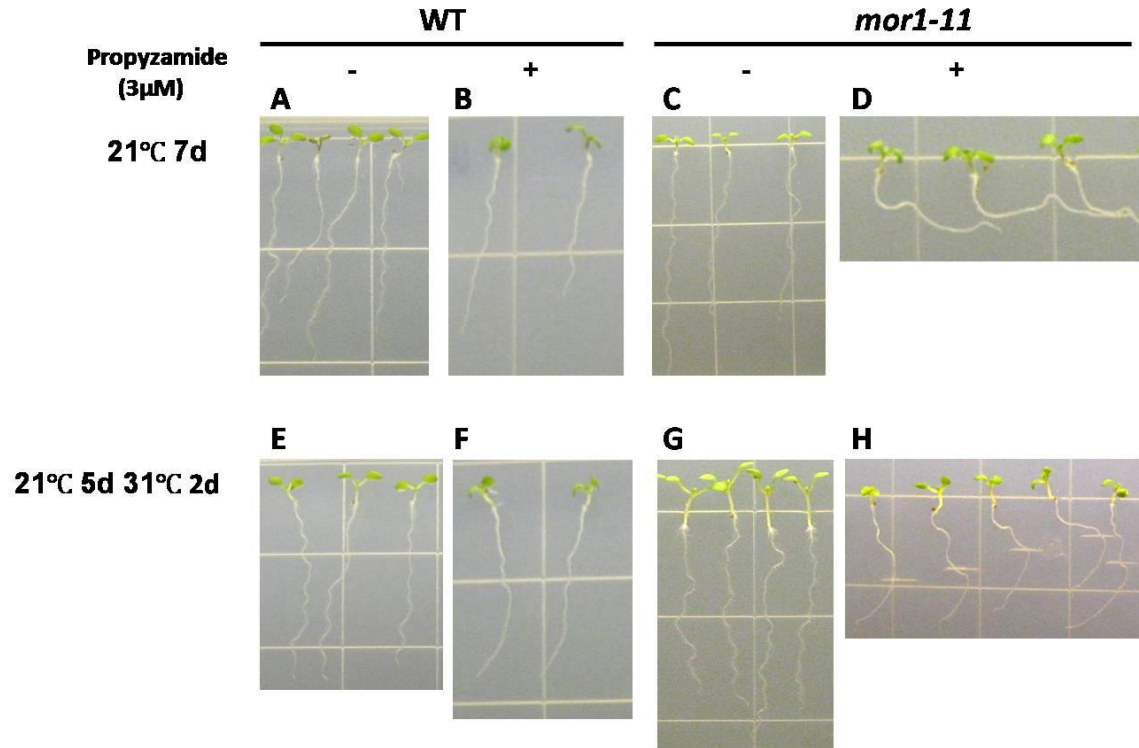
Figure 3- 15 Right-handed twisting of *mor1-11* roots was rescued by higher temperature treatment. (A, B). Wild type showed left-handed twisting roots when treated with 3 μM propyzamide at 21 ℃ for 7 days. (C, D). *mor1-11* showed right-handed twisting roots at 21 ℃ on 3 μM propyzamide, which is opposite to that of wild type. (E, F). Wild type kept left-handed twisting after shifting from 21 ℃ to 31 ℃ for 2 days on 3 μM propyzamide. (G, H) *mor1-11* shifted from right-handed twisting to left-handed twisting when temperature changed from 21 ℃ to 31 ℃ for 2 days.

3.3.4 Microtubule organization in *mor1-11* is altered by propyzamide

To see how the altered response to propyzamide in *mor1-11* is reflected in the organization of microtubules, I used anti-tubulin immunofluorescence microscopy to examine the arrangement of microtubules in cells from the late elongation zone of roots, which is the region in which cell file rotation (twisting) occurs. For this work I used 2.5 μM propyzamide because this concentration shows distinguishable twisting direction difference between wild type and *mor1-11* (as shown in Figure 3- 6 C. and D). 3 μM propyzamide causes the strongest right-handed twisting in *mor1-11* but has a relatively mild effect on the skewing angle of wild-type roots compared to 2.5 μM propyzamide. All treatments were for 7 days at 21 °C.

Consistent with its effects on the handedness of root twisting, propyzamide treatments had opposite effects on the orientation of cortical microtubules in wild type and *mor1-11* cells, shifting the net orientation of microtubules in wild type and *mor1-11* cells to right-handed and left-handed oblique arrays respectively. As shown in Figure 3- 16, 2.5 μM propyzamide generated a shallow right-handed oblique microtubule array in wild-type cells, with a mean orientation with respect to the cell long axis of 109.06±6.88 ° (transverse arrays are defined as 90 °), as compared with 94.14±6.36 ° in the absence of propyzamide. In *mor1-11* 2.5 μM propyzamide generated a shift in the mean orientation with respect to the cell long axis to 77.18±7.81 °, as compared to 91.67±8.41 ° measured in untreated cells. In addition the microtubules in *mor1-11* treated with propyzamide appeared to be shorter and less well ordered locally.
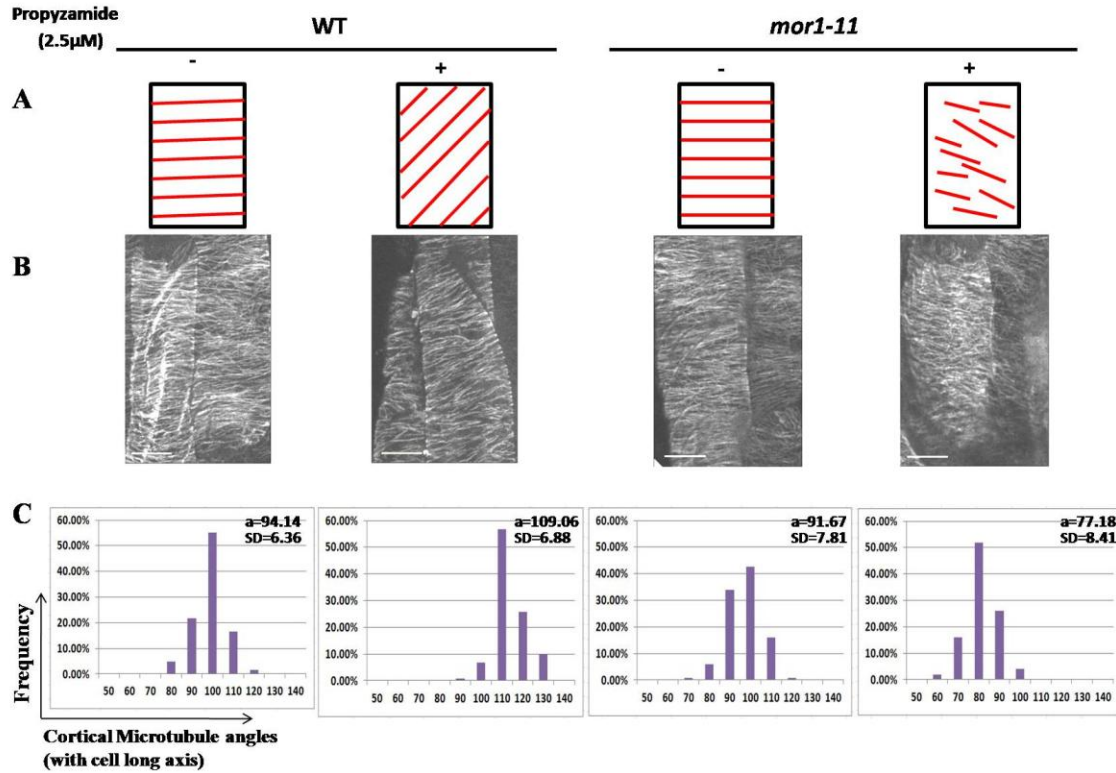
Figure 3- 16   Cortical microtubule organization in wild type and *mor1-11* with 2.5 μM propyzamide treatment for 7 days. Cortical microtubules appeared to be shorter and were oriented in left-handed oblique patterns in *mor1-11* after 2.5 μM propyzamide treatment for 7 days, in comparison to wild-type microtubules, which form right-handed oblique arrays. A. Schematic illustrations showing the general effects on cortical microtubules caused by 2.5 μM propyzamide. B. Representative immunofluorescence micrographs of epidermal cells in the late elongation zone of roots (Scale bar=10 μm). C. Frequency distributions of cortical microtubules angles with respect to the cell long axis in every treatment, with average angle (a) and standard deviation (SD) listed (data were collected from 120 microtubules from 12 cells in 3 roots for each treatment).

3.3.5 Propyzamide reduces microtubule dynamics in *mor1-11* at 21 ℃

To understand the cause of the altered cortical microtubule orientation patterns in *mor1-11* and wild type in the presence of propyzamide, I used live cell imaging with a spinning disc confocal microscope to measure plus end microtubule dynamics. For this work, I crossed the 35S::GFP-TUB6 microtubule reporter into the *mor1-11* mutant line, which enabled me to track the growth and shrinkage of microtubules. This reporter only works effectively in aerial tissues and not in roots but since propyzamide generates twisting in their petioles, I analyzed microtubule dynamics in epidermal cells of cotyledons. All seedlings were exposed continuously to $3 \mu M$ propyzamide or DMSO alone for 7 days. For each treatment, 10 to 12 plants were observed and, from each plant, 20 to 30 image time series were recorded for further data analysis.

Propyzamide at $3 \mu M$ caused a general decrease in microtubule plus end growth rates but the effect was greater in *mor1-11* than in wild type. In wild-type cells, the mean microtubule plus end growth rate decreased from 7.51 ± 0.94 μm/min in the DMSO control to 4.87 ± 1.12 μm/min in the propyzamide treated cells (Figure 3- 17 A. and B.; Figure 3- 18 A). In *mor1-11* the microtubule plus end growth rate was reduced from 7.10 ± 2.60 μm/min in the DMSO control to 3.05 ± 0.86 μm/min in propyzamide (Figure 3- 17 C. and D.; Figure 3- 18 C).

In contract, the effects of propyzamide on shrinkage rates were similar in the wild type and *mor1-11* (Figure 3- 17; Figure 3- 18 B. and D). Shrinkage rates were reduced from 17.63 ± 5.02 μm/min to 10.35 ± 3.81 μm/min in wild type (Figure 3- 17 A. and B.; Figure 3- 18 B) and from 17.17 ± 4.81 μm/min to 10.40 ± 0.98 μm/min in *mor1-11* (Figure 3- 17 C. and D.; Figure 3- 18 D) after propyzamide treatment.
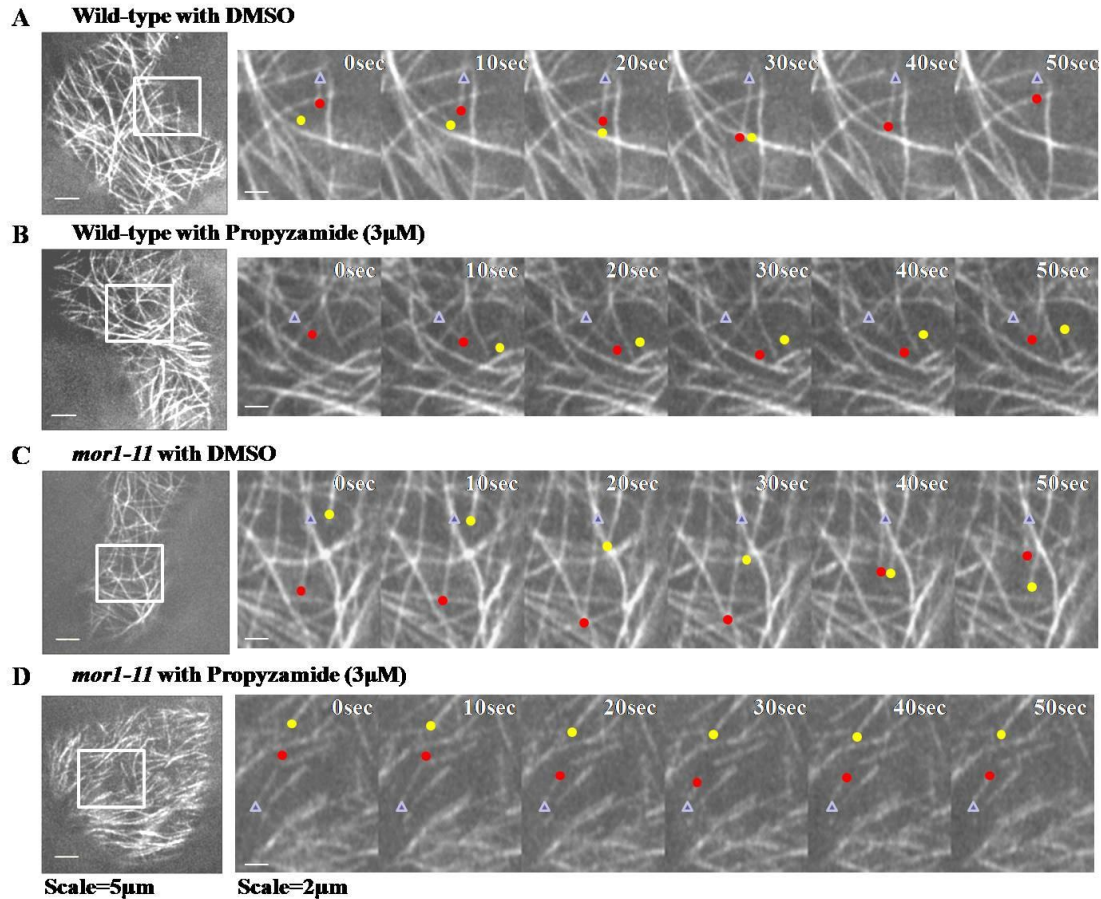
Figure 3- 17 Microtubule dynamics were altered by propyzamide treatment. Images were taken from 7 day old cotyledon epidermal cells after continuous treatment with propyzamide or DMSO. Red dots show microtubules growing and then shrinking during the time series, while the yellow dots indicate microtubules that continued to grow over the same time period.

A. Wild-type seedlings in DMSO control. Microtubules were organized in net-like patterns typical of pavement cells. The microtubules were highly dynamic, as indicated by the growth and shrinkage of the microtubule plus end labelled by a red dot.

B. Wild-type seedlings treated with 3μM propyzamide. The general netlike microtubule organization was not altered, but growth and shrinkage rates of microtubules appeared to be reduced after the treatment.

C. *mor1-11* seedlings without drug treatment. The organization and dynamics of microtubules were similar as in wild type.

D. *mor1-11* seedlings treated with 3μM propyzamide for 7 days. Microtubules are relatively short, sparsely distributed, and show relatively little contact and overlap with other microtubules. Growth and shrinkage also appear to be greatly reduced.

72
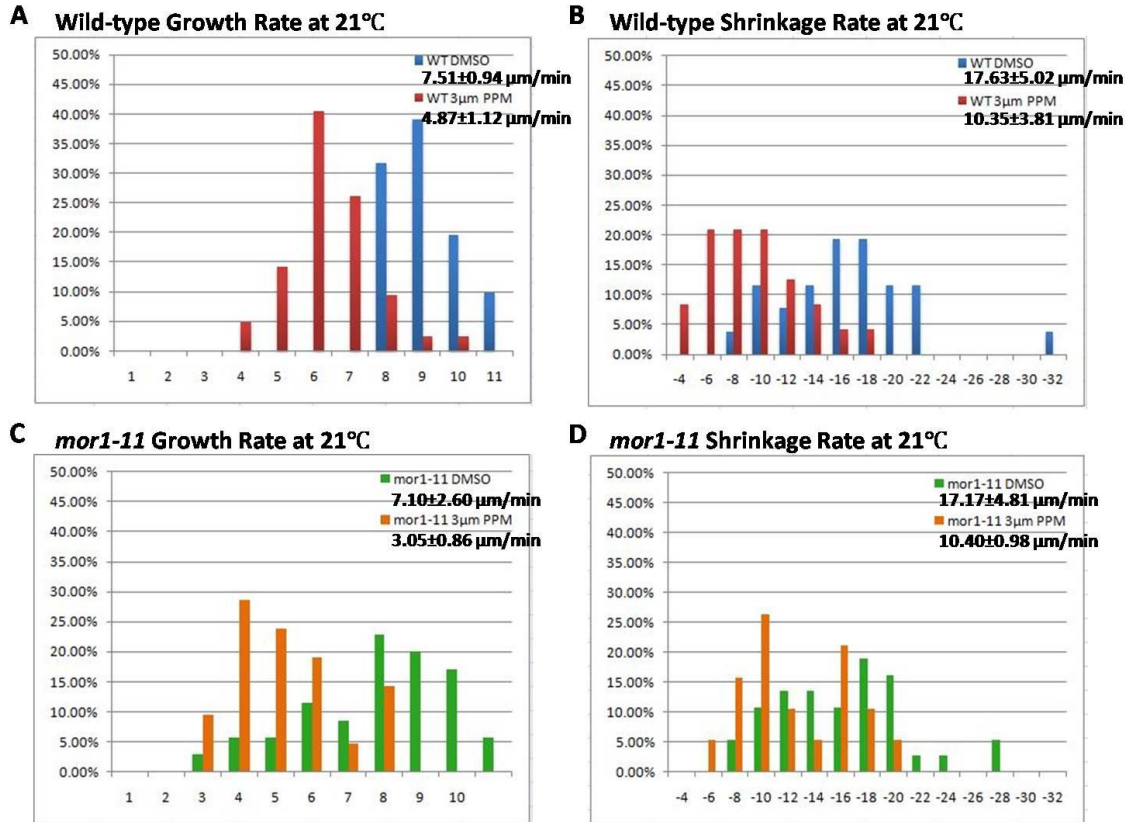
Figure 3- 18 Quantification of microtubule plus end dynamics in wild type and *mor1-11* without or with propyzamide treatment at 21 ℃. Frequency distribution histograms display the data we recollected from 50 microtubules from 12 cells from 9 plants for wild type with DMSO, 42 microtubules from 14 cells from 7 plants for wild type with 3μM propyzamide, 48 microtubules from 13 cells from 9 plants for *mor1-11* with DMSO, and 22 microtubules from 10 cells from 6 plants for *mor1-11* with 3μM propyzamide. Mean growth and shrinkage rates (±SD) are shown in the inset boxes.

73

3.3.6 Microtubule dynamics were recovered by 31 ℃ on propyzamide

Having established that the altered handedness of root twisting in response to propyzamide in *mor1-11* could be abolished at 31 ℃, I investigated the effects of higher temperature on microtubule dynamics in *mor1-11* and wild type after treatment with propyzamide. At 31 ℃, propyzamide had a similar effect of reducing the number of cortical microtubules in wild type (Figure 3- 19 A. and B) and *mor1-11* (Figure 3- 19 C. and D) cotyledon pavement cell arrays.

Microtubule dynamics increased dramatically in both wild type and *mor1-11* by shifting temperature from 21 ℃ to 31 ℃ (Figure 3- 20). At 31 ℃, propyzamide reduced the growth rate of microtubules from 12.55 ± 2.49 μm/min to 7.05 ± 2.11 μm/min in wild type (Figure 3- 20 A) and from 12.00 ± 2.94 μm/min to 5.54 ± 1.46 μm/min in *mor1-11* (Figure 3- 20 C). As observed at 21 ℃, the inhibition of microtubule growth rates was greater in *mor1-11* (a 54% decrease) than in wild type (a 44% decrease) (Table 3- 1).

Propyzamide also reduced the rate of microtubule disassembly but, in contrast to 21 ℃ at which the effect of propyzamide on shrinkage rates was almost identical in wild type and *mor1-11*, at 31 ℃, propyzamide had a greater inhibitory effect on both growth and shrinkage rates in *mor1-11* (Figure 3- 20 B. and D; Table 3- 1). Wild type shrinkage rates slowed from 36.05 ± 10.15 μm/min to 21.30 ± 6.65 μm/min when treated on 3 μM propyzamide (representing a 41% decline) (Figure 3- 20 B; Table 3- 1), while *mor1-11* rates were reduced by 51% from 31.74 ± 8.92 μm/min to 15.54 ± 5.93 μm/min (Figure 3- 20 D; Table 3- 1).
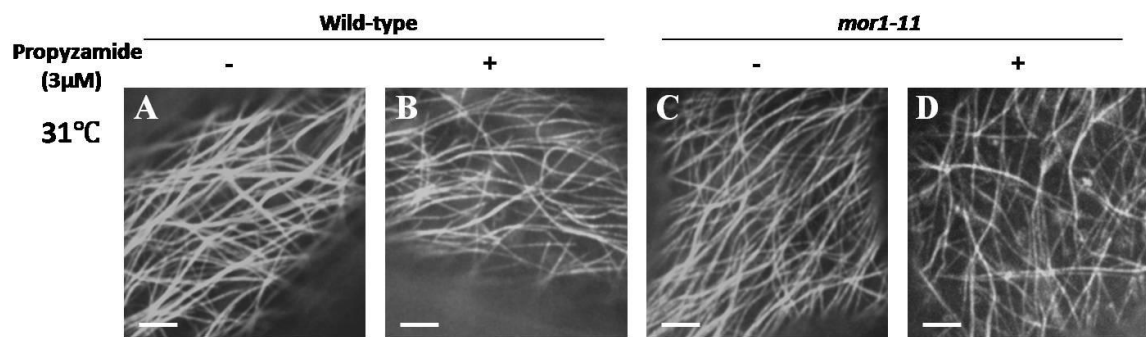
Figure 3- 19 Microtubule organization in wild type and *mor1-11* at 31 ℃ without or with propyzamide treatment. Propyzamide had a similar effect of reducing the number of cortical microtubules in wild type and *mor1-11* (B, D). But compared with the microtubule organization in *mor1-11* on propyzamide at 21 ℃, the microtubules in *mor1-11* with propyzamide at 31 ℃ recovered from the short length, which was observed at 21 ℃ (D). Scale =5 μm.
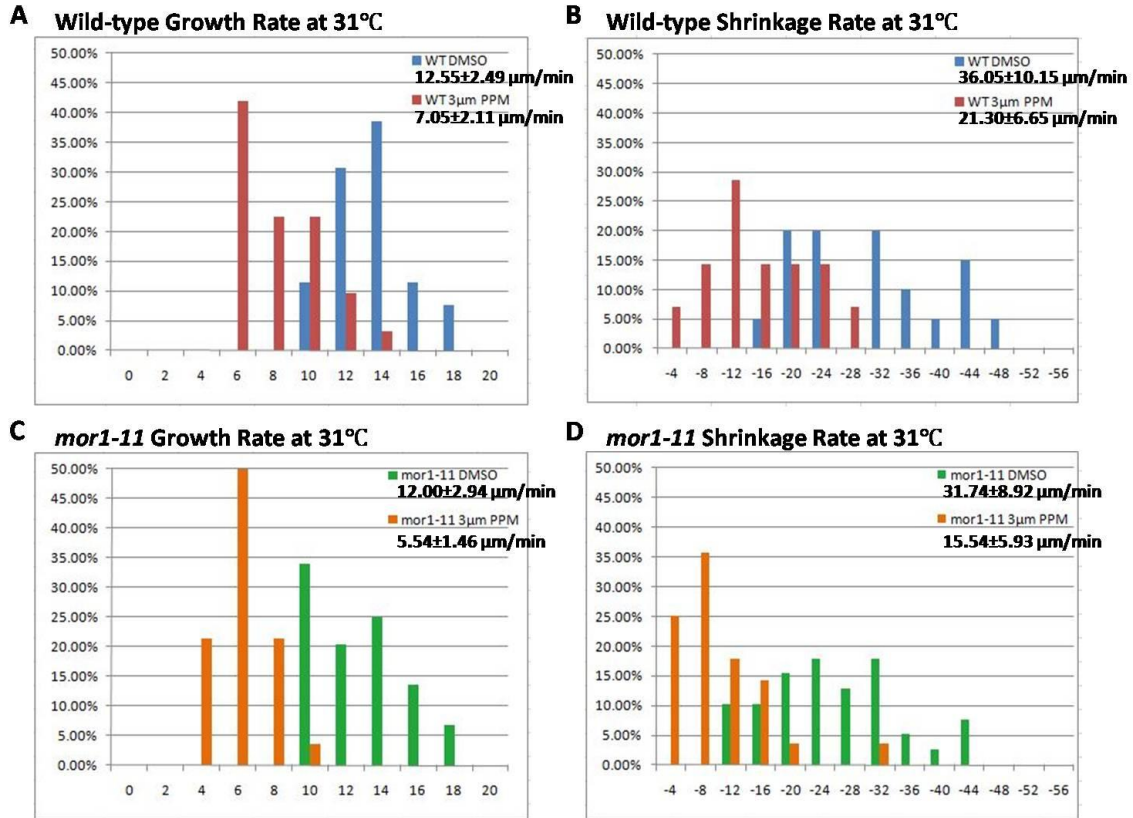
Figure 3- 20 At 31 ℃, propyzamide had a similar effect on wild type and *mor1-11* microtubule dynamics. The growth rate and shrinkage rate were promoted by higher temperature (A, B, C, D, DMSO controls), but the propyzamide affected microtubule behaved less-dynamic, with the similar fold change ((A, B, C, D, propyzamide treatment).

76

Table 3- 1 Effects of 3 μM propyzamide treatment on microtubule growth and shrinkage in *mor1-11* and wild type at 21 ℃ and 31 ℃.

Genotype and temperature	Microtubule Growth Rate (μm/min)		Microtubule Shrinkage Rate (μm/min)	
	-propyzamide	+propyzamide	-propyzamide	+propyzamide
Wild type at 21 ℃	7.5	4.9 (35% decrease)	17.6	10.5 (40% decrease)
***mor1-11* at 21 ℃**	7.1	3.1 (56% decrease)	17.2	10.4 (39.5% decrease)
Wild type at 31 ℃	12.6	7.1 (44% decrease)	36.1	21.3 (41% decrease)
***mor1-11* at 31 ℃**	12.0	5.5 (54% decrease)	31.7	15.5 (51% decrease)

3.3.7 Analysis of *mor1-11tua6*^{C213Y} double mutants

Based on the drug response assays, *mor1-11* has a propyzamide dependent semi-dominant right-handed twisting phenotype but will revert to left-handed twisting at 31 ℃. The *tua6*^{C213Y} mutant also has a similar semi-dominant propyzamide-induced right-handed twisting phenotype (Ishida and Hashimoto, 2007). It is possible that the altered response to the drug propyzamide in both cases happens as a result of an altered interaction between MOR1 protein and microtubules. It is also possible that the altered interaction between MOR1 and microtubules could alter the binding of propyzamide for its target, the identity of which remains unknown. To test these possibilities, analysis of genetic interactions between the *mor1-11* and *tua6*^{C213Y} mutants was carried out. Specifically I set out to determine, by phenotype analysis of the *mor1-11tua6*^{C213Y} double mutants, whether the propyzamide-sensitive phenotype is synergistic, additive or the same as that of the parent lines.

To construct double mutants, *mor1-11* was crossed with *tua6*^{C213Y}. Owing to the semi-dominant nature of both mutants, and the fact that both had similar propyzamide-specific phenotypes, it was not possible to use visual characters to identify double mutants. I therefore identified *mor1-11tua6*^{C213Y} double mutants and azygous control lines from the same F2 by genotyping using molecular markers. Single mutant, double mutant and wild-type segregants were then grown on the plates with or without 3 μM propyzamide and the effect of shifting the temperature from 21 ℃ to 31 ℃ determined (Figure 3- 21). On 3 μM propyzamide, the double mutant responded in the same manner as *tua6*^{C213Y} single mutant, with moderate right-handed twisting at 21 ℃ and a reduced skewing angle in comparison to *mor1-11* (Figure 3- 21 B. C. and D). And unlike the *mor1-11* mutant, the *tua6*^{C213Y} and the double mutant continued right-handed twisting when the temperature was shifted to 31 ℃ (Figure 3- 21 F. G. and H). Based on this phenotype analysis, the *tua6*^{C213Y} mutation appears to override the *mor1-11* phenotype, suggesting that the two mutations affect the same process but to different degrees.
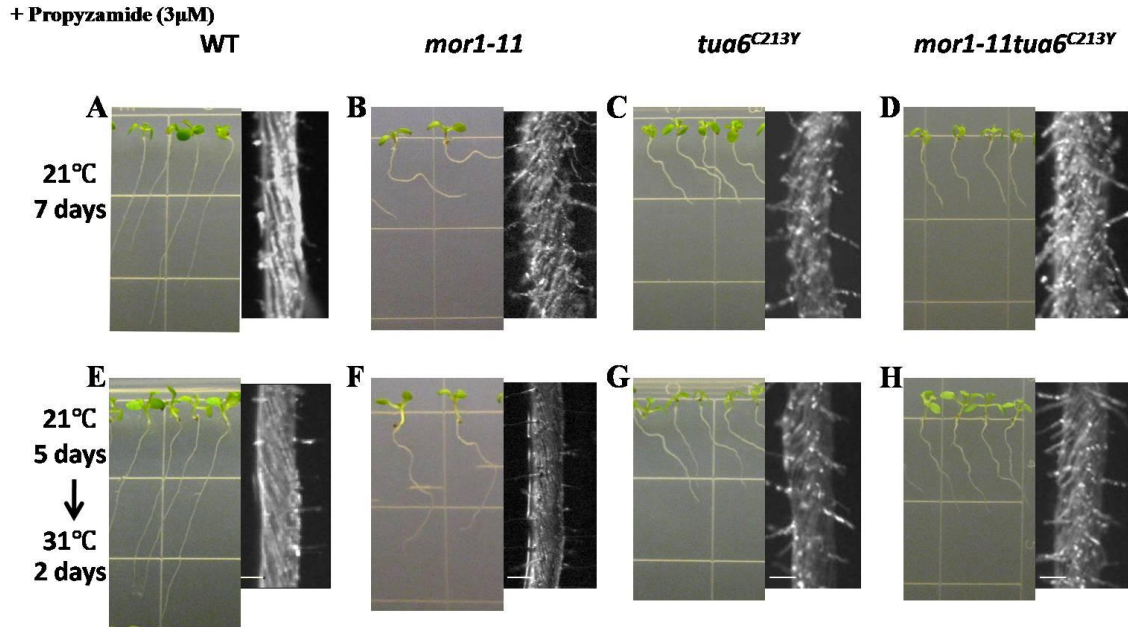
+ Propyzamide (3μM)

Figure 3- 21 Root twisting phenotypes of wild type, *mor1-11*, *tua6*^{C213Y} and *mor1-11tua6*^{C213Y} double mutants on 3μM propyzamide at different temperatures. Seedlings were planted on 3μM propyzamide plates at 21℃ for 7 days, or 21℃ for 5 days and 31℃ for 2 days for the temperature shift experiment. The wild type showed left skewing root and twisting cell files at both 21℃ (A) and 31℃ (E). *mor1-11* shifted from strong right-handed twisting at 21℃ (B) to left-handed twisting at 31℃ (F). *tua6*^{C213Y} maintained right-handed twisting root growth at both temperatures (C, G). The *mor1-11tua6*^{C213Y} double mutant showed a similar phenotype to the *tua6*^{C213Y} single mutant, with no altered root growth direction upon shifting the temperature to 31℃ (D, H).

3.4 Discussion

3.4.1 MOR1 TILLING alleles can provide novel insights into MOR1's function

For this part of study, I first organized the primary MOR1 TILLING data that had been accumulating in the Wasteneys lab to assess the current status of the program. Some of the TILLING alleles had been backcrossed once or twice, using relatively time-consuming and expensive sequencing reactions to genotype mutant alleles in the absence of obvious visual phenotypes. To reduce the high input and speed up the backcrossing process, I designed SNP primers for many of the TILLING alleles. This effective genotyping method promoted the study about *mor1-11*, one of the alleles located in the fifth TOG domain of MOR1, which had been suggested to be an essential part of MOR1's microtubule polymer-binding domain (Twell et al., 2002). This allele is the first of the ongoing studies to emerge from the MOR1 TILLING project.

One of the most intriguing aspects of this study is the finding that *mor1-11* has an opposite root twisting response from that of other alleles including *mor1-1*, which are located in the first TOG domain of the MOR1 protein (Figure 3- 22). This result demonstrates the value of identifying multiple alleles in genes, especially ones like *MOR1* that are essential, which makes null mutants lethal. MOR1 is also a large, multi-domain protein and it is reasonable to find as I have in this study that the specific mutation points of *mor1-1* and *mor1-11* cause distinct phenotypes. According to the model presented in Kawamura and Wasteneys (2008), the *mor1-1* mutation is found in a domain that is thought to function in interacting with incoming free tubulin dimers, while the *mor1-11* mutation is located in a region that would stabilize or mediate the interaction of MOR1 with the microtubule polymer lattice. Further studies on the *mor1-11* mutant could help to test this hypothesis and help to understand the function of this domain.

More broadly speaking, the results of the *mor1-11* study demonstrate the value of carrying out a reverse genetics strategy to identify novel alleles in MOR1. Studying the effects of TILLING alleles from other TOG domains should help us to figure out MOR1's function more comprehensively.
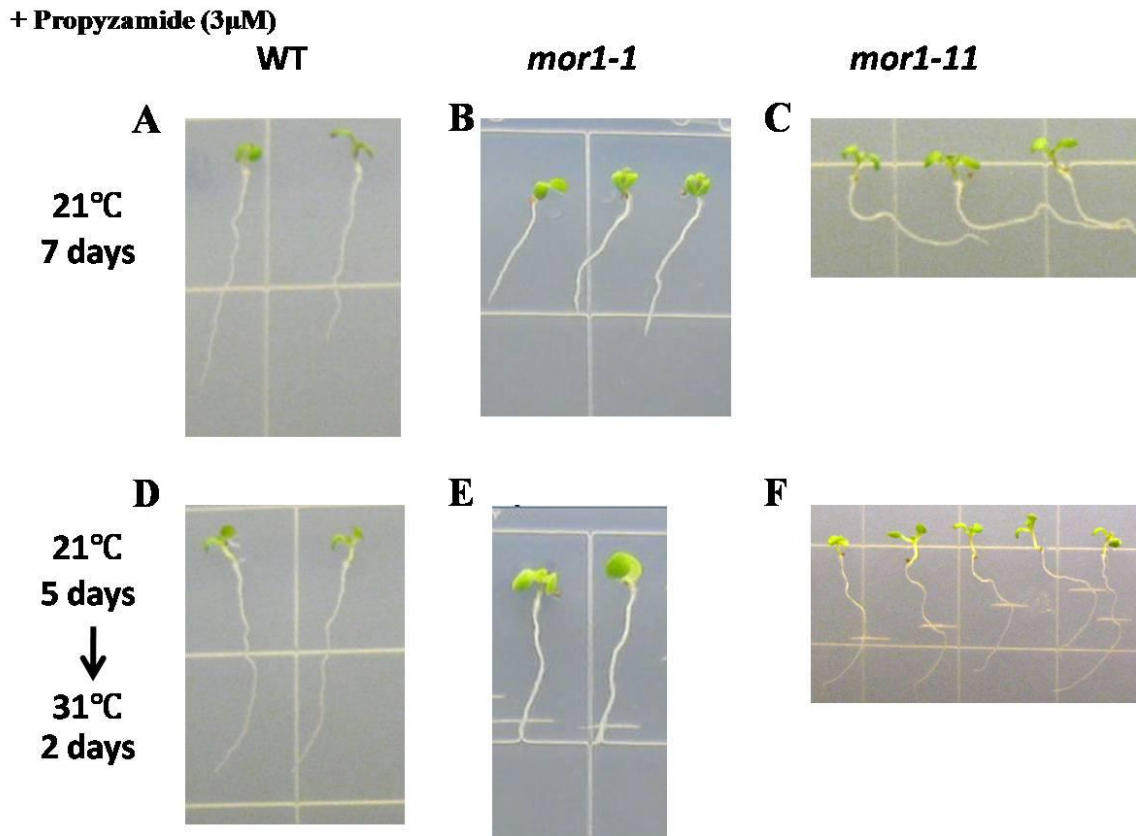
+ Propyzamide (3μM)

Figure 3- 22 *mor1-11* has an opposite root twisting response from that of *mor1-1* on 3μM propyzamide at 21 ℃ and 31 ℃. *mor1-1* had consistent left-handed twisting roots on propyzamide at 21 ℃ and 31 ℃ (B, E), whereas *mor1-11* showed temperature-dependent handedness twisting direction on propyzamide (C, F).

3.4.2 *mor1-11* has a propyzamide-specific defect

In the article that described the $tua6^{C213Y}$ propyzamide-dependent twisting phenotype, it was also reported that this mutant is hypersensitive to taxol, with 1 μM taxol causing stronger radial swelling of root epidermal cells than occurs in wild type (Ishida and Hashimoto, 2007). When I was measuring the effects of taxol on *mor1-11*, I observed no difference in terms of root radial swelling between wild type and the mutant (Data not shown). Thus, although the *mor1-11* and $tua6^{C213Y}$ propyzamide-dependent twisting phenotype and double mutant analysis suggests some allele-specific functional interaction, the differences in their phenotypes make it less likely that the domains affected by both mutations physically interact. However, the connection with propyzamide is compelling. Recently it was reported that the null allele of the MAP kinase phosphatise PHS1 also has a propyzamide-dependent right-twisting phenotype (Pytela et al., 2010). This finding could suggest that the *mor1-11* mutation defines a site that is a downstream target of MAP kinase signalling.

3.4.3 Microtubule organization and dynamics in *mor1-11* were affected by propyzamide

The microtubule-destabilizing drug propyzamide caused microtubules in *mor1-11* to become shorter and less well-organized, in comparison to the wild type. Several studies about twisting mutants describe the microtubules forming left-handed helices in right-handed twisting mutants (Ishida et al., 2007b; Ishida et al., 2007a). From the immunolabelled microtubule arrays in *mor1-11*, propyzamide appears to generate short microtubules that are tilted in a shallow left-handed orientation, but the arrangement does not resemble a helix. This is distinct from the description of the microtubule arrangement in the $tua6^{C213Y}$ mutant had shallow left-handed helical microtubule organization (as shown in Figure 3, Ishida and Hashimoto 2007). That suggests these two loci interact with propyzamide through different mechanisms.

3.4.4 Higher temperature can override the effect of propyzamide in *mor1-11*.

When *mor1-11* seedlings were moved from 21 °C to 31 °C on 3 μM propyzamide plates, the roots of seedlings shifted from right-handed twisting to left-handed twisting, which is the same twisting direction that occurs in wild type under these conditions. Based on this information, I hypothesised that microtubules in *mor1-11* at higher temperature have similar behaviour to microtubules in wild-type cells. The data from live cell imaging of microtubule dynamics measurement in *mor1-11* on 3 μM propyzamide at 31 °C, however, were inconsistent with this hypothesis. On the one hand, the short and less-organized microtubules were indeed replaced by longer and well organized ones after the temperature shift. On the other hand, the growth rate and shrinkage rates were both reduced to a greater extent in *mor1-11* than in wild type at 31 °C. One difference between the effects on propyzamide that might explain the right-handed twisting at 21 °C but not 31 °C in *mor1-11* is that at 21 °C, propyzamide had a much more dramatic effect on microtubule growth rates in *mor1-11* (a 56% reduction) than in wild type (a 35% reduction), but caused an identical reduction (40%) in the shrinkage rates. At 31 °C, both growth and shrinkage rates were reduced to a greater extent in *mor1-11* (54% and 51% respectively) than they were in wild type (44% and 41% respectively) but the fact that both were reduced by a similar amount might provide a clue as to why left- and not right-handed twisting took place. How these differences in the responses of microtubule dynamics to propyzamide in *mor1-11* and wild type relate to the spatial organization of cortical microtubules and the handedness of twisting remain unclear. Other aspects of microtubule dynamics, such as the relative time spent in growth, shrinkage and pause and the frequency of phase transitions might provide better insight into the overriding of the *mor1-11* propyzamide-induced right-handed twisting at higher temperatures.

3.4.5 *tua6*^{C213Y} can mask *mor1-11*'s effect in the interaction with propyzamide

It was shown that both *mor1-11* and *tua6*^{C213Y} have a propyzamide-conditional right-handed twisting phenotype. To understand the mechanism of the propyzamide-specific altered root twisting handedness, and to test whether *mor1-11* and *tua6*^{C213Y} share the same or a similar pathway in their response to propyzamide, double mutants of *mor1-11* and *tua6*^{C213Y} was generated. The phenotype of this double mutant suggested that the *tua6*^{C213Y} mutation masked the *mor1-11* phenotype. This suggests that the interaction between propyzamide and the domain defined by the *tua6*^{C213Y} point mutation might be more direct than that defined by the *mor1-11* mutation.

3.5 Future Directions

These studies on *mor1-11* led to more questions.

First, how does microtubules behaviour differ in *mor1-1* and *mor1-11*? These two point mutations are located in the same gene, but affect different domains, and show an opposite response in the presence of the drug propyzamide. Does this reflect distinct functions for the first TOG and the fifth TOG domains? Analysis of this will help to test the current interaction model for MOR1 and microtubules.

Second, what is the propyzamide binding site? If it is alpha tubulin, is the binding efficiency altered by substituting the cysteine at residue 213 for a tyrosine? To get clues for this question, more in depth analysis of microtubule dynamics in the *mor1-11tua6^{C213Y}* double mutant would be useful. Since *mor1-11* has a temperature-conditional phenotype, a wider range of temperature treatments is likely to be informative.

CHAPTER 4: Summary and Future Directions

4.1 Summary of major findings

In this thesis, two major projects were carried out to investigate the nature of interactions between TOG domains of the MOR1 microtubule-associated protein and tubulin dimers. Interaction was first tested between the first TOG domain of MOR1, through an extensive genetic strategy whereby phenotypes of various *mor1/tubulin* allelic combinations were compared. In the second project, a new allele of *mor1*, *mor1-11*, was identified in the fifth TOG domain. This study represents the first characterization of a mutant identified in a TILLING reverse genetics program that has identified numerous *mor1* alleles. This mutant's cryptic, semi-dominant phenotype comprised an unusual response to the drug propyzamide. The fact that a previous study identified an α-tubulin mutant with a similar phenotype prompted more in depth analysis of *mor1-11* in combination with the α-tubulin mutation.

The TOG1A-tubulin interaction was presented in Chapter 2. From 48 double mutants obtained by crossing 3 different *mor1* alleles with 16 *tubulin* mutants, it was determined that mutations in the interdimer region, where β-tubulin in protofilaments meets the α-tubulin of incoming free dimers, are especially prone to alter microtubule dynamics most severely in combination with mutations in MOR1's TOG1A domain. A mutation in the GTPase-activating domain of α-tubulin5 ($tua5^{D251N}$) caused seedling-lethality in combination with the *mor1-1* mutation in the 5th HR of TOG1A. This synthetic lethality was allele-specific, as it did not occur in when $tua5^{D251N}$ was crossed with *mor1-2* or *rid5* alleles.

In Chapter 3, the study of the novel *mor1-11* mutant was described. After removing other background mutations through six backcrosses, homozygous *mor1-11* mutants were found to have cryptic semi-dominant phenotypes upon application of low concentrations of propyzamide. At 3 μM propyzamide, *mor1-11* showed right skewing roots while wild type showed left skewing. However, the normal left skewing response to propyzamide treatment could be restored in *mor1-11* at a higher temperature (31℃) on propyzamide.

Microtubule dynamics in *mor1-11* were also restored to wild-type rates at 31℃ after being more severely affected at 21℃ by exposure to 3 μM propyzamide. Genetic interaction analysis between *mor1-11* and *tua6*^{C213Y} showed that the *tua6*^{C213Y} mutation masked the *mor1-11* phenotype, suggesting that the *mor1-11* propyzamide-dependent phenotype is dependent on a fully functional TUA6. In this sense, TUA6 may be upstream of MOR1 in a propyzamide-targeted pathway.

4.2 How does MOR1 interact with tubulins to regulate microtubule dynamics?

As hypothesized in the model presented in Chapter 1, MOR1 might bind along protofilaments with each TOG domain interacting with one tubulin dimer to control microtubule dynamics. This model predicts that the region in TOG1A where the *mor1-1*, *mor1-2* but not the *rid5* mutations are located is where TOG1A interacts with the exposed β-tubulin at the plus ends of protofilaments, to which incoming free tubulin dimers are added. Although the genetic interaction analysis identified some clear allele-specific phenotypes of double mutant combinations, the general conclusion is that the TOG1A domain is involved in mediating the interactions between the terminal tubulin dimer in each protofilament and the incoming free tubulin. The *mor1-11* mutation located in the fifth TOG domain did not induce stronger phenotypic effects in combination with α-tubulin6 modified by the substitution of the cysteine residue at position 213 by a tyrosine. Together these genetic approaches have provided us with insights into how MOR1-microtubule and MOR1-tubulin interactions regulate microtubule dynamics.

Currently, MOR1-microtubule binding and polymerization assays are being carried out by Dr. Bettina Lechner in our lab, using biochemical approaches. Various *MOR1* constructs will be cloned, including full-length MOR1, two types of C-terminally truncated, two types of N-terminally truncated, and TOG2A/TOG2B depleted constructs. *mor1-1* and *mor1-2* mutations will be introduced into the constructs containing TOG1A. Comparing how the different MOR1 constructs bind with free tubulins *in vitro*, it should

be possible to get clues as to the function of each TOG domain in microtubule and free tubulin interaction. Live cell imaging using fluorescently labelled tubulin and MOR1 will provide more information about how microtubule dynamics are regulated by MOR1 *in vivo*. The combination of *in vitro* and *in vivo* assays will be effective to determine MOR1's function in organizing microtubule arrays.

4.3 Is MOR1 involved in other processes?

Microtubule dynamics were altered by four point mutations in the MOR1 protein, as described in this thesis. Since microtubules are involved in various important processes inside the cell, it can be considered that MOR1 contributes to many functions that depend on the regulation of microtubule dynamics.

One of the most important outcomes of this thesis was the identification of a new allele of *mor1* and the fact that it has a propyzamide-dependent right-handed twisting phenotype. Interestingly, the *phs1-1* mutant identified in a screen for hypersensitivity to the drug Propyzamide Hypersensitive 1 (PHS1), unlike the *mor1-11*mutant, forms left skewing roots on 3 µM propyzamide. The *phs1-1* was also shown to enhance the *mor1-1* mutant root swelling phenotype (Naoi and Hashimoto, 2004). PHS1 was identified to be a putative mitogen-activated protein kinase (MAPK) phosphatase (Naoi and Hashimoto, 2004), and this function was recently confirmed in a collaborative project between Wasteneys and Ellis laboratories. This recent study by Ankit Walia determined that at least one MAP kinase, MPK18 can interact with and be dephosphorylated by PHS1 and that this signalling module is active in regulating cortical microtubule functions (Walia et al., 2009). The enhancement of the *mor1-1* phenotype by a mutation in the putative MAP-kinase docking domain of PHS1 as well as the propyzamide-dependent phenotype of *mor1-11* indicate that there is a functional link between MOR1 and MAP kinase/ MAP kinase phosphatise signalling. Further studies will investigate this link more extensively through the analysis of genetic interactions between *mor1-11* and *mpk18*, or *mor1-11* and

phs1-1, or *mor1-11* and null allele *phs1-3*, which was recently reported to also have a right-handed propyzamide-specific phenotype (Pytela et al., 2010).

4.4 What causes organ twisting?

As summarised in Chapter 1, altering microtubule organization and dynamics is often correlated with the generation of organ twisting, which can be either left-handed or right-handed. In the *spr1* mutants, right-handed twisting in elongating hypocotyls is associated with reduced cortex and endodermal cell elongation but normal epidermal cell elongation. A possible model was put forward that suggested that twisting growth might be caused by the differential rates of longitudinal cell expansion between tissue layers. Epidermal cells expanding at normal rates will be forced to rotate relative to the organ's long axis if the inner cell elongation rates are reduced (Hashimoto, 2002). This model does not, however, predict the handedness of twisting, which is suggested to be determined by the orientation of cortical microtubule arrays in oblique directions (Ishida et al., 2007a).

To test whether organ twisting is generated by different cell expansion rates in different tissue layers associated with abnormal microtubule organization, a series of promoters that drive tissue-specific expression of the fluorescent microtubule reporter protein GFP-MBD in roots is now being conducted in our lab. It was reported that overexpression of *p35S*:: GFP-MBD can alter microtubule dynamics and generate right-handed twisting roots (Abe and Hashimoto, 2005). When YFP-MBD expression was restricted to the vascular cylinder of roots by a secondary wall specific promoter (*pIRX3*:: YFP-MBD), this generated left-handed twisting, whereas the *p35S*:: GFP-MBD was found to be expressed predominantly in the outer tissue layer and confirmed to cause right-handed twisting (Paulus den Hollander, unpublished data). Together these results indicate the possibility that the handedness of twisting is also dependent on differential tissue expansion and not microtubule orientation per se. To further test this idea, YFP-MBD is now being cloned into a variety of plasmic vectors so that it can be expressed under the control of a wild range of tissue-specific promoters including *pUBQ1*for constitutive

expression, *pCOBRA* for epidermis-specific expression, *pSCARECROW* for endodermis-specific expression and *pWOODENLEG* for vascular cylinder-specific expression of YFP-tagged MBD (Yuan Ruan, ongoing project).

Several studies have demonstrated cortical microtubules could provide the template for cellulose microfibrils synthesis and to regulate the organization of cellulose microfibrils, as suggested by Ledbetter and Porter in 1963. However, there are some studies that do not support this idea. In the temperature-sensitive *mor1-1* mutant, microtubules were less organized and short at restrictive temperature, resulting in left-handed twisting and swelling roots but in these cells the cellulose microfibril orientation remained transverse to the cell long axis. When the microtubule-targeted drug oryzalin caused completed disassembly of microtubules, the parallel orientation of cellulose microfibrils was similarly not altered (Sugimoto et al., 2003). These observations were followed up by a study in which the cellulose microfibril orientation was first disrupted by the cellulose synthesis inhibitor DCB (2,6-dichlorobenzonitrile) in the *mor1-1* mutant and then cellulose synthesis restored by washing out the DCB at *mor1-1*'s restrictive temperature. Despite the lack of any pre-existing well-organized cellulose microfibril template, cellulose microfibrils were once again deposited in parallel, transverse patterns (Himmelspach et al., 2003). These studies indicate that in the left-handed root twisting *mor1-1*, neither the well-organized cortical microtubules nor a well-ordered microfibril template was required for the alignment of cellulose microfibrils. On the other hand, studies on the CesA1 mutant *rsw1-1* demonstrate that cellulose synthesis is itself an important factor in the orientation of microfibrils. The *rsw1-1* mutant has a temperature-sensitive radial swelling phenotype and reduced cellulose synthesis (Arioli et al., 1998) and the reduction in cellulose synthesis causes a loss of microfibril organization but no obvious change in the transverse orientation of cortical microtubules (Sugimoto et al., 2001). These studies demonstrate that cortical microtubules control the anisotropic expansion of plant cells by some as yet unknown mechanism other than cellulose microfibril orientation.

To determine whether the handedness of root twisting is defined by cellulose microfibril orientation or cortical microtubule orientation, I investigated cellulose microfibril orientation by field emission scanning electron microscopy (FESEM) as well as cortical microtubule orientation by immunofluorescence microscopy in a range of mutant alleles showing either left- or right-handed twisting root growth (see Appendix 3). Analysis of microfibril orientation in various tubulin mutants causing either left-handed (*lefty1*, *lefty2*) or right-handed (*tua4^{V62I}*, *tua5^{D251N}*) twisting, plus the left-handed twisting *rid5* allele of MOR1, indicated that the cellulose microfibrils did not co-align with cortical microtubules in these root twisting mutants. In conclusion, although there is a strong correlation between altered microtubule dynamics and organ twisting phenotypes, the handedness of twisting does not appear to be directed by changes in cellulose microfibril orientation, and the mechanism for determining the handedness of twisting remains undefined.

REFERENCES

Abe, T., and Hashimoto, T. (2005). Altered microtubule dynamics by expression of modified α-tubulin protein causes right-handed helical growth in transgenic *Arabidopsis* plants. The Plant Journal **43,** 191-204.

Abe, T., Thitamadee, S., and Hashimoto, T. (2004). Microtubule defects and cell morphogenesis in the *lefty1lefty2* tubulin mutant of *Arabidopsis thaliana*. Plant Cell Physiol. **45,** 211-220.

Akhmanova, A., Hoogenraad, C.C., Drabek, K., Stepanova, T., Dortland, B., Verkerk, T., Vermeulen, W., Burgering, B.M., De Zeeuw, C.I., Grosveld, F., and Galjart, N. (2001). CLASPs are CLIP-115 and -170 associating proteins involved in the regional regulation of microtubule dynamics in motile fibroblasts **104,** 923-935.

Al-Bassam, J., van Breugel, M., Harrison, S.C., and Hyman, A. (2006). Stu2p binds tubulin and undergoes an open-to-closed conformational change. J. Cell Biol. **172,** 1009-1022.

Al-Bassam, J., Larsen, N.A., Hyman, A.A., and Harrison, S.C. (2007). Crystal structure of a TOG domain: conserved features of XMAP215/Dis1-family TOG domains and implications for tubulin binding. Structure **15,** 355-362.

Arioli, T., Peng, L., Betzner, A.S., Burn, J., Wittke, W., Herth, W., Camilleri, C., ouml, fte, H., Plazinski, J., Birch, R., Cork, A., Glover, J., Redmond, J., and Williamson, R.E. (1998). Molecular analysis of cellulose biosynthesis in *Arabidopsis*. Science **279,** 717-720.

Bisgrove, S.R., Lee, Y.-R.J., Liu, B., Peters, N.T., and Kropf, D.L. (2008). The microtubule plus-end binding protein EB1 functions in root responses to touch and gravity signals in *Arabidopsis*. Plant Cell **20,** 396-410.

Brittle, A.L., and Ohkura, H. (2005). Mini spindles, the XMAP215 homologue, suppresses pausing of interphase microtubules in *Drosophila*. EMBO J **24,** 1387-1396.

Brouhard, G.J., Stear, J.H., Noetzel, T.L., Al-Bassam, J., Kinoshita, K., Harrison, S.C., Howard, J., and Hyman, A.A. (2008). XMAP215 is a processive microtubule polymerase. Cell **132,** 79-88.

Cassimeris, L., Gard, D., Tran, P.T., and Erickson, H.P. (2001). XMAP215 is a long thin molecule that does not increase microtubule stiffness. J Cell Sci **114,** 3025-3033.

Chan, J., Calder, G., Fox, S., and Lloyd, C. (2005). Localization of the microtubule end binding protein EB1 reveals alternative pathways of spindle development in *Arabidopsis* suspension cells. Plant Cell **17,** 1737-1748.

Collings, D.A., Lill, A.W., Himmelspach, R., and Wasteneys, G.O. (2006). Hypersensitivity to cytoskeletal antagonists demonstrates microtubule-microfilament cross-talk in the control of root elongation in *Arabidopsis thaliana*. New Phytologist **170,** 275-290.

Dixit, R., and Cyr, R. (2004). Encounters between dynamic cortical microtubules promote ordering of the cortical array through angle-dependent modifications of microtubule behavior. Plant Cell **16,** 3274-3284.

Furutani, I., Watanabe, Y., Prieto, R., Masukawa, M., Suzuki, K., Naoi, K., Thitamadee, S., Shikanai, T., and Hashimoto, T. (2000). The SPIRAL genes are required for directional control of cell elongation in *Aarabidopsis thaliana*. Development **127,** 4443-4453.

Gard, D.L., and Kirschner, M.W. (1987a). Microtubule assembly in cytoplasmic extracts of *Xenopus* oocytes and eggs. J. Cell Biol. **105,** 2191-2201.

Gard, D.L., and Kirschner, M.W. (1987b). A microtubule-associated protein from *Xenopus* eggs that specifically promotes assembly at the plus-end. J. Cell Biol. **105,** 2203-2215.

Gergely, F., Draviam, V.M., and Raff, J.W. (2003). The ch-TOG/XMAP215 protein is essential for spindle pole organization in human somatic cells. Genes & Development **17,** 336-341.

Hamada, T., Igarashi, H., Itoh, T.J., Shimmen, T., and Sonobe, S. (2004). Characterization of a 200 kDa microtubule-associated protein of tobacco BY-2 cells, a member of the XMAP215/MOR1 family. Plant Cell Physiol. **45,** 1233-1242.

Hashimoto, T. (2002). Molecular genetic analysis of left-right handedness in plants. Philosophical Transactions of the Royal Society of London. Series B: Biological Sciences **357,** 799-808.

Hashimoto, T. (2003). Dynamics and regulation of plant interphase microtubules: a comparative view. Current Opinion in Plant Biology **6,** 568-576.

Himmelspach, R., Williamson, R.E., and Wasteneys, G.O. (2003). Cellulose microfibril alignment recovers from DCB-induced disruption despite microtubule disorganization. The Plant Journal **36,** 565-575.

Hugdahl, J.D., Bokros, C.L., Hanesworth, V.R., Aalund, G.R., and Morejohn, L.C. (1993). Unique functional characteristics of the polymerization and MAP binding regulatory domains of plant tubulin. Plant Cell **5,** 1063-1080.

Ishida, T., and Hashimoto, T. (2007). An *Arabidopsis thaliana* tubulin mutant with conditional root-skewing phenotype. Journal of Plant Research **120,** 635-640.

Ishida, T., Thitamadee, S., and Hashimoto, T. (2007a). Twisted growth and organization of cortical microtubules. Journal of Plant Research **120,** 61-70.

Ishida, T., Kaneko, Y., Iwano, M., and Hashimoto, T. (2007b). Helical microtubule arrays in a collection of twisting tubulin mutants of *Arabidopsis thaliana*. Proceedings of the National Academy of Sciences **104,** 8544-8549.

Kawamura, E., and Wasteneys, G.O. (2008). MOR1, the *Arabidopsis thaliana* homologue of *Xenopus* MAP215, promotes rapid growth and shrinkage, and suppresses the pausing of microtubules *in vivo*. J Cell Sci **121,** 4114-4123.

Kawamura, E., Himmelspach, R., Rashbrooke, M.C., Whittington, A.T., Gale, K.R., Collings, D.A., and Wasteneys, G.O. (2006). Microtubule Organization 1 regulates structure and function of microtubule arrays during mitosis and cytokinesis in the *Arabidopsis* root. Plant Physiol. **140,** 102-114.

Konishi, M., and Sugiyama, M. (2003). Genetic analysis of adventitious root formation with a novel series of temperature-sensitive mutants of *Arabidopsis thaliana*. Development **130,** 5637-5647.

Ledbetter, M.C., and Porter, K.R. (1963). A "MICROTUBULE" in plant cell fine structure. The Journal of Cell Biology **19,** 239-250.

Matthews, L.R., Carter, P., Thierry-Mieg, D., and Kemphues, K. (1998). ZYG-9, a caenorhabditis elegans protein required for microtubule organization and function, is a component of meiotic and mitotic spindle poles. J. Cell Biol. **141,** 1159-1168.

McCallum, C.M., Comai, L., Greene, E.A., and Henikoff, S. (2000). Targeting Induced Local Lesions IN Genomes (TILLING) for plant functional genomics. Plant Physiol. **123,** 439-442.

Nakajima, K., Furutani, I., Tachimoto, H., Matsubara, H., and Hashimoto, T. (2004). SPIRAL1 encodes a plant-specific microtubule-localized protein required for directional control of rapidly expanding *Arabidopsis* cells. Plant Cell **16,** 1178-1190.

Nakamura, M., Naoi, K., Shoji, T., and Hashimoto, T. (2004). Low concentrations of propyzamide and rryzalin alter microtubule dynamics in *Arabidopsis* epidermal cells. Plant Cell Physiol. **45,** 1330-1334.

Naoi, K., and Hashimoto, T. (2004). A semidominant mutation in an *Arabidopsis* mitogen-activated protein kinase phosphatase-like gene compromises cortical microtubule organization. Plant Cell **16,** 1841-1853.

Neuwald, A.F., and Hirano, T. (2000). HEAT repeats associated with condensins, cohesins, and other complexes involved in chromosome-related functions. Genome Res. **10,** 1445-1452.

Nogales, E., Grayer Wolf, S., Khan, I.A., Luduena, R.F., and Downing, K.H. (1995). Structure of tubulin at 6.5 A and location of the taxol-binding site. Nature **375,** 424-427.

Ohkura, H., Garcia, M.A., and Toda, T. (2001). Dis1/TOG universal microtubule adaptors - one MAP for all? J Cell Sci **114,** 3805-3812.

Paredez, A.R., Somerville, C.R., and Ehrhardt, D.W. (2006). Visualization of cellulose synthase demonstrates functional association with microtubules. Science **312,** 1491-1495.

Park, S.K., and Twell, D. (2001). Novel patterns of ectopic cell plate growth and lipid body distribution in the *Arabidopsis gemini pollen1* mutant. Plant Physiol. **126,** 899-909.

Perry, J., and Kleckner, N. (2003). The ATRs, ATMs, and TORs are giant HEAT repeat proteins. Cell **112,** 151-155.

Pytela, J., Kato, T., and Hashimoto, T. (2010). Mitogen-activated protein kinase phosphatase PHS1 is retained in the cytoplasm by nuclear extrusion signal-dependent and independent mechanisms. Planta.

Sedbrook, J.C., and Kaloriti, D. (2008). Microtubules, MAPs and plant directional cell expansion. Trends in Plant Science **13,** 303-310.

Sedbrook, J.C., Ehrhardt, D.W., Fisher, S.E., Scheible, W.-R., and Somerville, C.R. (2004). The *Arabidopsis* SKU6/SPIRAL1 gene

encodes a plus end-localized microtubule-interacting protein involved in directional cell expansion. Plant Cell **16,** 1506-1520.

Shirasu-Hiza, M., Coughlin, P., and Mitchison, T. (2003). Identification of XMAP215 as a microtubule-destabilizing factor in *Xenopus* egg extract by biochemical purification. J. Cell Biol. **161,** 349-358.

Shoji, T., Narita, N.N., Hayashi, K., Asada, J., Hamada, T., Sonobe, S., Nakajima, K., and Hashimoto, T. (2004). Plant-specific microtubule-associated protein SPIRAL2 is required for anisotropic growth in *Arabidopsis*. Plant Physiol. **136,** 3933-3944.

Smertenko, A., Saleh, N., Igarashi, H., Mori, H., Hauser-Hahn, I., Jiang, C.-J., Sonobe, S., Lloyd, C.W., and Hussey, P.J. (2000). A new class of microtubule-associated proteins in plants. Nat Cell Biol **2,** 750-753.

Spittle, C., Charrasse, S., Larroque, C., and Cassimeris, L. (2000). The interaction of TOGp with microtubules and tubulin. Journal of Biological Chemistry **275,** 20748-20753.

Srayko, M., Kaya, A., Stamford, J., and Hyman, A.A. (2005). Identification and characterization of factors required for microtubule growth and nucleation in the early *C. elegans* embryo **9,** 223-236.

Sugimoto, K., Williamson, R.E., and Wasteneys, G.O. (2000). New Techniques enable comparative analysis of microtubule orientation, wall texture, and growth rate in intact roots of *Arabidopsis*. Plant Physiol. **124,** 1493-1506.

Sugimoto, K., Williamson, R.E., and Wasteneys, G.O. (2001). Wall architecture in the cellulose-deficient *rsw1* mutant of *Arabidopsis thaliana*: microfibrils but not microtubules lose their transverse alignment before microfibrils become unrecognizable in the mitotic and elongation zones of roots. Protoplasma **215,** 172-183.

Sugimoto, K., Himmelspach, R., Williamson, R.E., and Wasteneys, G.O. (2003). Mutation or drug-dependent microtubule disruption causes radial swelling without altering parallel cellulose microfibril deposition in *Arabidopsis* root cells. Plant Cell**,** tpc.011593.

Thitamadee, S., Tuchihara, K., and Hashimoto, T. (2002). Microtubule basis for left-handed helical growth in *Arabidopsis*. Nature **417,** 193-196.

Till, B.J., Reynolds, S.H., Greene, E.A., Codomo, C.A., Enns, L.C., Johnson, J.E., Burtner, C., Odden, A.R., Young, K., Taylor, N.E., Henikoff, J.G., Comai, L., and Henikoff, S. (2003). Large-scale

discovery of induced point mutations with high-throughput TILLING. Genome Research **13,** 524-530.

Tournebize, R., Popov, A., Kinoshita, K., Ashford, A.J., Rybina, S., Pozniakovsky, A., Mayer, T.U., Walczak, C.E., Karsenti, E., and Hyman, A.A. (2000). Control of microtubule dynamics by the antagonistic activities of XMAP215 and XKCM1 in *Xenopus* egg extracts. Nat Cell Biol **2,** 13-19.

Twell, D., Park, S.K., Hawkins, T.J., Schubert, D., Schmidt, R., Smertenko, A., and Hussey, P.J. (2002). MOR1/GEM1 has an essential role in the plant-specific cytokinetic phragmoplast. Nat Cell Biol **4,** 711-714.

Walia, A., Lee, J., S. , Wasteneys, G., and Ellis, B. (2009). *Arabidopsis* mitogen-activated protein kinase MPK18 mediates cortical microtubule functions in plant cells. The Plant Journal **59,** 565-575.

Wang, P.J., and Huffaker, T.C. (1997). Stu2p: A microtubule-binding protein that is an essential component of the yeast spindle pole body. J. Cell Biol. **139,** 1271-1280.

Wang, X., Zhu, L., Liu, B., Wang, C., Jin, L., Zhao, Q., and Yuan, M. (2007). *Arabidopsis* Microtubule-Associated Protein18 functions in directional cell growth by destabilizing cortical microtubules. Plant Cell **19,** 877-889.

Wasteneys, G.O. (2004). Progress in understanding the role of microtubules in plant cells. Current Opinion in Plant Biology **7,** 651-660.

Wasteneys, G.O., and Collings, D. (2006). The cytoskeleton and co-ordination of directional expansion in a multicellular context. . (Berlin: Springer-Verlag).

Wasteneys, G.O., and Ambrose, J.C. (2009). Spatial organization of plant cortical microtubules: close encounters of the 2D kind. Trends in Cell Biology **19,** 62-71.

Weigel, D., and Glazebrook, J. (2002). *Arabidopsis*: a laboratory manual. (Cold Spring Harbor, New York: Cold Spring Harbor Laboratory Press).

Whittington, A.T., Vugrek, O., Wei, K.J., Hasenbein, N.G., Sugimoto, K., Rashbrooke, M.C., and Wasteneys, G.O. (2001). MOR1 is essential for organizing cortical microtubules in plants. Nature **411,** 610-613.

Yasuhara, H., Muraoka, M., Shogaki, H., Mori, H., and Sonobe, S. (2002). TMBP200, a microtubule bundling polypeptide isolated from

telophase tobacco BY-2 cells is a MOR1 Homologue. Plant Cell Physiol. **43,** 595-603.

APPENDICES

Appendix 1: Supplemental Data of *tubulin-mor1* Double Mutants

Phenotypes of all 48 *tubulin-mor1* double mutants at 21 ℃ and 31 ℃ are listed in Table A1-1, including the handedness of hypocotyl twisting, root skewing direction and handedness of root cell file twisting at two temperatures. Related crosses information is presented in Table A1-2 and details can be found in Cross Records for the Wasteneys Lab according to the cross code.

Table A1- 1 Phenotypes of *tubulin-mor1* double mutants. Significant differences among *tubulin-mor1* double mutants are labelled in red color. Locations of the tubulin mutations are noted. Direction of hypocotyl twisting is defined as left-handed twisting (L), right-handed twisting (R) and no twisting (N). Cell files are described as left-handed twisting (L), right-handed twisting (R) and no twisting (N) observed. Relatively, the root skewing directions are left skewing (L), corresponding with right-handed twisting, and right skewing (R) corresponding with left-handed twisting. If the roots with no skewing direction, straight (S) growth direction will be labelled.

* *tua5^{D251N}mor1-1* double mutants are seedling lethal.

** The diameters of swollen roots in *tua2^{R2K}mor1-1* and *tua2^{R2K}mor1-2* are bigger than that in *mor1-1* and *mor1-2* single mutants.

	Hypocotyl	21 ℃			31 ℃		
		Cell file twisting	Root skewing		Cell file twisting	Root skewing	Root swollen
tub4^{G96D}	Interdimer αβ-tubulin region						
tub4^{G96D}mor1-1	N	R	L		L	R	Y
tub4^{G96D}mor1-2	N	R	L		L	R	Y
tub4^{G96D}rid5	**L**	R	L		L	R	Y
tua6^{T56I}	Lateral contact region						
tua6^{T56I}mor1-1	R	R	L		L	R	Y
tua6^{T56I}mor1-2	R	R	L		L	R	Y
tua6^{T56I}rid5	R	R	L		**N**	R	Y
tua6^{P325S}	Interdimer αβ-tubulin region						
tua6^{P325S}mor1-1	L	R	L		L	R	Y
tua6^{P325S}mor1-2	L	R	L		L	R	Y
tua6^{P325S}rid5	L	R	L		L	R	**N**
tua5^{D251N}	GTPase-activing region						
tua5^{D251N} mor1-1**	R	R	L		L	R	Y
tua5^{D251N}mor1-2	R	R	L		L	R	Y
tua5^{D251N}rid5	R	R	L		L	R	Y
tub4^{P220S}	Interdimer αβ-tubulin region						
tub4^{P220S}mor1-1	L	R	L		**N**	**S**	Y
tub4^{P220S}mor1-2	L	R	L		**N**	**S**	Y
tub4^{P220S}rid5	L	R	L		**R**	**L**	Y
tub3^{P287L}	Lateral contact region						
tub3^{P287L}mor1-1	L	R	L		L	R	Y
tub3^{P287L}mor1-2	L	R	L		L	R	Y
tub3^{P287L}rid5	L	R	L		L	R	Y

		21℃		31℃		
	Hypocotyl	**Cell file twisting**	**Root skewing**	**Cell file twisting**	**Root skewing**	**Root swollen**
tua2^{E284K}	Lateral contact region					
tua2^{E284K}mor1-1	L	R	L	L	R	Y
tua2^{E284K}mor1-2	L	R	L	L	R	Y
tua2^{E284K}rid5	L	R	L	L	R	Y
tua2^{R2K}	Near GTPase-activating region					
tua2^{R2K}mor1-1	R	R	L	L	N	Y**
tua2^{R2K}mor1-2	R	R	L	L	N	Y**
tua2^{R2K}rid5	R	R	L	L	N	Y
tua4^{V62I}	Lateral contact region					
tua4^{V62I}mor1-1	L	R	L	L	R	Y
tua4^{V62I}mor1-2	L	R	L	L	R	Y
tua4^{V62I}rid5	L	R	L	L	R	Y
tua4^{M268I}	Lateral contact region					
tua4^{M268I}mor1-1	L	R	L	L	R	Y
tua4^{M268I}mor1-2	L	R	L	L	R	Y
tua4^{M268I}rid5	L	R	L	L	R	Y
tua6^{S277F}	Lateral contact region					
tua6^{S277F}mor1-1	L	R	L	L	R	Y
tua6^{S277F}mor1-2	L	R	L	L	R	Y
tua6^{S277F}rid5	L	R	L	L	R	Y
tua6^{A281T}	Lateral contact region					
tua6^{A281T}mor1-1	L	R	L	L	R	Y
tua6^{A281T}mor1-2	L	R	L	L	R	Y
tua6^{A281T}rid5	L	R	L	L	R	Y
tub1^{S96F}	Interdimer αβ-tubulin region					
tub1^{S96F}mor1-1	L	R	L	L	R	Y
tub1^{S96F}mor1-2	L	R	L	L	R	Y
tub1^{S96F}rid5	L	R	L	L	R	Y
tub2^{P287L}	Lateral contact region					
tub2^{P287L}mor1-1	L	R	L	L	R	Y
tub2^{P287L}mor1-2	L	R	L	L	R	Y
tub2^{P287L}rid5	L	R	L	L	R	Y
tub4^{P287L}	Lateral contact region					
tub4^{P287L}mor1-1	R	R	L	L	R	Y
tub4^{P287L}mor1-2	R	R	L	L	R	Y
tub4^{P287L}rid5	R	R	L	L	R	Y

Table A1- 2 Record of crosses. Every cross is named with a cross code in the Wasteneys lab, and detail information can be found in Cross Records folder. All of sixteen *tubulin* mutants were crossed with three *mor1* mutants separately. Since *tubulin* mutants have the semi-dominant phenotype, every allele was crossed with wild type to provide information about the phenotypes of heterozygous *tubulin* for further analysis. For the microtubule dynamic observation, before the double mutants were segregated, every tubulin mutant was crossed with four different GFP reporter lines, *Pro35S*::EB1-GFP (labelled as EB1-GFP in table), *ProEB1*::EB1-GFP (EB1-GFP (pEB1), *Pro35S*::GFP-TUB (GFP-TUB6) and *Pro35S*::GFP-TUA6 (GFP-TUA6), to ensure to have backup material. The Wasteneys lab has already generated *mor1-1* mutant background with *Pro35S*::EB1-GFP and *Pro35S*::GFP-TUB reporters. Every tubulin mutant was crossed with these two GFP-fused *mor1-1* alleles for the same backup purpose.

		mor1-1	mor1-2	rid5	WT	EB1-GFP	EB1-GFP(pEB1)	GFP-TUB	GFP-TUA6	mor1-1×GFP-EB1	mor1-1×GFP-TUB
tua2	E284K	4V18 5A13	4V19	5A16	5B3	4Y19		4W16		4X24	5D24
tua4	R2K	4R23 5A14	4X15	5A17	5C12	4Y21		5G10	5G11	**4Z3** 5A18	**5B13**
	T56I	4V17	4V24	5A20 5B2	5B4		5H9	5H4	4X1	4X21	4Y2 5B15
	V62I	4T21	4X14	**5B6** 5F12	4Z13 5C13			5A5	5A1	4Z7 5B24	4Z1
	M268I	4T15	4X11	5C17	4Z12 5C23	4Z23		5A6	5A2	4Z8	5C16
	S277F	4T23 4T24	4X10 5F4	5A23 5D18	5B5	5G14		5G13		4X23 5A19	4Y4 5F3
tua5	D251N	4T22 5F7	4X12 5D22	5C18	4Z9 5C24	4Z24		5A7		4Z4	4Y23
tua6	S277F	4V15	4V22	5D15 5C14	4Z15	4Z25			4V4	4Z5	4Y24 5B16
	A281T	4V13	4V21	5E24 5G5	5C7			4V5	4V3	4X25	5B17
	P325S	4W20	4W23	5B1 5E25	4Z16 5C6		5H18	5H17		5C2	5B18
tub1	S96F	4W18	4W21	5F1 5G6	4Z17					5B23	5B19
tub2	P287L	4W19	4W22	5B8	5C8			4W15		5B25	5B20
tub3	P287L	4U8 4X17	4X13	5B9 5C21	5C9		5H10	5H5		5C3	4Y7
tub4	G96D	4S8	4V20	5B10 5D19 5F2	5C10		5H8	5H3	4W25	5C4 5E1	4Y1 5D25
	P220S	4R8 4R22	4R24 5D23	5B11 5C22	4Z14 5C15	4Y20	5I18	5G15		4Z6 5C5	4Y25 5B21
	P287L	4U7 4V16 4W17	4V23	5B12	5C11	4V10			4W24	5C1	5B22

Appendix 2: SNP Primer Design for MOR1 TILLING Project

A3.1 Introduction

Microtubule Organization1 (MOR1) in *Arabidopsis thalina* is the first identified higher plant member of the MAP215/Dis1 MAPs family, proteins characterized by having five N-terminal TOG domains. In the first TOG domain, *mor1-1*[L174F] and *mor1-2*[E195K] were identified as temperature-sensitive mutants, with altered microtubule dynamics. Besides *mor1-1* and *mor1-2*, more *mor1* mutations have been identified in the TOG4 and TOG5 domains by the reverse genetics TILLING (Targeted Induced Local Lesions IN Genomes) method. These new alleles include 3 point mutations in TOG4, 5 in TOG5 and 9 in the C terminal region. Analysis of microtubule dynamics with these mutants can provide more perceptions about MOR1's function on microtubule organization, besides that of *mor1-1* in the first TOG domain. Before taking any phenotypic analysis, these mutants need to be backcrossed with the wild-type *Arabidopsis* parental line several times to remove undesired non-specific background mutations.

Since the TILLING alleles harbor point mutations, during the backcross progress, good molecular markers are needed for confirming the genotype of the progeny population. Traditionally, homozygous mutants from every BC-F2 generation will be crossed with - plants. However, effective molecular markers can confirm the presence of specific point mutations and dramatically reduce backcrossing times by identifying heterozygotes in sequential F1 generations, instead of identifying homozygotes in F2 generation. These primers also can enhance double mutant segregation analysis by distinguishing heterozygotes and homozygotes.

I have now tested four different strategies for designing single nucleotide polymorphism (SNP) primers, resulting in the successful implementation of primer sets for genotyping the *mor1-1*[L174F] and *mor1-11*[G1399R] mutant alleles. This experience in molecular marker design enabled me to gain expertise in developing similar protocols for the lab's future primer design needs.

A3.2 Design methods and process

A3.2.1 Step 1: SNP primer design

There are four different strategies involved. (Here I use *mor1-11*^{G1399R} as an example)

Col sequence: 5'—CCAAGGATATGGAGAAAAGAAGAGAA**G**GGAAACCTGGGG—3'

mor1-11 sequence: 5'—CCAAGGATATGGAGAAAAGAAGAGAA**A**GGAAACCTGGGG—3'

The mutation is a G to A change in *mor1-11*.

<u>**Regular SNPs**</u>: The length of primers is around 20bp. Set the last base of the forward primer to correspond with the point mutation. Two forward primers, each specific to WT (*mor1-11*_M) and *mor1-11* (*mor1-11*_m) allele respectively, will be synthesized and used for reciprocal PCR analysis. As listed below, *mor1-11*_M stands for the forward primer for the wild type while *mor1-11*_m is the forward primer for the mutant.

Col sequence: 5'—CCAAGGATATGGAGAAAAGAAGAGAA**G**GGAAACCTGGGG--3'

*mor1-11*_M: 5'----------AGGATATGGAGAAAAGAAGAGAA**G**----------------------3'

mor1-11 sequence: 5'—CCAAGGATATGGAGAAAAGAAGAGAA**A**GGAAACCTGGGG--3'

*mor1-11*_m: 5'--------AAGGATATGGAGAAAAGAAGAGAA**A**----------------------3'

The regular size of the genotyping PCR is around 500bp. Thus the reverse primer should be placed about 500bp downstream of the site of mutation. Please be aware that gene families are common in the *Arabidopsis* genome. Therefore the designed genotyping primer should be able to distinguish the gene of interest from other paralogous genes.

2 Mismatch SNPs: This method uses primers that are around 20bp in length. The forward primers specific to the mutant allele contain two mismatches compared to wild type alleles, one corresponding to the point mutation at the very 3'end and the other is the base immediately upstream of the mutation site, as shown below with the blue highlight.

Col sequence: 5'—CCAAGGATATGGAGAAAAGAAGAGA**A****G**GGAAACCTGGGG--3'

*mor1-11*_M: 5'---------AGGATATGGAGAAAAGAAGAGA**GG**----------------------3'

mor1-11 sequence: 5'—CCAAGGATATGGAGAAAAGAAGAGA**A****A**GGAAACCTGGGG--3'

*mor1-11*_m: 5'--------AAGGATATGGAGAAAAGAAGAGA**GA**----------------------3'

3rd or 4th position SNPs: These primers are around 20bp in length. For the primer specific to the mutant allele, set the third or fourth base pair from 3' end in forward primers to correspond with the mutation point.

Col sequence: 5'—CCAAGGATATGGAGAAAAGAAGAGAA**G**GGAAACCTGGGG--3'

*mor1-11*_M: 5'--------------GATATGGAGAAAAGAAGAGAA**G**GG--------------------3'

mor1-11 sequence: 5'—CCAAGGATATGGAGAAAAGAAGAGAA**A**GGAAACCTGGGG--3'

*mor1-11*_m: 5'---------------GATATGGAGAAAAGAAGAGAA**A**GG--------------------3'

Short SNPs: To maximize the difference in annealing thermo-dynamics caused by an introduced mismatch, primers were designed with low Tm. Forward primers are just 15bp in length and with the mutation point placed at the 3' end.

Col sequence: 5'—CCAAGGATATGGAGAAAAGAAGAGAA**G**GGAAACCTGGGG--3'

*mor1-11*_M: 5'---------AGGATATGGAGAAAAGAAGAGAA**G**----------------------3'

mor1-11 sequence: 5'—CCAAGGATATGGAGAAAAGAAGAGAA**A**GGAAACCTGGGG--3'

*mor1-11*_m: 5'------------------------GGAGAAAAGAAGAGAA**A**----------------------3'

A common reverse primer can be used for all of the four strategies. All the designed primers were analyzed with online tools Primer3 (http://frodo.wi.mit.edu/primer3/) and Primer-Blast (http://www.ncbi.nlm.nih.gov/tools/primer-blast/index.cgi?LINK_LOC=BlastNoResAd) to ensure they are suitable for PCR reaction and specific to the target gene.

A3.2.2 Step 2: Test the annealing temperature with designed primers

After obtaining the synthesized oligos, it is necessary to run trial PCR reactions with gradient annealing temperatures (Tm) to find out the best condition for analytical specificity and robustness of amplification.

Figure A2- 1 A. shows an example of a desired SNP genotyping reaction system when it functions well. The wild-type primers would only recognize wild-type DNA but not the mutant DNA, producing one single bind around 500bp. Meanwhile, the mutant primer set is specific to produce a 500bp band when running PCR with mutant's DNA. Based on this, if the sample is azygous, there will be one band only shown with the sample's DNA amplified by the wild-type primer set. If it is a homozygous mutant, one band will be shown when sample's DNA added with mutant's primer set, none with wild type's (Figure A2- 1 B).
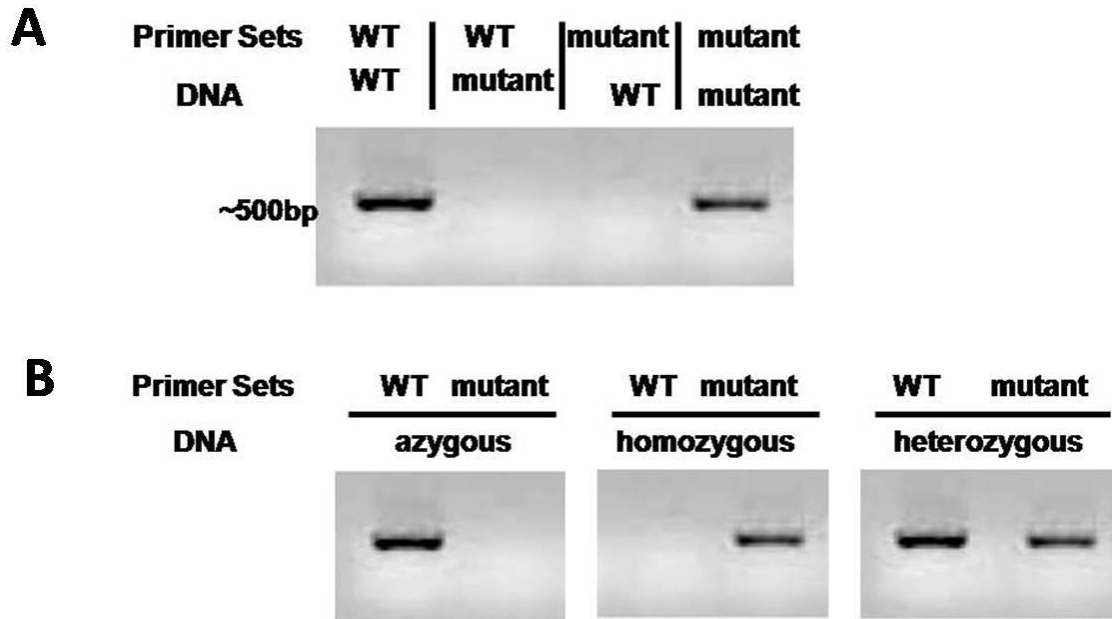
Figure A2- 1 Gel images showing desired SNP genotyping reaction system. A. Primer sets for wild type would only recognize wild-type DNA but not the mutant DNA, while the mutant primers specifically recognize the mutant DNA but not wild-type DNA. B. SNP genotyping can identify the sample is a homozygous or heterozygous or azygous mutant.

The PCR reaction is prepared as following: (Note: the DNA extraction is according to standard Wasteneys lab DNA extraction protocol)

dH$_2$O	15.7µl
10×PCR buffer	2.5µl
50mM MgCl$_2$	0.8µl
10mM dNTPs	0.5µl
Forward primer (10µM)	1.0µl
Reverse primer (10µM)	1.0µl
Taq polymerase	0.3µl
DNA	1.0µl

The PCR reaction was performed as following:

96 ℃	2min	
94 ℃	30sec	
Desired Annealing Temperature	30sec	35×
72 ℃	35sec	
72 ℃	5min	
4 ℃	∞	

Run the Tm test PCR reaction with <u>Regular SNP</u> primer sets:

  for wild type: Fwd-AAGGATATGGAGAAAAGAAGAGAA**G** (Tm=57.82℃)

                        Rev-TTCCAGTCTGTAGGGCCATT (Tm=59.95℃) (length: 526bp)

  for *mor1-11*: Fwd-AAGGATATGGAGAAAAGAAGAGAA**A** (Tm=58.14℃)

                        Rev-TTCCAGTCTGTAGGGCCATT (Tm=59.95℃) (length: 526bp)

In the gel picture shown in Figure A2- 2, *clasp-1* wild type primer set (C) and wily type DNA (M) were used as control to determine whether the PCR reaction was successful. Between 50℃ to 65℃, 7 gradient temperatures were chosen to indicate at which one the SNP markers could function well to distinguish mutation point from genomic point. As shown in Figure A2- 2, at 63℃, the specificity of the wild-type primer set (*mor1-11*_M) and mutant primer set (*mor1-11*_m) is significant.
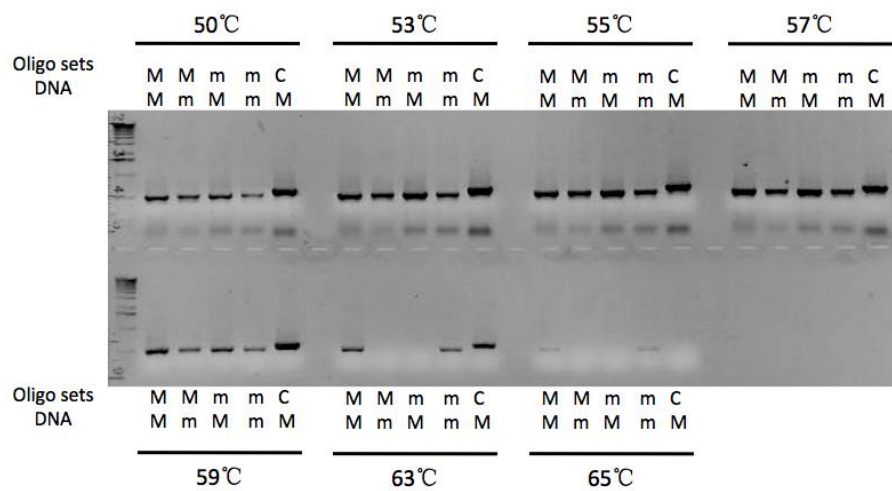
Figure A2- 2 PCR reaction is run with gradient melting temperatures to indicate at which one the mutation point and genomic point can be detected by the SNP markers.

However, <u>2 Mismatch SNP</u> primer and <u>3rd or 4th position SNP</u> primer cannot recognize the mutation specifically.

With <u>Short SNP</u> primer sets, a PCR reaction was run with gradient Tm from 50 ℃ to 60 ℃. With wild-type primers, PCR was run with an annealing temperature of 63 ℃, while a temperature of 52 ℃ was used for the *mor1-11* <u>Short SNP</u> primer set (Figure A2-3).
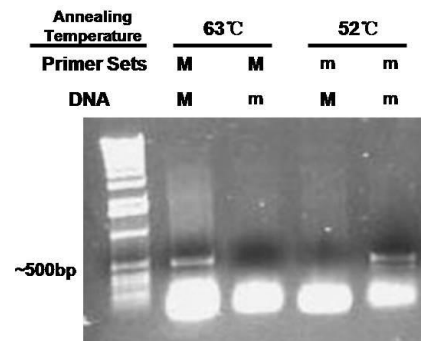
Figure A2- 3 PCR reaction with <u>Short SNP</u> **primer sets for** *mor1-11***. As shown on the gel image, the wild-type primers recognized wild-type DNA with 63 ℃ as melting temperature, while mutant primers were functional at 52 ℃.**

So far, both <u>Regular SNP</u> primer sets and <u>Short SNP</u> primer sets can provide specific binding with certain genotypes. However, <u>Short SNPs</u> worked more consistently than <u>Regular SNP</u> primers.

A3.2.3 Step 3: Optimize the PCR system if necessary

Sometimes, the primers work well but the band on the gel is not bright due to a low amount of PCR product. In this case, optimization of the PCR system is needed. The simplest way is to increase the amount the DNA sample or to increase the number of PCR cycles. Moreover, it is also helpful to adjust the amount of other components in the PCR reaction.

A 3.2.4 Step 4: Try CAPS markers if SNP markers cannot work

If none of the SNP markers worked well, another approach to consider is CAPS (Cleaved-Amplified Polymorphic Sequence) markers. In this method, a restriction enzyme is used to cut the PCR product at the mutation site. However, this technique requires the point where the mutation exists to be a restriction enzyme cutting site, either in the wild-type or mutant sequence.

A3.3 Summary of designed primers

A3.3.1 SNP primers for *mor1-11*

The M3 generation of *mor1-11* seedlings has right-handed root twisting on regular Hoaglands medium. However, it is unclear whether this phenotype is caused by the *mor1-11* mutation. In that case, backcross progress needs to focus on the point mutation change, not the phenotype.

Four sets of primers were designed according to the above strategies (Table A2- 1). Upon testing, the Short SNP primer was found to work best, providing clear and specific binding to detect and amplify the mutant sequence. When using this primer set for genotyping, adding a larger amount of DNA is preferable (e.g. 2µl DNA from the standard Wasteneys lab DNA extraction protocol) to the PCR reaction for robust amplification. Regular SNP primers also can be used for genotyping, but with inconsistent results. Overall, the Short SNP primer set was used during the backcrossing process.

Table A2- 1 SNP primer sets for *mor1-11*.

Primer sets	Sequence	Length	PCR	DNA
Genomic	Fwd: 5' AGGATATGGAGAAAAGAAGAGAAG 3'	526bp	63℃	1μl
(WT)	Rev: 5' TTCCAGTCTGTAGGGCCATT 3'		35×	
Short SNP	Fwd: 5' GGAGAA AAGAAGAGA A**A** 3'	518bp	52℃	2μl
(*mor-11*)	Rev: 5' TTCCAGTCTGTAGGGCCATT 3'		35×	
Regular SNP	Fwd: 5' AAGGATATGGAGAAAAGAAGAGAA**A** 3'	526bp	63℃	1μl
(*mor-11*)	Rev: 5' TTCCAGTCTGTAGGGCCATT 3'		40×	
2 Mismatch	Fwd: 5' AAGGATATGGAGAAAAGAAGAGA**GA** 3'	526bp	—	—
(*mor-11*)	Rev: 5' TTCCAGTCTGTAGGGCCATT 3'			
3rd position	Fwd: 5' GGATATGGAGAAAAGAAGAGAA**A**GG 3'	523bp	—	—
(*mor-11*)	Rev: 5' TTCCAGTCTGTAGGGCCATT 3'			

A3.3.2 SNP primers for *mor1-1*

mor1-1 is a temperature-sensitive mutant, showing left-handed twisting root growth and root swelling at restrictive temperature. According this phenotype, backcrosses were done smoothly. However, if *mor1-1* is combined with other mutations and we need to confirm its presence and status, molecular primers will be needed.

mor1-1^{L174F} is a C to T point mutation.

Col: 5'----TCCACCTAAAAGGATTTTAAAGATG**C**TTCCTGAACTTTT----3'

mor1-1: 5'----TCCACCTAAAAGGATTTTAAAGATG**T**TTCCTGAACTTTT----3'

After testing different primer sets, the <u>Short SNP</u> primer was chosen to use for *mor1-1*'s genotyping. In the PCR reaction, 2µl DNA was added to identify the mutation in existence, with 52 ℃ as annealing temperature, 35 cycles (Table A2- 2).

Table A2- 2 SNP primer sets for *mor1-1*.

Primer sets	Sequence	Length	PCR	DNA
Genomic	Fwd: 5' CCTAAAAGGATTTTAAAGATG**C** 3'	400bp	63℃	1μl
(WT)	Rev: 5' GAGAATAAATAAAAATTCAAGTGT 3'		35×	
Short SNP	Fwd: 5' AAGGATTTTAAAGATG**T** 3'	394bp	52℃	2μl
(mor1-1)	Rev: 5' GAGAATAAATAAAAATTCAAGTGT 3'		35×	
Normal SNP	Fwd: 5' ACCTAAAAGGATTTTAAAGATG**T** 3'	400bp	—	—
(mor1-1)	Rev: 5' GAGAATAAATAAAAATTCAAGTGT 3'			
2 Mismatch	Fwd: 5' CCTAAAAGGATTTTAAAGAT**TT** 3'	526bp	—	—
(mor1-1)	Rev: 5' GAGAATAAATAAAAATTCAAGTGT 3'			

A3.4 Supplemental data about MOR1 TILLING mutants

Table A2- 3 SNP primers for some MOR1 TILLING alleles.

Line	Mutation	Primer Set (primer #)	Primer Type	Length	Note
mor1-6^{splice869} 88077	TGC->TGA Stop Codon	Fwd1:5'GAGTCTTTTAAACTTTTGTAGATG**C**3' (#37) Fwd2:5'TTGAGTCTTTTAAACTTTTGTAGATG**A**3' (#39) Fwd2':5'TTTAAACTTTTGTAGATG**A**3' (#38) Rev: 5'CTCAAGTACTTGGTAAAAATGGC3' (#40)	Regular Short	~450bp	Check** Unclear
mor1-7^{T891I} 87379	ACT->ATT uncharged to nonpolar	Fwd1:5'GGCTAATAAACGTATCCAACCAA**C**3' (#12) Fwd2:5'AGGCTAATAAACGTATCCAACCAA**T**3' (#13) Rev: 5'CACCAAGCCACAAGTCAAGA3' (#14)	Regular	~450bp	Bad*
mor1-8^{G920E} 87625	GGA->GAA nonpolar to negative				
mor1-9^{T1242I} 86190	ACA->ATA uncharge to nonpolar				
mor1-10^{R1274K} 85555	AGA->AAA positive to positive				
mor1-11^{G1399R} 85722	GGG->AGG nonpolar to positive	Fwd1:5'AGGATATGGAGAAAAGAAGAGAA**G**3' (#15) Fwd2:5'AAGGATATGGAGAAAAGAAGAGAA**A**3' (#16) Fwd2':5'GGAGAAAAGAAGAGAA**A**3' (#34) Rev: 5'CTCAAGTACTTGGTAAAAATGGC3' (#17)	Regular Short	~500bp	Good Better
mor1-12^{G1402R} 87514	GGG->AGG nonpolar to positive				

Line	Mutation	Primer Set (primer #)	Primer Type	Length	Note
mor1-13^{E1403K} 87020	GAG->AAG negative to positive	Fwd1:5'GAGAAGGGAAACCTGGG**G**3' (#1) Fwd2:5'AGAGAAGGGAAACCTGGGA**A**3' (#2) Rev: 5'TAGAAGCCACGTGAACACCA3' (#10)	Regular	~400bp	Bad*
mor1-14^{R1683C} 90852	CGT->TGT positive to nonpolar				
mor1-15^{R1685K} 93670	AGA->AAA postitive to positive	Fwd1:5'GGAATGGAAGAGATACGTAGGA**G**3' (#21) Fwd2:5'GGAATGGAAGAGATACGTAGGA**A**3' (#22) Rev: 5' GGTGAAGGATTGTTGGCTGT 3' (#23)	Regular	~500bp	Bad*
mor1-16^{P1764S} 94083	CCT->TCT nonpolar to uncharged	Fwd1:5'CAGATTCAACAGCCAACAAT**C**3' (#24) Fwd2:5'ACAGATTCAACAGCCAACAAT**T**3' (#25) Rev: 5' GGGTTCATCAAAGGCTTCAC 3' (#26)	Regular	~500bp	Bad*
mor1-17^{V1773I} 91302	GTT->ATT nonpolar to nonpolar				
mor1-18^{G1795D} 92312	GGT->GAT nonpolar to negative	Fwd1:5'CAAACAAACTTCCACAATTG**G**3' (#4) Fwd2:5'ACAAACAAACTTCCACAATTGA**A**3' (#5) Rev: 5' CGCAAGGAAGGACAAAGAAG3' (#11)	Regular	~500bp	Check*
mor1-19^{A1838V} 90666	GCT->GTT nonpolar to nonpolar	Fwd1:5'CTGTAGGTTGAGAAGAATGCAG**C**3' (#18) Fwd2:5'TCTGTAGGTTGAGAAGAATGCAGT**T**3' (#19) Rev: 5' TGGGTGTGTGTGGACTGTCT 3' (#20)	Regular	~500bp	Bad*
mor1-20^{R1841K} 91169	AGA->AAA positive to positive				
mor1-21^{R1878K} 87986	AGA->AAA positive to positive	Fwd1:5'GAAGCCTTTGATGAACCCTA**G**3' (#27) Fwd2:5'GAAGCCTTTGATGAACCCTAA**A**3' (#28) Rev: 5' TCCAAAGCTTGGGGTCTCTA 3' (#29)	Regular	~400bp	Unclear

Line	Mutation	Primer Set (primer #)	Primer Type	Length	Note
mor1-22^{M1907I} 93798	ATG->ATN nonpolar to nonpolar				

Notes: Primer details can be found in Yi Zhang's primer folder in the Wasteneys lab, catalogued by primer number (#).

Bad*-- Current primers do not have specific binding and new primer sets need to be designed. Try Short SNPs first.

Check*-- From primary PCR result, the primer sets worked well at 65 ℃ (see Yi Zhang's notebook TILLING#1 page 55). The reaction system needs to be confirmed and optimized.

Check**-- From primary PCR results, the Regular SNP primer sets worked well at 59 ℃ (see Yi Zhang's notebook TILLING#2 page 9 and page 36). The reaction system needs to be confirmed and optimized.

Unclear--Not sure. Need to run trail PCR reaction with gradient annealing temperatures (Tm) first.

Appendix 3: Orientations of Cortical Microtubules and Cellulose Microfibrils in Twisting Mutants

This project was presented in the poster section of 2009 Annual CSPP Meeting.

Yi Zhang, Regina Himmelspach and Geoffrey O. Wasteneys. Probing the role of microtubules in plant cell wall formation. 2009 Annual CSPP Meeting, June 2009 (Vancouver, Canada).

A3.1 Introduction

Cellulose is the major component of plant cell walls that provides the rigidity of plant bodies. During plant development, anisotropic cell expansion requires cellulose microfibrils and microtubules, which was indicated by several studies using cellulose synthesis inhibiters or microtubule drugs to alter the normal regulation (Himmelspach et al., 2003; Sugimoto et al., 2003; Nakamura et al., 2004). Traditionally, cellulose synthesis is hypothesized to be guided by microtubules (Ledbetter and Porter, 1963) and through the enzymatic activities of the Cellulose Synthesis Complex (Paredez et al., 2006). However, this could be an incomplete model not covering all complexity as both supporting and inconsistent experimental evidences exist. Previous analysis of the role of microtubules in cellulose synthesis relies on modifying microtubule behaviours by either treating with microtubule-disrupting chemicals such as oryzalin or genetic disturbance such as the *mor1-1* mutant followed by observing cellulose depositions (Sugimoto et al., 2003; Wasteneys, 2004). These experiments have yield invaluable knowledge but may not be comprehensive enough as only one chemical, oryzalin, and one mutant (*mor1-1*) has been used.

Until now, it is still unclear whether cellulose microfibrils or microtubules principally define the altered cell expansion observed when certain mutants undergo organ twisting, which appears to be manifested by cell file orientation. To investigate this question, a large scale study is presented here in which microtubule orientation was altered by mutations in tubulin genes *(lefty1*, *lefty2*, *tua4^{V62I}*, *tua5^{D251N}*) or by mutation in the

microtubule associate protein MOR1, generating either left-handed or right-handed root twisting. The orientation of microtubules and cellulose microfibrils were measured in these mutants backgrounds together with wild-type controls using immunofluorescence and field emission scanning electron microscopy (FESEM) respectively.

A3.2 Materials and methods

A3.2.1 Growth conditions

lefty1, lefty2, tua5^{D251N} and *tua4^{V62I}* seeds were provided by the Hashimoto Lab at the Nara Institute of Science and Technology, Japan. *rid5* seeds were from the Sugiyama Lab at the University of Tokyo, Japan.

Seeds were sterilised by 3% (v/v) hydrogen peroxide and 50% (v/v) ethanol in distilled water for 2 min, then rinsed in distilled water three times. Sterilised seeds then were planted on nutrient-solidified Hoaglands' medium (90 µM Fe-EDTA, 5mM Ca(NO$_3$)$_2$, 1mM KH$_2$PO$_4$, 2mM KNO$_3$, 2mM MgSO$_4$, 46 µM H$_3$BO$_3$, 9.2 µM MnCl$_2$, 0.77 µM ZnSO$_4$, 0.32 µM CuSO$_4$, 0.11 µM MoO$_3$, 530 µM Inositol (Sigma), 50 µM Thiamine Hydrochloride (Lancaster Synthesis), 3% (w/v) Sucrose (Fisher Chemical), 1.2% (w/v) Bacto Agar (BD Chemical). Approximately 20 seeds were planted for every mutant and placed at 21℃ for 7 days ready for use.

A3.2.2 Roots preparation and field emission scanning electron microscopy (FESEM)

The Wasteneys lab has already developed the FESEM sample preparation and observation protocol for roots (Sugimoto et al., 2000) for study the cellulose microfibrils in the innermost cell wall layers, and modified for inflorescence stems (Miki Fujita, unpublished methods). The mutants I used for this part of the work have either right- or left-handed handedness twisting roots and the twisting occurred in elongation zone, especially the late elongation zone, where good cryo-sectioning surfaces are needed. All the steps for FESEM were based on the protocol from Sugimoto in 2000. Some improvements were made for better results. The detailed protocol is attached at the end and major steps are described as following.

7 day old whole roots were fixed in fixation buffer containing 4% formaldehyde, 1% glutaraldehyde in 1x PME (50mM PIPES, 1mM MgSO$_4$ and 5mM EGTA, pH7.2) for 40

min under the same temperature as at which seedlings were grown. Then samples were rinsed with 1x PME 3 times, for 10 min each. Before cryo-sectioning, fresh glass knives were prepared and placed in the vibratome at an angle of 6 °(Leica Ultracutting). Seedlings kept in1x PME were transferred to 25%DMSO in PME for 10 min, and then transferred to 50%DMSO in PME for 10 min. For a better view to tell where the elongation zone is located during the sectioning process, seedlings were placed into 1% Toluidine Blue and 1% Borate in 1x PME containing 50%DMSO for 1 min to add color, which can be removed later by DMSO and caused no damage to the samples. Then approximately 2 cm lengths roots from the root tips were cut and embedded in Tissue-Tek at the center of pins. Sectioning was done at -120℃, at 0.6mm/s and at a feed rate of 200nm. Sectioned samples were put into 50% DMSO in PME and then transferred to1x PME. After the ultracutting, the outer surfaces of epidermal cells were pealed to expose the inner surfaces. To exact other cell wall materials except cellulose microfibrils, roots were placed in 0.1% NaHCl for 10 min, and rinsed 3 times with distilled water, 10 min. Osmication was done in 2% osmicate solution followed by 3 times distilled water rinsing, 10 min. Root sections were then dehydrated with a series concentrations of ethanol (30%, 50%, 70%, 95% and 100%) 30 min every step and 3 times with 100% ethanol, and critical point drying (Supercritical Autosamdri 815B, Tousimis). The dried sections were mounted on aluminum stubs with two side sticky carbon tapes on the top, and coated with platinum or with gold for 5nm thickness (Crossington Sputter Coater 208HR).

Cellulose microfibrils were observed and images were taken with scanning electron microscopy (Hitachi S-4700) under the settings of 3kV, 10 μA, objective aperture at 2 and condenser aperture at 1, using upper detector and a 5mm working distance.

Orientation angles of cellulose microfibrils were measured using ImageJ software. Images were rotated to place the root vertically and the angles were measured relative to the cell long axis, from 25 around randomly picked cellulose microfibrils per image, 2 to 3 images per cell, 2 to 3 cells per root, approximately 10 roots per treatment. All data were collected from the images taken on the elongation zone.

A3.2.3 Whole root immunofluorescence and confocal laser scanning microscopy

To do the immunolabelling on whole roots, 7 day old seedlings were fixed in small Petri dishes with 4% formaldehyde (v/v), 0.1% glutaraldehyde made up in 1x PMEG (25mM PIPES, 0.5mM $MgSO_4$, 2.5mM EGTA and 2% glycerol, pH6.9) for 1 hour. Then PBS containing 0.05% Triton X-100 was used to rinse 3 times, for 5 min. After this, whole seedlings were transferred to digestion solution (0.1% pectolyase, 0.05% cellulase, 0.5% Triton X-100, dissolved in PME buffer) for 30 min, and then were rinsed again twice with PME for 10 min. The samples were then treated for 1 hour in 3%BSA/PBS to block non-specific binding. To remove the lipids from the samples for better antibody diffusion, seedlings were detergent extracted in PME containing 0.5% Triton for 30 min, then rinsed 3 times for 5 min each time in PBS (with no Triton X-100).

For immunolabelling, DM1A (FITC-conjugated anti-tubulin) was used at a 1:1000 dilution in 3%BSA/PBS for 1hour. If needed, this step can be done at 30℃ incubation. Finally, the seedlings were rinsed in PBS (no Triton X-100) 3 times for 10 min. During the rinsing, slides used for mounting were coated twice with poly-L-Lysine (Sigma 1524, at 1 or 0.5 mg/ml in distilled water). To mounting samples, 20μl Citifluor (#AF1, Electron Microscope Science) was applied to the centre of each slide, then roots were cut off 2cm above the tip and placed in the mounting medium. Cover slips were then applied, sealed with nail polish, and the samples stored at 4℃.

To study cortical microtubule organization in *Arabidopsis* root, images were taken in the late elongation zone, where cell file twisting was observed (Sugimoto et al., 2000). All the immunolabelled roots were observed using an upright AxioImager M1 microscopy (Carl Zeiss, Germany), housing a Zeiss Pascal Excite two channel scan head. A 63×oil-immersion lens (Zeiss) was used to collect images using fluorescence generated by the 488nm laser, and 488nm to 505nm emission filter.

ImageJ software was used for microtubule array measurements. Images were rotated to place the root vertically, with the tip at the bottom. The orientation of microtubules was

measured relative to the cell long axis, from 10 randomly picked microtubules per cell, 4 to 5 cells per root, 3 to 4 roots per treatment.

A3.3 Results

The question of whether the cellulose microfibril or cortical microtubule is the principal feature defining organ twisting handedness has led to various studies on cellulose microfibrils and cortical microtubules. The orientations of these two components of cytoskeleton in handedness root twisting mutants were studied in this work and will provide insight into understanding the role of microtubules and cellulose microfibrils in plant cell wall formation.

The information about cortical microtubule orientation was collected from the outer face of epidermal cells by spinning disk scanning confocal microscopy. However, due to technical limitations, the cellulose microfibril orientation was observed at the inner face of epidermal cells, which was exposed by cyro-sectioning. Based on the cortical microtubule helical arrangement as suggested in Ishida et al, (2007a), microtubule orientations were converted to how they would appear at the inner face of epidermal cells for comparison.

A3.3.1 Microtubule orientation and cellulose microfibril orientation in left-handed twisting mutants

It has been repeatedly demonstrated that the cortical microtubules oriented transversely (Thitamadee et al., 2002; Ishida et al., 2007b), and the cellulose microfibrils formed similar parallel arrays in wild type under normal growth condition (Sugimoto et al., 2000; Himmelspach et al., 2003; Sugimoto et al., 2003).

As the control, the cortical microtubules in wild-type outer face of epidermal cells in elongation zone formed transverse arrays, at a mean angle of 91.06±8.07 relative with cell long axis Figure A3- 1 C). And the cellulose microfibrils detected at the inner face of epidermal cells were parallel aligned, having an 89.35±4.27 degree relative to cell long axis (Figure A3- 1 B).
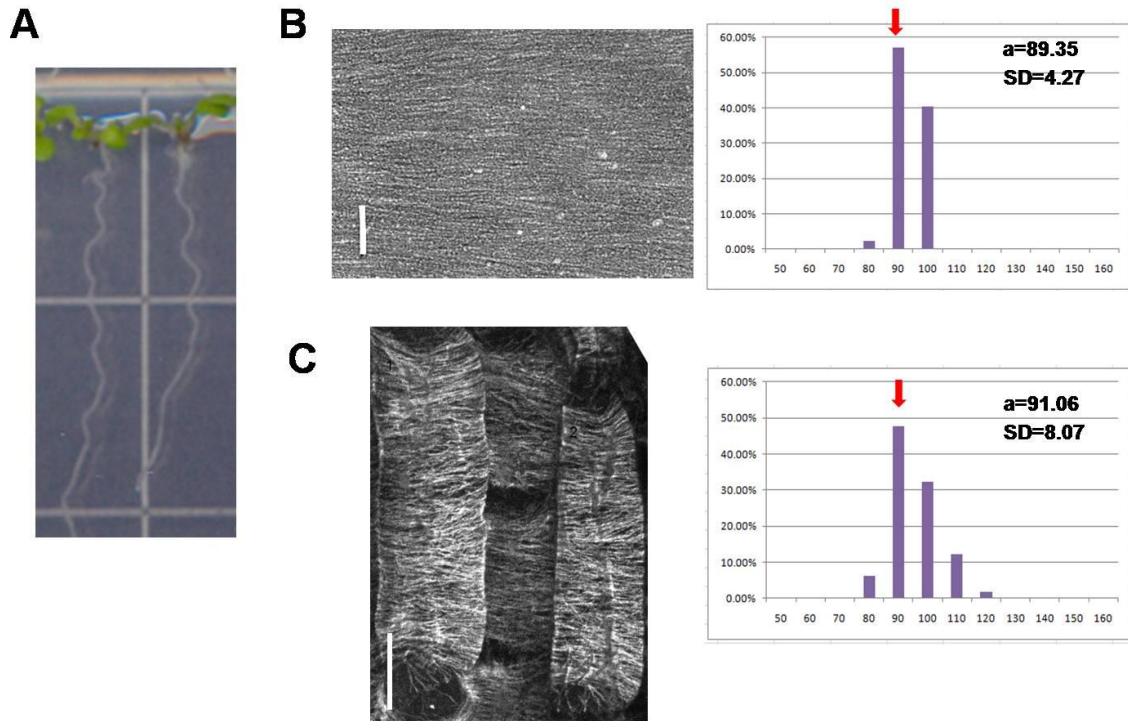
Figure A3- 1 Cellulose microfibril orientation and cortical microtubule orientation in wild type. A. Wild type grown under normal growth conditions had an overall straight root growth. The slight waving and slanting of roots is common when seedlings are planted on Hoagland's medium. B. Cellulose microfibrils at the inner face of root epidermal cells in the elongation zone were transversely oriented, at an angle of 91.06 ±8.07 relative to the cell long axis. (Scale bar = 200nm) C. Cortical microtubule orientation at the outer face of epidermal cells was transverse, at an angle of 89.35 ±4.27 relative to cell long axis. (Scale bar = 10 μm) Red arrows indicated the mean microtubule angles.

It has been reported that in left-handed organ twisting *lefty* mutants, which had mutation points in α-tubulin, left-handed epidermal cell file rotation was observed and the cortical microtubules at the outer face of epidermal cells formed right-handed helices (Thitamadee et al., 2002). To figure out whether cellulose microfibrils and microtubules have co-alignment in *lefty* alleles, organization of cellulose microfibrils was detected by FESEM (Regina Himmelspach, unpublished data). As shown in Figure A3- 2 A. and B, both *lefty1* and *lefty2* displayed right skewing roots, but the cellulose microfibrils did not align the same direction as what microtubules did. The *lefty1lefty2* double mutants had stronger defect of root growth, generating short and swollen roots. But the cellulose microfibril organization was not as same as any single mutant, which was totally disorganized (Figure A3- 2 C).
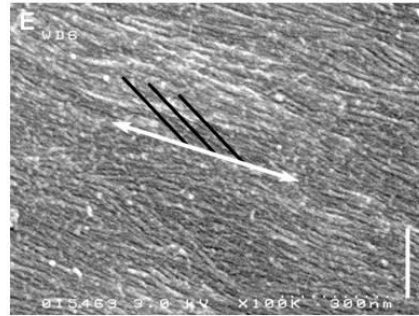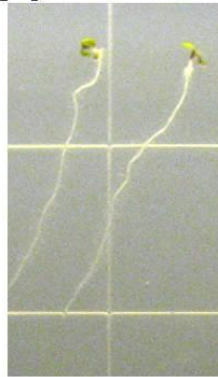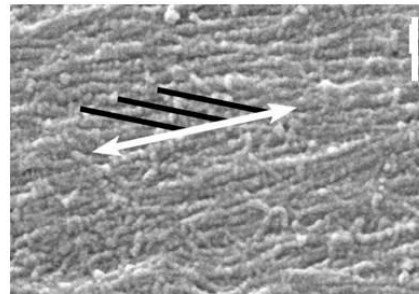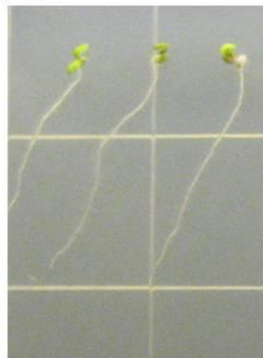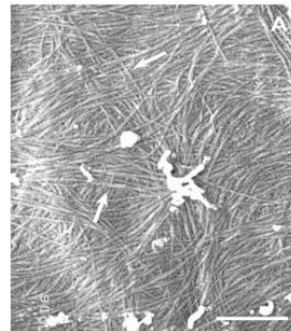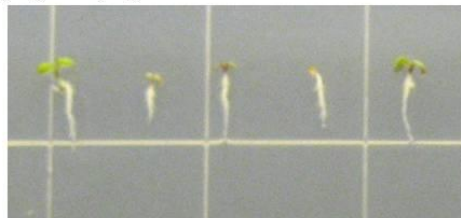
Figure A3- 2 Cellulose microfibril orientation in *lefty* mutants (FESEM was done by Regina Himmelspach). A. and B. *lefty1* and *lefty2* mutants showed left-handed twisted roots and right skewing growth direction. Images of cellulose microfibrils were taken from the elongation zone. White double-ended arrows show the transverse axis of the cells and black lines show the orientation of microtubules reported in (Thitamadee et al., 2002). (Scale bar = 200nm, in A and B) C. *lefty1lefty2* double mutants had strong root growth defects and the cellulose microfibrils in the swollen root cells were disorganized. (Scale bar = 300nm)

Another left-handed twisting *rid5* mutant was from *MOR1*, the gene encoding with microtubule-associate proteins. Cellulose microfibrils were measured having a 93.24±8.96 (average±SD) degree angle relative to the cell long axis, which is close to transverse (Figure A3- 3 B). However, the cortical microtubules were oriented in right-handed helices, at 103.54±8.70 relative to the cell long axis (Figure A3- 3 C). Cellulose microfibril orientation did not reflect microtubule arrangement (as shown in Figure A3- 3 B).
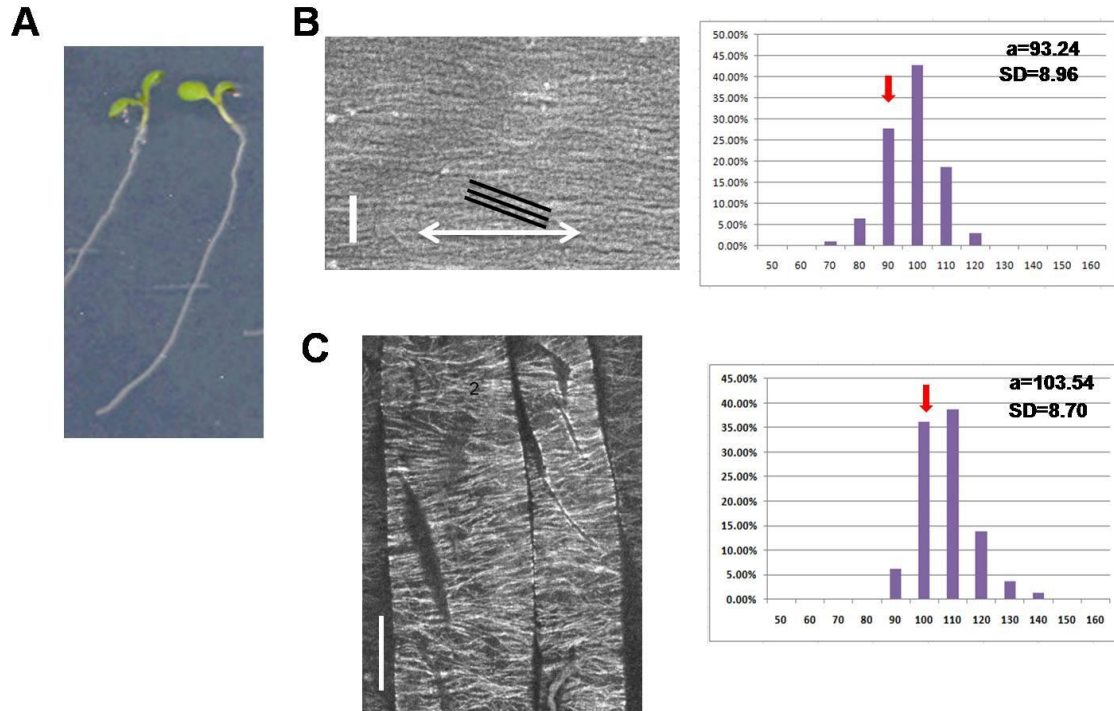
Figure A3- 3 Cellulose microfibril orientation and cortical microtubule orientation in *rid5*. Cellulose microfibrils (B) are predominantly oriented along the transverse axis of cells (as shown by the white arrow), and black lines indicated the angle of microtubule orientation extrapolated from C. (B. Scale bar = 200nm, C. Scale bar = 10 μm) Red arrows indicated the mean microtubule angles.

A.3.3.2 Microtubule orientation and cellulose microfibril orientation in right-handed twisting mutants

Two alleles having point mutation in tubulin-encoding gene were used for further analysis. These two mutants, *tua5^{D251N}* and *tua4^{V62I}*, have been reported to have altered microtubule orientations (Ishida et al., 2007b). The root cell files were rotated in right-handed helices and microtubules at outer layer of epidermal cells formed left-handed oblique arrays (Figure A3- 4 Figure A3- 5). In *tua5^{D251N}*, cellulose microfibrils from inner layer of epidermal cells were not transversely aligned as previous studied in three left-handed twisting mutants, forming 111.08±4.45 degree relative to cell long axis (Figure A3- 4 B). The left-handed helical microtubules from outer face of epidermal cells were oriented on average at 75.46±8.75 °relative to the cell long axis (Figure A3- 4 C). However, when the tilted microtubule angles were helical converted from the outer layer to the inner layer, the alignment was similar to that of the cellulose microfibrils (Figure A3- 4 B).

A similar correlation was also found in another tubulin mutant *tua4^{V62I}* (Figure A3- 5).
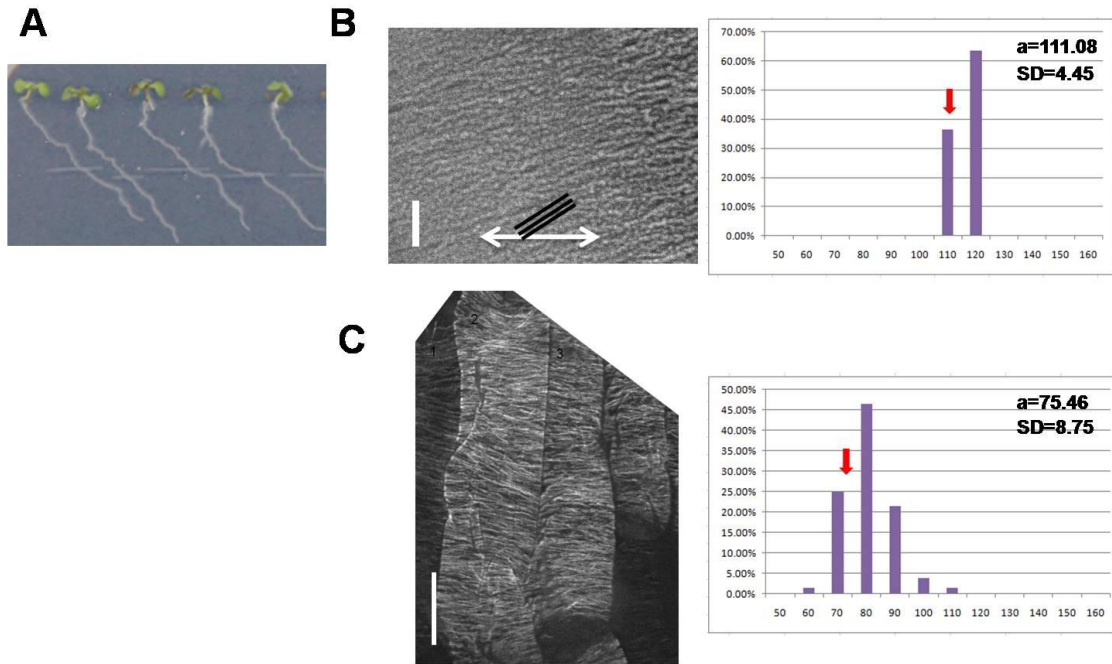
Figure A3- 4 Cellulose microfibril orientation and cortical microtubule orientation in *tua5*^{D251N}**. The cellulose microfibrils at the inner face of epidermal cells were not transversely oriented, tilted at a 111.08±4.45 angle to cell long axis (B). When converted the left-handed helical microtubule arrays (75.46±8.75) (C) from outer layer to inner layer (as the black lines shown in B), a weak alignment correlation between cellulose microfibrils and microtubules was observed. (B. Scale bar = 200nm, C. Scale bar = 10 μm) Red arrows indicated the mean microtubule angles.**
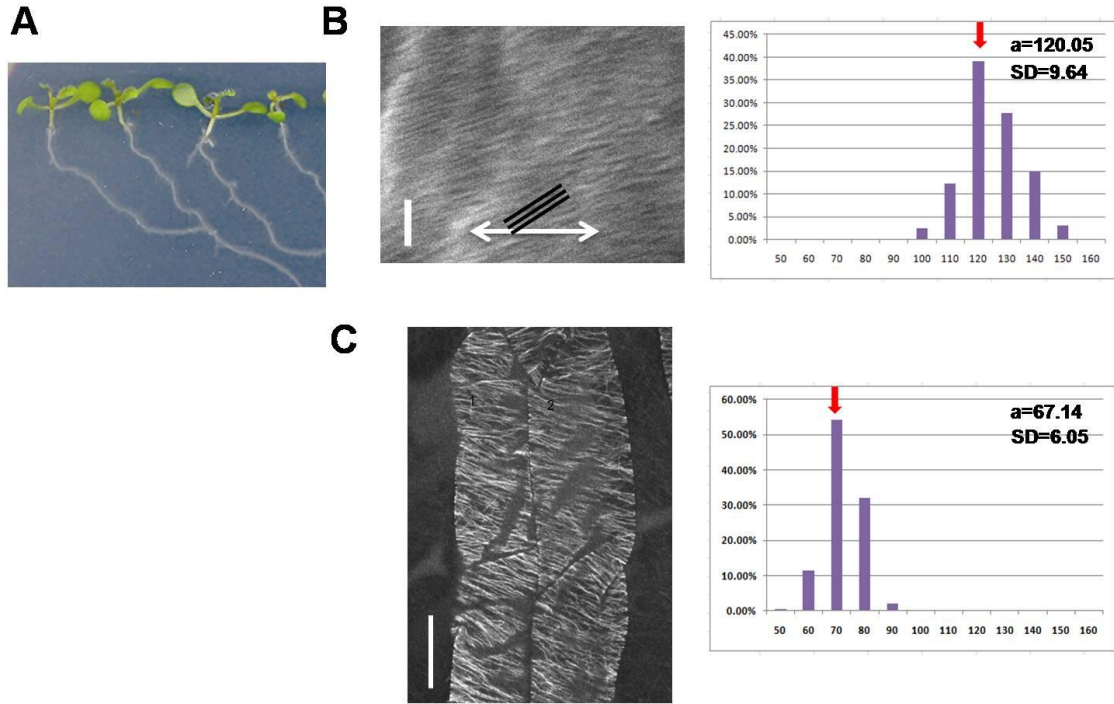
Figure A3- 5 Cellulose microfibril orientation and cortical microtubule orientation in *tua4*[V62I]**. A weak correlation between cellulose microfibril orientation (A) and microtubule orientation (B) was also observed as shown in** *tua5*[D251N]**. (B. Scale bar = 200nm, C. Scale bar = 10 μm) Red arrows indicated the mean microtubule angles.**

A3.4 Discussions

The four α-tubulin mutants, *lefty1, lefty2, tua5*^{D251N} and *tua4*^{V62I}, generated either left-handed or right-handed root twisting phenotypes. All of them showed helical microtubule orientation in epidermal cells of elongating roots. However, it was clearly observed that the transverse arrays of cellulose microfibrils did not reflect the obliquely oriented microtubules in left-handed twisting mutants (Figure A3- 6 C). Another interesting finding was that in right-handed twisting mutants, there were weak correlations between microtubule arrays and cellulose microfibril arrays (Figure A3- 6 D). The loss of coordination between microtubule and cellulose microfibril orientation was suggested to be due to the specific consequence of tubulin mutations (Ishida et al., 2007a). To address this, the orientations of microtubules and cellulose microfibrils in *mor1* allele, *rid5*, were also compared and not found to be correlated.
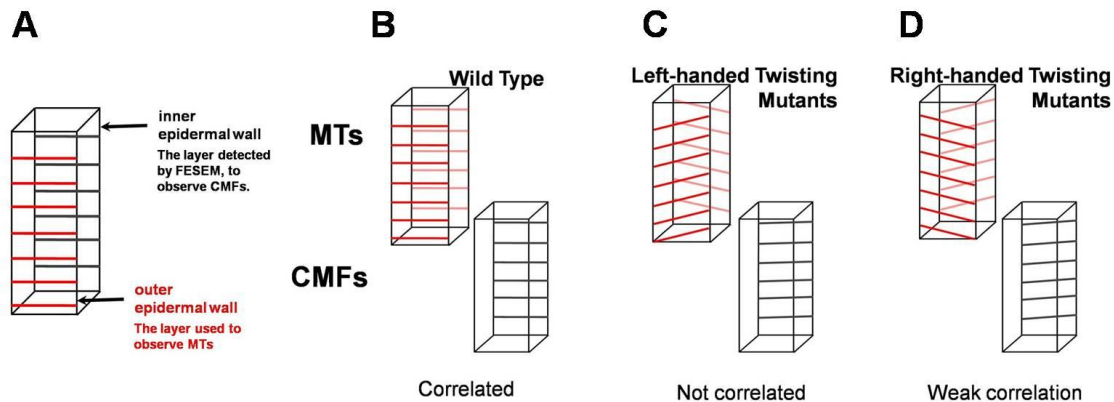
Figure A3- 6 Diagrams to explain the relationship between cellulose microfibril orientation and microtubule orientation in twisting mutants. A. The layers of epidermal cells at which microtubules and cellulose microfibrils were observed, including the outer periclinal surface where microtubules were observed and the inner periclinal surface where cellulose microfibrils were detected by FESEM. B. In wild type, both microtubules and cellulose microfibrils were well organized as transverse arrays. C. In left-handed twisting mutants, right-handed helical microtubule orientation detected in outer face of the cell when adjusted for the inner surface predicted an opposite cellulose microfibril orientation at the inner face of the cell but this was not reflected by the transverse cellulose microfibril orientation observed. D. In right-handed twisting mutants, there was a weak correlation between the alignments of cellulose microfibrils and microtubules.

From this study, it has been investigated that the handedness twisting phenotype had a strong link with altered microtubules caused by point mutations in either tubulins or MAPs, but that there was no apparent correlation with cellulose microfibril orientation. This suggested there might be some other factors involved in the defining of organ twisting directions, such as discoordination of growth cessation between tissues. Meanwhile, improvement of cyro-sectioning technique for FESEM will be required in order to accurately assess cellulose microfibril arrays at the outer periclinal surface of epidermal cells. That will provide unambiguous evidence for the relationship between the orientation of cellulose microfibrils and microtubules, and organ twisting behaviours.

FESEM preparation protocol   **Yi Zhang 2008**

For root: 7 days
For hypocotyl: 3 days

Solutions:

Stock (keep at 4℃)

    100mM PIPES pH7.2 (MW302.4; 15.12g in 500ml; use KOH to adjust pH)

    100mM MgSO$_4$ (MW246.47; 2.46g in 100ml)

    100mM EGTA   (MW380.4; 3.8g in 25ml 100mM PIPES)

2×PME (keep at 4℃; 3 months) 50mM PIPES, 1mM MgSO$_4$, 5mM EGTA, pH7.2

    100ml   100mM PIPES stock

    2ml   100mM MgSO$_4$ stock

    10ml   100mM EGTA stock

    88ml   dH$_2$O

    pH7.2   200ml in total

1×PME (keep at 4℃; 3 months) 25mM PIPES, 0.5mM MgSO$_4$, 2.5mM EGTA, pH7.2

    Diluted from 2×PME

50%DMSO in 1×PME (keep at room temperature)

    DMSO will be precipitated at 4℃

    50ml   2×PME

    50ml   DMSO

25%DMSO in 1×PME (keep at room temperature)

    50ml   2×PME

    25ml   DMSO

    25ml   dH$_2$O

Ethanol

    30% 50% 70% 95% 100%

Check:

Fixation buffer: 5ml for each treatment

16% FA	1.25ml
25% GA	200 μl
2×PME	2.5ml
dH$_2$O	1.05ml

1×PME

Vials (should be with tight lids to prevent the GA and FA being exposed to air), forceps, brushes, glass Petri dishes

1. Add 2.5ml 2×PME and 1.05ml dH$_2$O into each vial (for roots, it's better to use Petri dishes). Put the vials and forceps in the growth cabinet (if there is a temperature treatment)   **30min**

2. Bring the GA and FA to the growth cabinet, add 1.25ml 16% FA and 200 μl 25% GA to the vials, mix well.

3. Pick up the seedlings into the vials. If the interested sample is root, should be care of it. If the samples tend to float on the surface of the buffer, swirl the vial.

4. Incubate for 40min in growth cabinet.   **40min**

5. Bring the vials to the fume hood. Pour the samples and solutions to the glass Petri dishes.

6. Wash with 1×PME 10min, 3 times.   **40min**

7. Leave the samples in 1×PME, put at 4℃, O.N.

Check:

Glass, forceps (with curved tip), large forceps, brushes, liquid N$_2$ container (with a small beaker), timer, pipettes, toothpicks, blades, glass slides

Pins (clean, in a vial), glass Petri dishes (25% DMSO in PME, 50% DMSO in PME, 50% DMSO in PME for cut sample, 1×PME for melting sample—4 for each sample)

25% DMSO in PME, 50% DMSO in PME, 1×PME, Tissue-Tek

For roots, need to use 1%Toluidine Blue+1% Na Borate to stain the tissue so that it can be more easily seen. (10 μl 1%Toluidine Blue+1% Na Borate, 990 μl 50% DMSO in 1× PME, fix 1min)

Making glass knives (Leica)

Use the glass 8mm thick. If need, wash it with warm water.
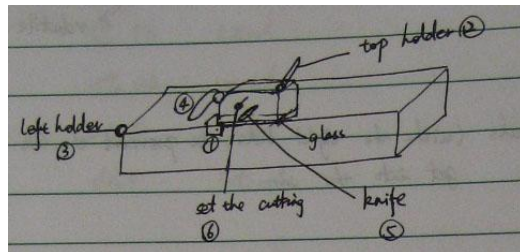
1. Put the glass at the centre of the cutting area, then use ① to fix the glass in the middle point.
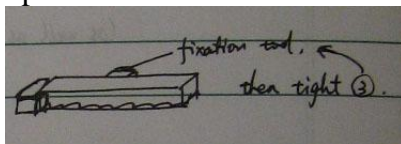
               check the bottom!

2. Make sure the top handle ② is at the very left side and check that the knife ⑤ is at the back position.
    For the square cutting, put ⑥ into the long line, cut the whole width;

    For the tri-angle cutting, put ⑥ into the short line, cut the center part.

3. Pull ④ towards you, fix it tightly.

4. Pull the knife ⑤ towards you, just one time!

5. Move the handle ② slowly, from the left to right side. It can gently break the grass, producing the smooth surface.

6. Then cut the square glass to tri-angle ones.

Good knives:
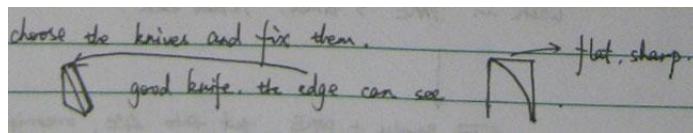
It has the flat and shape edge.

choose the knives and fix them.
good knife. the edge can see → flat, sharp.

Cryo-planing set up (Leica Ultracutting)

Machine

X. machine central part.

liq. N₂.

operation for the cutting   cutting chamber   operation for the temperature, liq N₂ ...

Cutting part:

Return	decide the speed return.
Counter	Σ run (how much advanced) decide the thickness of the sample. don't need to change.
Reset	move the sample holder back!! 0 — very back. full — close. when beeping, press it and wait it turn to 0.

Window set the "start" and "end"
· decide the region for cutting.
· use the handle at the right side of the chamber to change sample holder's position, then set it.

Approach
· when change the samples, move to end
· to move the samples close or far away from the glass knives.
· can use it to set the "window".

Illum
Light { top / side / bottom } both. (generally)

when watching the space between sample and knife. use the bottom light.

| Speed | 0.6 mm/s |
| Feed | 200 nm⌀. the speed of sample container move. |

Cut ... to cut.
⇓ ⇑ when knife holder position is adjusted, cut direction should be ⇓ direction. (also for the "Reset")

Temperature part:

| temperature | sample holder ⇒ | knives △ | TG | all set to -120℃ |

| Memory | we don't need. |
| Operation | control the liq. N₂. |

(LN₂ STOP)   STOP   (H)
((((·))))

When liq N₂ light get to one left.
it will beep, press the "STOP".
but still can use for 1 hour around.

When finish cryo-planing:
take out the knife holder and sample holder.
stop liq. N₂ uptake
press the "H" for heating.
make sure all knobs are loosen.

143

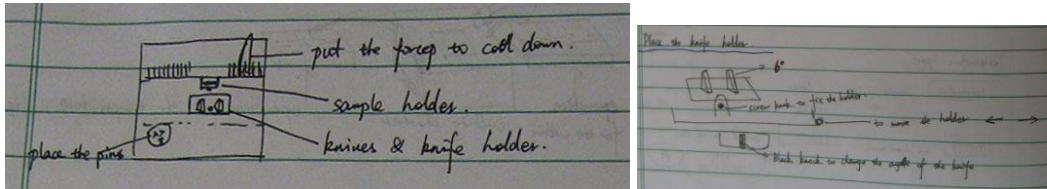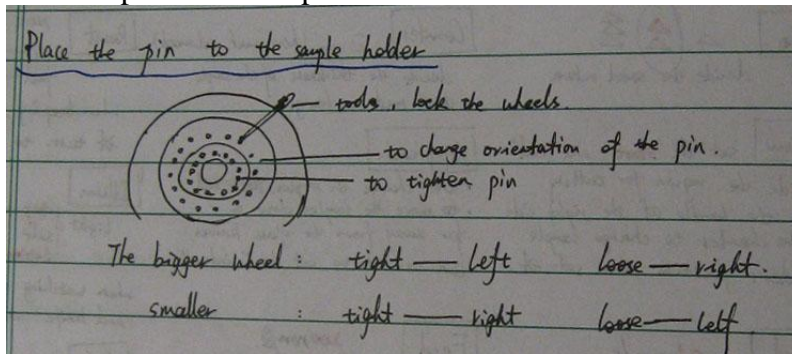**Cryo-planing set up (Leica Ultracutting)**

Chamber

1. Choose two glass knives and fix them on the knives holder. Remember to lock the holder.

2. Fix the pin in the sample holder.

3. Adjust the position of the pin and the knife. It's better to use the left edge of the knife.

4. Start cutting. For the root sample, it's hard to observe the cutting surface, so it's better to start with manual cutting.

Sample prep.

Samples were kept with 1×PME at 4℃.

1. Transfer samples from 1×PME to 25% DMSO in PME, by brush.   **10min**

2. Transfer samples from 25% DMSO in PME to 50% DMSO in PME, by brush.10min

3. Use small forceps to pick up the pin, and then put the Tissue-Tek at the top of the pin with toothpick. When applying the sample, use brush to pick up the seedling and try to put the interested region at the center of the pin.

Note: For the root sample, it's necessary to cut it before putting on the pin. 1%Toluidine Blue+1% Na Borate is used to incubate the whole seeding for 1 or 2min. Then directly cut the interested region with the blade, using microscopy to visualize the process; no need to wash it before cutting.

4. Use big forceps to hold the pin and gently put it into the liquid N2. Cannot drop it! That will damage the sample.

5. Move the pins inside the chamber and then fix the pin in sample holder.

Check the setting on the machine:

> Temperature: -120℃
>
> Glass knives: 6°
>
> Cutting speed: 0.6mm/s
>
> Feed: 200nm
>
> After adjusting the position of pin and knife, set the "Start" and "End", if need auto cutting.

When finish:

> Take out the pin and put it into 50% DMSO in PME. Wait until the samples come off from the pin, then transfer it into $1 \times$ PME.
>
> Keep at 4℃.

When all cutting is done:

> Take out the knife holder and the sample holder.
>
> Stop liquid N_2 uptake and press the "H" for heating.
>
> Make sure all knobs are loosened.
>
> Turn off the power of machine part, not the temperature control part.

Pin cleaning (Bransonic Ultrasonic Cleaning)

> Add 100% EtOH into a small beaker and put used pins inside.
>
> Use the heavy metal to prevent it floating.
>
> Put the beaker into the chamber (filled with water). Make sure the top of the beaker is higher than the water level.
>
> Turn on the power and set the timer for 10min.
>
> It will stop automatically.

When finished:

> Add new 100% EtOH into a vial.
>
> Put the clean pins into the vial.

Day 3: Extraction ≈1.5h

Check:

Beakers or glass Petri dishes, brushes, pipettes

Extraction solution: 0.1% NaHCl (from a new bleach bottle), dH_2O

1. Making the extraction solution (probably 3-5ml for each sample)

2. Using brushes to transfer the cryo-planed samples from $1 \times PME$ to extraction solution.

3. Remember to label the beaker or glass Petri dishes.

4. Put the beakers or glass Petri dishes on a shaker. Sit for 10min, slowly.   **10min**

5. Prepare a new beaker or glass Petri dishes with dH_2O for each sample.

6. After 10min, transfer the samples from extraction solution to dH_2O. Wash 10min, 3 times.

Day 3: Osmication ≈1.5h

Check:

2% Osmicate (OsO_4), dH_2O

Brushes, pipettes, parafilm

In Fume hood! OsO_4 is TOXIC!

1. Get parafilm and place it inside the fume hood. Use water to fix parafilm to the bottom.

2. Put a drop of dH_2O on the parafilm, for each sample.

3. Transfer the samples to the water drop. Remember to label!

4. Use small disposable pipette to take out the drop of dH_2O then put a drop of 2% OsO_4 on the samples. Samples will turn black.

5. Cover the drops with the lid of the Petri dishes to avoid drying out. Allow it to sit for 1h.

6. Remove the 2% OsO_4 with a small pipette to the OsO_4 waste bin.

7. Put a drop of dH_2O onto the samples. Wash 10min, 3times.

147

Check:

Brushes, curved tip forcep, white baskets (with dH$_2$O), glass Petri dishes

dH$_2$O, 30% EtOH, 50% EtOH, 70% EtOH, 95% EtOH, 100% EtOH

1. Transfer the samples into small white baskets by brush. Remember to label it!

2. Put the white baskets on a paper towel. 5sec later, put the baskets into 30% EtOH
Petri dishes. Make sure the level of EtOH is higher than the lid of the basket.

3. Sit on shaker for 30min.   **30min**

4. After 30min, put the white baskets onto the paper towel to get rid of excess EtOH.

5. Then put them into 50% EtOH for 30min.   **30min**

6. Then 70% EtOH 30min.   **30min**

7. Then 95% EtOH 30min.   **30min**

8. Then 100% EtOH 30min. 3 times.   **3×30min**

9. Keep at 4℃.

Check:

Forceps, 100%EtOH, a dry glass Petri dish

Put the white baskets from the overnight 100% EtOH to a new 100% EtOH Petri dish.

Critical Point Dry (Supercritical Autosamdri 815B, Tousimis)
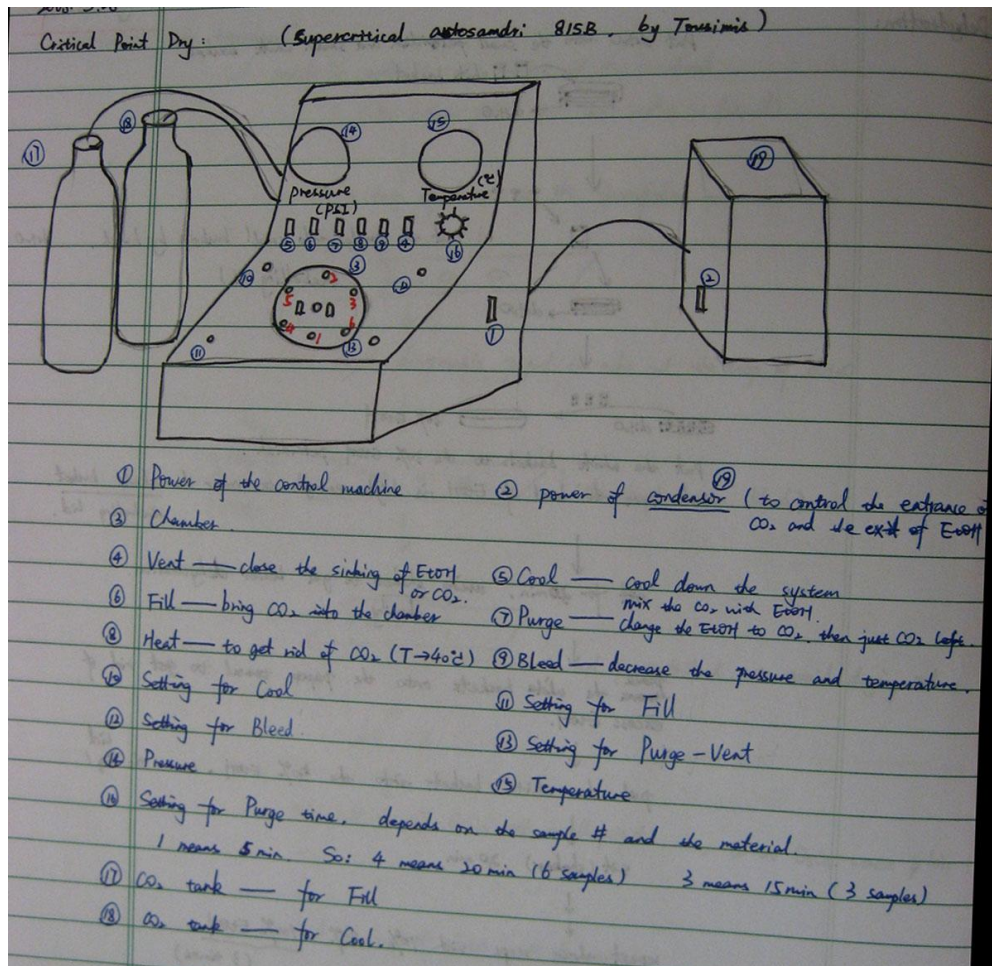
Check the setting:

Cool: 0.90   Fill: 0.65   Bleed: 0.20   Purge-Vent: 0.35

Purge time: 4—20min, depends on the sample number

Pressure (PSI): 0   Temperature (℃): N/A

1. Turn on the powers ① and ②.

2. Open chamber ③, unscrew the knobs in order, 1-6, and lift up the lid. Press "Vent", the light should be blinking; this means the chamber is closed.

3. Fill the chamber with 100% EtOH. If needed, take out the Teflon adapters. Fill half chamber first, and then put the white baskets inside. Make sure the EtOH lever is higher than the basket lid. Finally, fill the chamber full.

4. Put the lid back on, and then put the knobs in order, 1-6.

5. Open the CO_2 tanks. Anti-clock 2-3 rounds.

6. Check everything is right!

7. Press "Cool".

8. When the temperature gets around $0℃$, press "Fill".

9. The following steps will be automatically processed. From Fill to Vent will take approx. 1h.

<u>When finished:</u>

1. When the temperature reaches 0PSI, close the CO_2 tanks.

2. Open the chamber to pick up baskets, put into a dry Petri dish.

3. Turn off all power.

Check:

  Brushes, aluminum stubs, carbon sticky tape

1. Get aluminum stubs and put carbon sticky tape on the top.

2. Under the dissection microscope, use brush to move the samples onto the stubs. Put the cut side up and press it gently to fix it. Leave some space among the samples for better coating.

3. Draw the picture to label the samples.

Check:

Forceps, gloves

Sputter Coating (Crossington Sputter Coater 208HR)
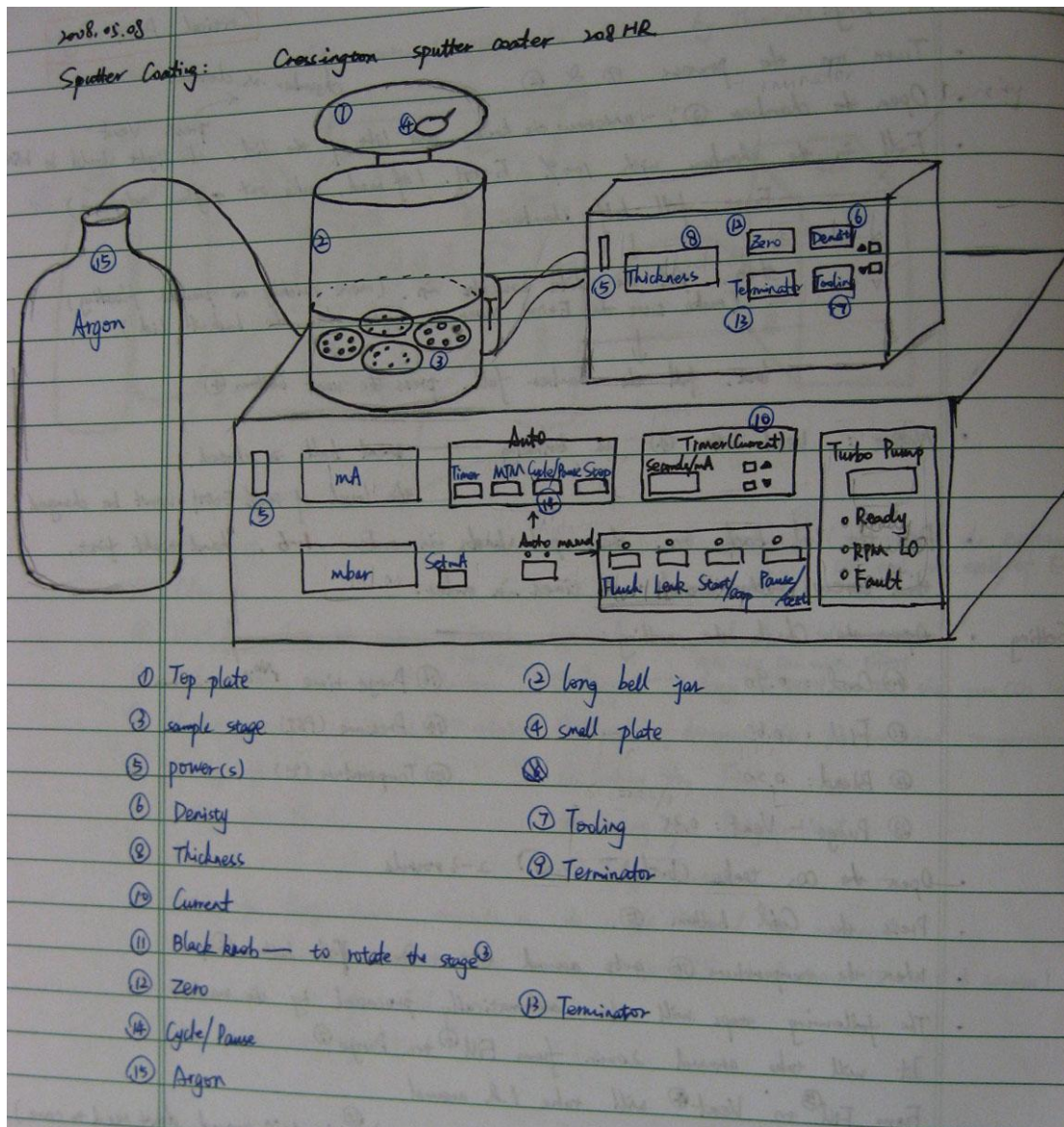
1. Check the plate on the top, make sure it's Platinum. (80/20) Pt/Pd, Density 19.52g/cm^3.

2. Take out the long bell jar and set the samples. Turn the back black knob ⑪ to move around the stub stage, for better coating. **Adjust the detector.**

3. Put the long bell jar back, and then close the top lid, with the small plate in the center position—to prevent the electron diffraction at the very beginning.

4. Turn on the powers and turn on the Argon tank.

5. Setting:

    Density: 19.52g/cm^3 Tooling: 1nm   Thickness: 5nm

    Terminator: 5nm   Current: 20mA

6. After 5min (Timer!), press "Zero", "Terminator" and "Cycle".

7. Wait…at the beginning cannot see the blue light, after around 1min, it is easy to see the light at the top. After 1 to 2min, move the small plate from the center to the side.

8. When the thickness gets to 5nm, it will stop automatically.
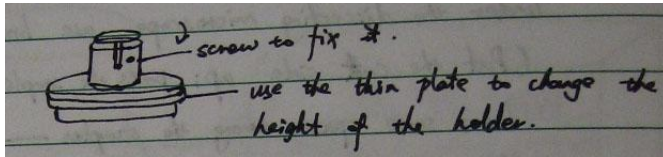

When finished:

1. Open the long bell jar, pick up the stubs.

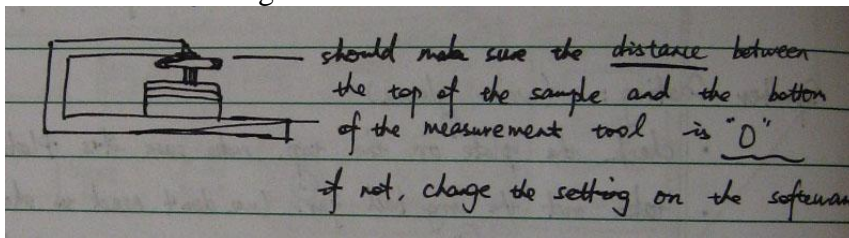2. Turn off all the power and the Argon tank.

Check:

  Forceps, gloves, FESEM data form

FESEM (Hitachi S-4700)   Wear gloves!

1. Put the stub onto stub holder and fix it.

2. Measure the height.

3. Press "AIR" on the machine (from Vacuum to Air).

4. Screw sample holder into the rod.

5. Close the chamber, press "Evac". Wait until vacuum is done, and then open MV1 (C →O).

6. Push the sample inside, put on the stage. Unscrew the rod and pull it back. **(to the very end)**

7. Close the MV1 (O→C).

8. FESEM software setting.

9. Observe the samples. Take pictures. Save the images.